National Calibration Facility for Retroreflective Traffic Control Materials

Prepared for:

National Cooperative Highway Research Program

TRANSPORTATION RESEARCH BOARD
OF THE NATIONAL ACADEMIES

Submitted by:

C. Cameron Miller
Todd Heimer
Edward Early
National Institute of Standards and Technology
Gaithersburg, Maryland

April 2005

THE NATIONAL ACADEMIES
Advisers to the Nation on Science, Engineering, and Medicine

The **National Academy of Sciences** is a private, nonprofit, self-perpetuating society of distinguished scholars engaged in scientific and engineering research, dedicated to the furtherance of science and technology and to their use for the general welfare. On the authority of the charter granted to it by the Congress in 1863, the Academy has a mandate that requires it to advise the federal government on scientific and technical matters. Dr. Bruce M. Alberts is president of the National Academy of Sciences.

The **National Academy of Engineering** was established in 1964, under the charter of the National Academy of Sciences, as a parallel organization of outstanding engineers. It is autonomous in its administration and in the selection of its members, sharing with the National Academy of Sciences the responsibility for advising the federal government. The National Academy of Engineering also sponsors engineering programs aimed at meeting national needs, encourages education and research, and recognizes the superior achievements of engineers. Dr. William A. Wulf is president of the National Academy of Engineering.

The **Institute of Medicine** was established in 1970 by the National Academy of Sciences to secure the services of eminent members of appropriate professions in the examination of policy matters pertaining to the health of the public. The Institute acts under the responsibility given to the National Academy of Sciences by its congressional charter to be an adviser to the federal government and, on its own initiative, to identify issues of medical care, research, and education. Dr. Harvey V. Fineberg is president of the Institute of Medicine.

The **National Research Council** was organized by the National Academy of Sciences in 1916 to associate the broad community of science and technology with the Academy's purposes of furthering knowledge and advising the federal government. Functioning in accordance with general policies determined by the Academy, the Council has become the principal operating agency of both the National Academy of Sciences and the National Academy of Engineering in providing services to the government, the public, and the scientific and engineering communities. The Council is administered jointly by both the Academies and the Institute of Medicine. Dr. Bruce M. Alberts and Dr. William A. Wulf are chair and vice chair, respectively, of the National Research Council.

The **Transportation Research Board** is a division of the National Research Council, which serves the National Academy of Sciences and the National Academy of Engineering. The Board's mission is to promote innovation and progress in transportation through research. In an objective and interdisciplinary setting, the Board facilitates the sharing of information on transportation practice and policy by researchers and practitioners; stimulates research and offers research management services that promote technical excellence; provides expert advice on transportation policy and programs; and disseminates research results broadly and encourages their implementation. The Board's varied activities annually engage more than 5,000 engineers, scientists, and other transportation researchers and practitioners from the public and private sectors and academia, all of whom contribute their expertise in the public interest. The program is supported by state transportation departments, federal agencies including the component administrations of the U.S. Department of Transportation, and other organizations and individuals interested in the development of transportation. **www.TRB.org**

www.national-academies.org

TABLE OF CONTENTS

       Problem Statement and Research Approach
       Summary of Instrument Requirements
       Instrument Overview

       Strip Lamp Projection System
       Sphere Projection System

       General Construction Requirements
       Goniometer Communications
       Three Axes of Rotation
       Three Axes of Translation
       Sample Holder and Depth Positioning
       The Rail System and Distance Dependence

       Three Axes Detector Stages
       Photometric Detection
       Spectroradiometric Detection

       Setting the Illumination Axis
       Absolute NIST Entrance Angle Components Alignment
       Absolute Observation Angle Alignment
       Absolute Rotation Angle Alignment

LIST OF FIGURES

LIST OF TABLES

ACKNOWLEDGMENTS

ABSTRACT

Congress has directed the United States Department of Transportation to establish "a standard for a minimum level of retroreflectivity that must be maintained for pavement markings and signs which apply to all roads open to public travel." Presented are the final capabilities of the NIST Center for High Accuracy Retroreflection Measurements. The requirements for the reference retroreflectometer are based on the data collected from national and international standards and meeting with various people knowledgeable in the field of retroreflective measurements. This final report on the reference retroreflectometer includes details concerning the source, the goniometer and the detectors and an in depth description of how the reference retroreflectometer is aligned and absolutely calibrated for the angular parameters, $\alpha, \beta_1, \beta_2, \varepsilon$. The reference retroreflectometer has been analyzed and characterized for over forty different aspects that are components in the overall uncertainty budget for the calibration of retroreflective material including signage and pavement marking material. The calibration of a typical retroreflective sheeting material for coefficient of luminous intensity can expect a relative expanded uncertainty of 1 % ($k=2$). Typical pavement marking material calibration will have a slightly higher relative expanded uncertainty of 2 % ($k=2$).

SUMMARY

Retroreflective traffic control devices are widely used for nighttime visibility and safety. Congress has directed the United States Department of Transportation to establish "a standard for a minimum level of retroreflectivity that must be maintained for pavement markings and signs which apply to all roads open to public travel." Establishing a national standard for minimum levels of retroreflectivity will require accurate methods to measure retroreflectivity. Before this project there were no traceable methods in the United States to determine the accuracy of measurements, because national calibration standards for retroreflectivity did not exist. The primary mission of the National Institute of Standards and Technology (NIST) is to provide such national calibration standards in a variety of areas important to government or industry. The objective of this project was two-fold. First, to develop a dedicated reference instrument for measuring retroreflective materials, and second, to develop a calibration program that provides traceability to the relevant national scales maintained by NIST.

The Center for High Accuracy Retroreflection Measurements at NIST is composed of three components, the source, the goniometer, and the detector, and how these components are absolutely aligned. Each component is briefly described. The source is composed of a 100 W strip lamp that is imaged by an Abbe projector. The source luminance varies less than ± 0.056 % ($k=2$) over a day due to the current setting. Experimentally, once the lamp has stabilized, the intensity fluctuation is less than ± 0.025 %. The correlated color temperature produced by the system is 2856 K ± 10 K ($k=2$). The uniformity of the illuminance at the source aperture was determined to be within ± 3 % of the mean value. The uniformity of the illuminance at the retroreflector aperture surface was determined to be within ± 1.8 % of the mean value. The overall expanded uncertainty to the measurement of R_L due to the source system is 0.33 % ($k=2$). A second system consists of a 5 cm diameter sphere made from Zenithpolymer pumped by light from four 410 W reflector lamps. The exit port is imaged by an Abbe projection system similar to the system used in the strip lamp system. The sphere system provided similar characteristics to the strip lamp system with more operating complications. The real advantage of the sphere projection system is that any light can be coupled into the sphere without changing any of the projection optics. The high intensity discharge (HID) lamps that are available in cars have a very distinct spectral pattern. The retroreflectance of devices can be calculated if spectral coefficients

of retroreflection are measured, but to experimentally verify the results, the sphere projection system is the best option.

The goniometer of the reference retroreflectometer is mounted on a rail system. The illumination distance is variable from 5 to 35 m and will have an absolute uncertainty of 0.005 m ($k=2$). The pitch and yaw axes have an absolute expanded uncertainty of 0.02° ($k=2$) and both axes have a range of ± 95°. The rotation axis, ε, has an absolute expanded uncertainty of 0.36° ($k=2$). The largest retroreflective device the goniometer can accommodate is a device 95 cm in diameter, and it has a clear view to allow almost any length of pavement marking. The sample mounting plate uses vacuum cups to hold the retroreflective devices against a precision register. The mounting bracket has an adjustable depth to accommodate different sample thicknesses. The detector package can also be mounted to the sample plate, to measure the illuminance at the sample plane. In addition to the three automated rotation axes, the goniometer is able to translate along three axes using stepping motors providing an accuracy of 0.25 mm along the illumination axis and 0.05 mm perpendicular to the illumination axis. These translations are for research purposes such as studying uniformity of the source and the sample.

The detector is supported by the observation angle positioner, which is comprised of a 2 m translation stage, a rotation stage and a 0.2 m translation stage. Each of these motions has an optical encoder to ensure accuracy. The absolute expanded uncertainty of the entrance angle, α, is 0.0002° ($k=2$). The observation distance is maintained equal to the illumination distance to an absolute expanded uncertainty of 0.005 m ($k=2$). The observer apertures will range from 3 to 20 arc minutes. An f_1'= 1.6% was determined for our complete optical detection system. With this detector system and source the detection limit (signal-to-noise of 2:1) for the NIST reference retroreflectometer is 0.17 mcd/m^2/lx. A calibration limit can be defined as the magnitude of the coefficient of retroreflected luminance where the signal-to-noise does not dominated the uncertainty budget (typically 1000:1, in this case 500:1); therefore the calibration limit for the NIST reference retroreflectometer is 42 mcd/m^2/lx.

The reference retroreflectometer has been analyzed and characterized for over forty different aspects that are components in the overall uncertainty budget for the calibration of retroreflective material including signage and pavement marking material. The typical calibration of a white encapsulated bead retroreflective sheeting material for coefficient of retroreflected luminous intensity is expected to have a relative expanded uncertainty of 1 %

(k=2). The uncertainty will be somewhat higher, up to 2 % (k=2) for microprismatic and/or colored materials. Typical white or yellow pavement marking material will have a relative expanded uncertainty of 2 % (k=2).

Traceability requires the establishment of an unbroken chain of comparisons to stated reference artifacts or materials. NIST assures the traceability of results of measurements or values of standards that NIST itself provides or calibrates. Other organizations are responsible for establishing the traceability of their own results or values to those of NIST. The role of this project was to develop a calibration program to provide the stated references. NIST also assists in helping laboratories establish traceability of their measurements through a variety of support mechanisms, which include round robin comparisons, workshops, the Measurement Assurance Program, and the National Voluntary Laboratory Accreditation Program.

CHAPTER 1

INTRODUCTION AND OVERVIEW

Presented in this Final Report for Project 05-16 "National Calibration Facility for Retroreflective Traffic Control Materials" are the details required to construct and validate the reference retroreflectometer. Chapter 1 contains the problem statement along with the research approach for solving this problem. The requirements for the reference retroreflectometer are presented based on the data collected from national and international standards and meeting with various people knowledgeable in the field of retroreflective measurements. The conclusion of Chapter 1 presents a general overview of the Center for High Accuracy Retroreflection Measurements.

Chapters 2, 3 and 4 discuss the source, the goniometer and the detectors. Each section describes the operation and capabilities of the component along with the contributions to the final uncertainty budget. Chapter 5 gives an in depth description of how the reference retroreflectometer is aligned and absolutely calibrated for ($\alpha, \beta_1, \beta_2, \varepsilon$) parameters. Additional components of uncertainty not addressed in chapters 2, 3, and 4 are discussed. Chapter 6 provides the overall uncertainty budgets for the calibration of retroreflective material. Uncertainty analysis for additional angular parameters that are important in other representations: Intrinsic, Application and Road Marking ($\omega_s, \gamma, a, b, e, d$) are discussed in the Appendix B.

Chapter 7 describes the calibration procedure, which includes a statement of traceability to NIST. The role of accreditation through the National Voluntary Laboratory Accreditation Program (NVLAP) or the Measurement Assurance Program (MAP) is discussed.

PROBLEM STATEMENT AND RESEARCH APPROACH

Retroreflective traffic control devices are widely used for nighttime visibility and safety. Congress has directed the U.S. Department of Transportation to establish "a standard for a minimum level of retroreflectivity that must be maintained for pavement markings and signs which apply to all roads open to public travel." Establishing a national standard for minimum levels of retroreflectivity will require accurate methods to measure retroreflectivity. Instruments are commercially available for measuring the retroreflectivity of signs and markings, and

documented standards establish procedures for such measurements. However, there can be significant variability among instruments measuring the same object, and the standards do not ensure accuracy of the instruments. There are currently no traceable methods in the United States to determine the accuracy of measurements, because national calibration standards for retroreflectivity do not exist. The primary mission of the National Institute of Standards and Technology (NIST) is to provide such national calibration standards in a variety of areas important to government or industry. Within NIST, the Optical Technology Division maintains standards and provides calibrations for measurements involving optical radiation.

The measurement of retroreflectivity is essentially a measurement of the reflectance of materials under specified geometrical and spectral conditions. It therefore involves the areas of photometry and spectrophotometry within the Optical Technology Division. While the distinction between these two areas can overlap, in general photometry maintains the national scales for luminous intensity, illuminance and luminance, while spectrophotometry maintains the national scales for spectral reflectance and transmittance.

NIST was previously involved in retroreflectivity with a reference instrument and a Measurement Assurance Program. However, retirement of essential personnel and lack of modernization of the reference instrument, particularly automation, ended this program. The range used by the reference instrument and some of its components were used in the new reference instrument. A workshop held in 1997 stressed the need for NIST to again become involved in retroreflectivity, and so NIST personnel began to participate in national and international organizations dealing with retroreflectivity, namely the American Society of Testing and Materials (ASTM) and the International Commission on Illumination (CIE).

The objective of this project was two-fold. First, to develop a dedicated reference instrument for measuring retroreflective materials, and second, to develop a calibration program that provides traceability to the relevant national scales maintained by NIST. The expertise of the personnel in the specific area of retroreflectivity and in the broader areas of photometry and spectrophotometry, the existing facilities, and the mission of NIST, has assured that the objective was attained.

The research detailed in this report was directed toward developing a reference instrument that provides the basis for a national calibration facility for retroreflectivity measurements. This research was divided into two phases. Phase I consisted of those tasks

necessary to design the reference instrument, while the instrument was built and characterized in Phase II.

The specific tasks in Phase I was as follows.

Task 1. Literature review. This review included all of the existing national and international calibration and measurement methods of, and specifications for, retroreflective traffic control materials, with particular attention to the material, geometric, and spectral requirement capabilities. The review included visits to facilities to assess current retroreflectivity measurements, such as the 3M Company in Minnesota and the Turner Fairbanks Highway Research Center in Virginia. Facilities at the British Standards Institute (BSI) in England and the Federal Institute for Materials Research and Testing (BAM) in Germany have been visited. The list of standards is presented in Appendix A.

Task 2. Requirements. These requirements describe all of the parameters necessary to calibrate retroreflective traffic control materials based upon the literature review conducted in Task 1. These parameters include the materials and sizes of retroreflecting materials, the geometry of the entrance and observation angles, apertures, and the spectral conditions. Also, included in this task are the requirements necessary to measure and characterize fluorescent materials. Specifically, a bi-spectral measurement is not included in this research plan. Task 2 is included in the Chapter 1 Summary of Instrument Requirements.

Task 3. Preliminary design. A preliminary design for the reference instrument was produced, based upon the requirements identified in Task 2. This design included all of the components needed for the source, goniometer, detector, and data acquisition and control systems, as well as a plan for characterizing the operation of the instrument to ensure that it meets the requirements. The preliminary design was presented at the Annual Meeting of the Council for Optical Radiation Measurements, meeting on May $6^{th} - 8^{th}$, 2002, specifically at OP4 "Retroreflection," and at the 16th Biennial Symposium on Visibility and Simulation hosted by the Transportation Research Board and the University of Iowa on June $2^{nd} - 4^{th}$, 2002. The preliminary design was described in the Interim Report to NCHRP and published as NISTIR 6940, "National Calibration Facility for Retroreflective Traffic Control Materials – Phase I."

Task 4. Uncertainty analysis. Based upon the design in Task 3, the uncertainties in the components of the reference retroreflectometer were calculated. The overall uncertainty budget

for calibration of typical retroreflective traffic control materials was finalized in this report and is presented in Chapter 7.

Task 5. Traceability to NIST. Possible mechanisms for providing traceability of calibrated standards to NIST were investigated. There is not now, nor will there be, the resources for calibrating many samples in a rapid, inexpensive manner. Therefore, several mechanisms were developed to provide traceability to NIST that is agreeable both to NIST and to the customers. They include accreditation of secondary laboratories through NVLAP, measurement assurance program sets, and guidelines for customer standards submitted for the calibration service. The possibility of generating standard reference materials is discussed in Chapter 7.

Task 6. Interim report. An interim report was prepared documenting Tasks 1 to 5 and including a detailed work plan for Phase II. This report was submitted to NCHRP and published as NISTIR 6940, "National Calibration Facility for Retroreflective Traffic Control Materials – Phase I."

Task 7. Meet with the project panel. This meeting occurred July 18th, 2002 at the National Academy of Sciences in Washington DC.

The construction and validation of the reference instrument occurred in Phase II. In general terms, the goals for the instrument were divided into two categories. First, the instrument satisfies all the current requirements detailed in relevant documentary standards for materials, geometrical, and spectral conditions. Second, the instrument can accommodate additional geometrical and spectral capabilities to increase its utility in the future as standards change and develop. The specific tasks in Phase II were as follows.

Task 8. Final design. A final design of the instrument was prepared based upon the results from Phase I.

Task 9. Construct instrument. The components were acquired and assembled to produce a reference instrument for measuring the retroreflectivity of traffic control materials based upon the design in Task 8.

Task 10. Validate instrument. The performance of the instrument was fully characterized to ensure that it meets the requirements and uncertainties identified in Tasks 2 and 4.

Task 11. Demonstrate. On October 27th, 2003 a demonstration was conducted at NIST for the Project Panel to show the capabilities and operation of the instrument.

Task 12. Calibration program. The details of the calibration service described in Task 5 are finalized and presented in Chapter 7. The calibration service will be available starting the fall of 2004.

Task 13. Final report. A final report was prepared that documents the entire research effort in Tasks 1 to 12, in conformance with guidelines set forth by the NCHRP.

SUMMARY OF INSTRUMENT REQUIREMENTS

No one document specifies the necessary requirements for a reference retroreflectometer. Appendix A is a list of the national and international retroreflection standards collected. The requirements presented here are the minimum based on these retroreflection standards, related support standards, and interviews with knowledgeable sources.

The source of the reference retroreflectometer should be a projector type capable of uniformly overfilling the specimen. The uniformity of illuminance should be within 5% of the mean value obtained normal to the source. For most applications the relative spectral power distribution of the source should be equal to CIE standard illuminant A (2856 K) with an uncertainty of 20 K. The source should also be capable of providing other important relative spectral power distributions such as the new HID lamps. The source illuminance should not vary more than 1 % over the course of the measurement and should emit unpolarized light. Included in the source design is the source aperture. The recommended aperture sizes are 3, 6, 10, and 20 arc minutes for signage and 20 x 10 arc minutes for road marking materials. The uniformity of the source at the aperture has to be sufficiently uniform so as not to add positional uncertainty to the centroid of the aperture.

The goniometer of the reference retroreflectometer should be capable of movement in three axes, entrance angle component β_1, entrance angle component β_2 and rotation angle, ε. Figure 1 shows the CIE system for specifying and measuring retroreflectors. The uncertainty in setting β_1 and β_2 should be less than 0.1° and the resolution should be better than 0.02°. The uncertainty in setting ε should be less than 0.2° and the resolution should be better than 0.04°. The goniometer should be able to accommodate sign specimens 0.3 meters square and pavement markings panels 10 to 15 cm wide and 60 to 120 cm long. The goniometer has to be able to substitute the detection system and the retroreflector specimen easily. Also associated with the goniometer is the illumination distance, which is the distance between the center of the

goniometer and the source aperture. The illumination distance needs to be variable from 7.5 to 30 m and should have an uncertainty less than 0.01 m.

The detection system is composed of the observation angle positioner and photometer head. The observation angle positioner is designed to support and separate the photometer head from the light source. The observation distance should be maintained equal to the illumination distance with an uncertainty less than 0.01 m. The observation angle, α, should be set with an uncertainty less than 0.002°. The recommended aperture sizes for the photometer head aperture are 3, 6, 10, and 20 arc minutes. The responsivity and range of the photometer head should be sufficient that readings of the light source and the test retroreflector have a resolution of at least 1 part in 50. The linearity of the detection system over the range of the measurement should be within 1%. Correction factors may be used to correct non-linearities. The relative spectral responsivity of the photometer head should match the CIE $V(\lambda)$-function with an f_1' tolerance of at most 3%. Spectral mismatch corrections may be applied to the $V(\lambda)$-function. The readings of the photometer head from a constant source should not vary more than 1%. The specifications for nighttime color measurements or retroreflected color are not well specified. The spectroradiometer requirements are that it has a very good linear response and its wavelength scale must be calibrated.

INSTRUMENT OVERVIEW

The capabilities of the Center for High Accuracy Retroreflection Measurements at NIST are briefly described in this section and in more detail in the following chapters. Figure 2 is a conceptual drawing that shows the position of the devices in the tunnel. The source and detection system are on a 1.52 by 3.65 m optic table and the goniometer is on a rail system. The source and detector systems are behind a shield to reduce scattered light. Also, to reduce scattered light, a 3 square meter light trap is positioned at the end of the rail system and baffles mount on the rail system and slide into appropriate positions or can be removed.

The source is composed of a 100 W strip lamp that is imaged by an Abbe projector. The uncertainty of the source luminance varies less than ± 0.056 % (k=2) over the course of a day. Experimentally, once the lamp has stabilized, the intensity fluctuation is less than ± 0.025 % (A-type uncertainty). The correlated color temperature produced by the system is 2856 K ± 10 K (k=2). The uniformity of the illuminance at the source aperture was determined to be within ± 3

% of the mean value. The uniformity of the illuminance at the retroreflector aperture surface was determined to be within ± 1.8 % of the mean value. The overall expanded uncertainty to the measurement of R_L due to the source system is 0.33 % ($k=2$). A second system consists of a 5 cm diameter sphere made from Zenithpolymer[*] pumped by the light from four 410 W reflector lamps. The exit port is imaged by an Abbe projection system similar to the system used in the strip lamp system. The sphere system provided similar characteristics to the strip lamp system with more operating complications. The real advantage of the sphere projection system is that any light can be coupled into the sphere without changing any of the projection optics. The high intensity discharge (HID) lamps that are available in cars have a very distinct spectral pattern. The retroreflectance of devices can be calculated if spectral coefficients of retroreflection are measured, but to experimentally verify the results, the sphere projection system is the best option.

The goniometer of the reference retroreflectometer is mounted on a rail system. The illumination distance is variable from 5 to 35 m and has an absolute uncertainty of 0.005 m ($k=2$). The pitch and yaw axes have an absolute uncertainty of 0.02° ($k=2$) and both axes have a range of ± 95°. The rotation axis, ε, has an absolute uncertainty of 0.36° ($k=2$). The largest retroreflective device the goniometer can accommodate is a device 95 cm in diameter, and it has a clear view to allow almost any length of pavement marking. The sample mounting plate uses vacuum cups to hold the retroreflective devices against a precision register. The mounting bracket has an adjustable depth to accommodate different sample thicknesses. The detector package can also be mounted to the sample plate, to measure the illuminance at the sample plane. In addition to the three automated rotation axes, the goniometer is able to translate along three axes using stepping motors providing an accuracy of 0.25 mm along the illumination axis and 0.05 mm perpendicular to the illumination axis. These translations are for research purposes such as studying uniformity of the source and the sample.

The detector is supported by the observation angle positioner, which is comprised of a 2 m translation stage, a rotation stage and a 0.2 m translation stage. Each of these motions has an optical encoder to ensure accuracy. The absolute uncertainty of the entrance angle, α, is 0.0004°

---

[*] Certain commercial equipment, instruments, or materials are identified in this paper to foster understanding. Such identification does not imply recommendation or endorsement by the National Institute of Standards and Technology, nor does it imply that the materials or equipment identified are necessarily the best available for the purpose.

($k=2$). The observation distance is maintained equal to the illumination distance to an absolute uncertainty of 0.005 m. The observer apertures range from 3 to 20 arc minutes. An f_1'= 1.6% was determined for our complete optical detection system. With this detector system and source the detection limit (signal-to-noise of 2:1) for the NIST reference retroreflectometer is 0.17 mcd/m^2/lx.   A calibration limit can be defined as the magnitude of the coefficient of retroreflected luminance where the signal-to-noise does not dominated the uncertainty budget (typically 1000:1, in this case 500:1); therefore the calibration limit for the NIST reference retroreflectometer is 42 mcd/m^2/lx.

CHAPTER 2

SOURCE CHARACTERISTICS

The source was designed to meet or exceed the requirements listed in the documentary standards. The source uses an Abbe projection system to image a uniformly illuminated field aperture at the specimen location through a source aperture of defined angular extent. Two systems for achieving a uniformly illuminated field aperture were investigated – an imaged 100 W tungsten strip lamp and a pumped integrating sphere.

STRIP LAMP PROJECTION SYSTEM

The first system is a 100 W tungsten strip lamp imaged onto the field aperture. This is the system used in the NIST retroreflectance facility in the 1980s. Figure 3 shows a schematic of the projection system. An aspheric lens with a diameter of 60 mm and a focal length of 39 mm images the 2 mm x 18 mm tungsten strip on a 5 mm field aperture. The 5 mm field aperture limits the transmitted light such that the image is from a 0.83 mm diameter circle of the tungsten strip. One of a variety of a chromatic projection lenses is chosen to image the field aperture at the retroreflective device after passing through the source aperture. If the image of the field aperture is larger than the size of the retroreflective device, then the device is the aperture stop of the source and the source aperture is the field stop. However, if the image of the field aperture is smaller than the size of the retroreflective device, for example if a smaller field aperture is used, then the image is the field stop and the source aperture is the aperture stop. Table 1 lists the lenses and image sizes for various distances to the retroreflector device.

The strip lamp system is the source that will be used on a routine basis for calibrations and research activities. A summary of the requirements determined from standards and the characterization of the strip lamp projection system is presented in Table 2.

Stability and Correlated Color Temperature

The stability of the source is primarily dependent on the current control of the lamp. The lamp is powered by a constant current power supply that is analog controlled from the output of two 12-bit digital-to-analog controllers. One analog output is divided by 4096 and then added to the second analog output to achieve a 22-bit signal. Two bits of signal are lost in the addition. The 22-bit signal controls the current supply with a resolution of 0.004 mA. The digital-to-

analog controller is programmed based on the voltage drop across a calibrated shunt resistor. Over the course of a year setting the current has an uncertainty of 0.013 % (k=2), as calculated from Table 3. This table follows the procedure used in the "Guide to the Expression of Uncertainty in Measurement" (*GUM*) published by the International Organization for Standardization (ISO).(*1*) This *Guide* establishes general rules for evaluating and expressing uncertainty in measurement. Listed in the table are the dependent quantities for the final result, the symbol for these quantities, the value and the standard uncertainty, the unit of the quantity, the type of evaluation method, which is Type A for statistically based and Type B for all others, the degrees of freedom, which for a Type A measurement is typically the number of repetitions and the sensitivity coefficient, which is the partial derivative of the model or equation with respect to the quantity. The sensitivity coefficient can be calculated or determined experimentally. The uncertainty contribution is the standard uncertainty times the sensitivity coefficient. The combined standard uncertainty is the sum of the squares of the uncertainty contributions. Therefore, the last line in the table gives the resultant, the unit and the combined uncertainty. Typically, uncertainties are expressed as an expanded uncertainty with a coverage factor, k. A coverage factor of 2 is similar to a confidence interval of 95.45 % if the degrees of freedom are large. Using this feedback loop the current will vary over 24 h by less than 0.008 % (k=2), as calculated from Table 4. The difference is the calibration of the voltmeter for a day versus a year. The luminance of a tungsten lamp is approximately proportional to the current raised to the power of 7. Therefore, the luminance of the tungsten lamp will vary less than ± 0.056 % (k=2) over a day from the current setting. Figure 4 shows that once the lamp has stabilized, the intensity fluctuation is less than ± 0.025 %, which is within the expected uncertainty.

The correlated color temperature (CCT) is determined by a spectrometer that is calibrated against the NIST photometric color temperature standards using a pressed PTFE plaque. The PTFE plaque is placed in front of the projection system and viewed by the spectrometer, and the current is set so that the light has a 2856 K ± 10 K (k=2) spectral distribution. The CCT of the strip lamp changes 1 K for every 7 mA at the operating current for Illuminant A. Since the current is controlled to ± 0.008 % (k=2) or ± 2 mA over a 24 h period, the CCT should not change by more than ± 0.3 K. Figure 5 shows that the CCT only changes within the ± 1 K resolution of the spectrometer used to monitor the CCT. The final uncertainty budget

dependence on the CCT is more complex. The correction factor based on the CCT is the set CCT divided by the expected CCT. Since the expected CCT is 2856 K and the set CCT is 2856 K, the correction factor is 1. However, the expected CCT has no uncertainty where as the set CCT has an uncertainty of 10 K ($k=2$). The sensitivity coefficient used in the final uncertainty budget depends on the detector spectral response and the reflectance factor of the sample measured. The most time effective method of determining the sensitivity coefficient in this case is through simulation. The final results of the simulation are in Figure 6 and the calculation method is described below.

The calculation is normalized to the values calculated at 2856 K. For example, since the illuminance measured at the sample is dependent on the spectral response of the detection system, ideally the spectral luminous efficiency function, V_λ, the voltage of the detector system has to be calculated with a given CCT spectral distribution and divided by the voltage of the detector system with the given CCT spectral distribution at 2856 K. The illuminance ratio is then divided by the ratio at the detector, which is now dependent on the reflectance factor of the sample directing the light to the detector. Equation 1 expresses this mathematically,

$$Norm.R_L = \frac{\int \Phi_{CCT}(\lambda)s_r(\lambda)d\lambda}{\int \Phi_{2856K}(\lambda)s_r(\lambda)d\lambda} \Big/ \frac{\int \Phi_{CCT}(\lambda)R_s(\lambda)s_r(\lambda)d\lambda}{\int \Phi_{2856K}(\lambda)R_s(\lambda)s_r(\lambda)d\lambda} \tag{1}$$

where $\Phi_{CCT}(\lambda)$ is the spectral power distribution of the source at a given CCT, $\Phi_{2856K}(\lambda)$ is the spectral power distribution of the source at 2856 K, $s_r(\lambda)$ is the spectral response of the detection system, $R_s(\lambda)$ is the retroreflectance factor for a given sample, and the integration is over the visible region. The retroreflectance factor curves used in this calculation are measurements and are shown in Figure 7. The difference between the V_λ function and the spectral response of the NIST detection system is not visible in a figure and therefore is not shown here.

The slopes of the curves in Figure 6 are the sensitivity coefficients. Table 5 summarizes the slope of the curves for the different materials and shows the relative expanded uncertainty for each material. The relative expanded uncertainty is the contribution that the CCT uncertainty will have on the final uncertainty budget for the measurement of the coefficient of retroreflected luminance, R_L.

Source Aperture Uniformity and Size

The uniformity of luminous flux at the apertures of the projection system is important because it affects the uncertainty budget in several ways. The uniformity of the illuminance at the source aperture determines the weighting of the observation angles that are integrated within the aperture area. The uniformity was measured by scanning a photometer with a 3 mm aperture horizontally and vertically perpendicular to the source aperture. The uniformity of the illuminance at the source aperture was determined to be within ± 3 % of the mean value and is shown in Figure 8. To determine the effect the source aperture illuminance uniformity has on the overall uncertainty budget, we developed a simulation based on the aperture synthesis procedure described in Appendix D of the document CIE 54.2 "Retroreflection: Definition and Measurement."(2) The definition of R_L uses the angles α, β_1, β_2, and ε, which are defined originating from points. The definition is understood as the limiting value for infinitesimally small source and observer apertures. The measurement using an aperture of reasonable size generally introduces approximations to this theoretical definition. For calibration purposes the aperture size is fixed. For example, a measurement may define the distance to be 15 m and the apertures to have an angular extent of 6' from the sample. Therefore, the aperture should have a diameter of 26.18 mm. Any deviation from 26.18 mm causes uncertainty in the measurement. The source aperture made at NIST was measured at the Absolute Aperture Area Facility and has a diameter of 26.01216 mm with an uncertainty of 0.00087 mm (k=2).

The aperture synthesis procedure uses a large number of R_L measurements made using extremely small source and observer apertures. The reader can image a small area that is near the edge of the source aperture that is farthest from the detector aperture and vertically offset higher as shown in Figure 9. The light emerging from that small area goes to the sample and is retroreflected back to a small area near the edge of the detector aperture that is farthest from the source aperture and vertically offset lower. This path of light has a larger observation angle and a significantly different rotation angle than the path of light from the centers of the source and observer apertures. If the amount of light is much less or more at the edge of the aperture than the center, the average R_L value determined for this aperture size will be different than that determined for a uniformly illuminated source aperture. By treating the small areas as vectors as described in CIE 54.2, the simulation was calculated rather easily. The simulation showed that

the relative standard uncertainty due to the NIST non-uniformity at the source aperture for an encapsulated bead sign material is 0.000012 %. The non-uniformity of the sample and the detector are not considered in this quantity, and will be included in their respective chapters. For prismatic material, the R_L dependence on rotation angle was modeled as a sine wave that has three periods over 2π and oscillates from 0.8 % to 1.2 % of the R_L at 0°. The relative standard uncertainty for a prismatic sign material is 0.0026 %, given the NIST source aperture illuminance uniformity. The initial angle values used in the simulation were $\alpha = 0.33°$, $\beta_1 = -5°$, $\beta_2 = 0°$, and $\varepsilon = 0°$. When these values were changed, no large changes in the relative standard uncertainties were observed.

NIST modeled some of the systems encountered in the initial survey of instruments available. One such instrument had a rather non-uniform source aperture illuminance because it produced an image of the lamp filament next to a reflected lamp filament image. The reflected filament image is typically 20 % less in flux than the filament image. To model this situation a continuous curve that peaks in the center and is 20 % less on one side was used. A plot of this curve is shown in Figure 10. The vertical axis in the plot is along the observation plane in this system. The correction for beaded material with this system is 0.016 % and for prismatic material the correction climbs to 0.20 %. If the center of the filament image was placed perpendicular to the observation plane, the correction for beaded material is 0.22 % and for prismatic material the correction drops to -0.20 %. The instrument examined positions the non-uniformity in the most favorable geometry. However, this may not be the case for all instruments.

The aperture synthesis procedure was also used to model the uncertainty dependence on the size of the aperture. The relative R_L values were calculated for apertures of 23 mm and 29 mm versus a 26 mm aperture for beaded sign material and prismatic sign material. The results are shown in Figure 11. As stated above, the diameter of the source aperture is 26.01216 mm; therefore, Δd is -0.16779 mm. The correction factor calculated using the equations in Figure 11 is 0.99996 for beaded material and 0.99993 for prismatic material. Since the simulation is not based on detailed information for a particular material, the correction factor is included in the total uncertainty budget. The relative expanded uncertainty due to the size of the aperture is 0.0086 % (*k*=2) for beaded material and 0.014 % (*k*=2) for prismatic material.

Retroreflector Aperture Surface Uniformity and the Illuminance Measurement

Document CIE 54.2 defines the retroreflector aperture surface as the area illuminated by the source and viewed by the detector given either by the retroreflector itself or by a diaphragm enclosing part of the retroreflector. Retroreflector aperture refers to the angular dimensions from the source point of reference to the retroreflector aperture surface. The uniformity of the illuminance at the retroreflector aperture surface has a strong dependence on the illuminance measurement method and on the light retroreflected to the detector in association with the uniformity of the coefficient of retroreflection for the device. The uniformity of the illuminance at the retroreflector aperture surface was determined to be within $\pm$ 1.8 % of the mean value and is shown in Figure 12. The uniformity was measured by scanning a photometer with a 5 mm aperture across the beam over a 40 cm range in both x and y perpendicular to the beam. The uniformity of the illuminance at the retroreflector aperture surface was scanned many times over several days after burning the lamp for days at a time. The structure of the uniformity did not change by more than 0.10 %. The absolute flux fluctuated less than 0.30 % on a day-to-day basis. Based on this data the illuminance for the given day can be measured by sampling the retroreflector aperture surface instead of performing a complete scan. To measure the illuminance the detector is positioned on the goniometer in the center of the retroreflector aperture surface. The center is measured and then the detector is moved in a circle 5 cm away from the center point where 8 additional measurements are made. The 9 voltages are averaged then adjusted by a correction factor based on the size of the sample to be measured. For example, if a 20 cm by 20 cm sample is measured, the average voltage is multiplied by 0.99585, because the average illuminance on the 20 cm by 20 cm area is less than the average illuminance of the area sampled. The relative expanded uncertainty for the correction factors and therefore the illuminance measurement is 0.212 % (k=2) based on the uniformity measurement, the sampling, and the expected change over time. The illuminance is based on the projected area of the sample; therefore, the illuminance needs to be re-calculated for every movement of the entrance angles.

For the measurement of pavement marking material, an adjustable rectangular aperture in place of the 5 mm aperture in the projection system regulates the size of the illuminated area on the pavement marking material. The image formed is small enough that instead of sampling the

illuminance, the complete image is scanned and the voltages averaged. The relative expanded uncertainty of the illuminance measurement for pavement marking material is 0.06 % (k=2).

The effect of uniformity of the retroreflective device would be insignificant if the illuminance at the retroreflector aperture surface were perfectly uniform. Since it is not, each retroreflective device needs to be examined for uniformity. The standard deviation of the illuminance for the NIST retroreflectometer across the retroreflector aperture surface for a sample 20 cm by 20 cm is ± 0.85 %. If the uniformity of the device were not sampled, the standard deviation of the illuminance would have to be included in the final uncertainty budget. To not correct for this means the final relative expanded uncertainty would be ± 1.7 % (k=2), based on given knowledge of the uniformity of the sample.

To sample the uniformity of the retroreflective device, a small aperture flips into position immediately after the 5 mm aperture in the Abbe projector. This new field stop produces an illuminated area 3 cm in diameter at the retroreflector device. Through an automated process the goniometer moves the sample in a grid, 6 steps wide by 6 steps tall, adjusting the angles and the distance to make all 36 measurements as if the source was illuminating them in their centered original positions. Therefore, the observation, rotation, and entrance angles are adjusted slightly. Figure 13 shows a demonstration of the angles and distance changes required. The 36 R_L measurements are mapped onto the illuminance uniformity of the projection source and a correction factor is determined. The correction factor is close to one and the relative expanded uncertainty is about ± 0.20 % (k=2). The magnitude for the correction factor and uncertainty depend on the magnitude of R_L for the material and the change in R_L across the device.

The uniformity of R_L for pavement marking samples is typically poor. The uniformity of the projection system is ± 1.8 % of the mean value from top to bottom. Changing the vertical width of the adjustable rectangular aperture assesses the uniformity of pavement marking materials. The uniformity of a typical marking sample may change over 40 % from top to bottom or along the length. Mapping the projection system illuminance uniformity onto the R_L uniformity of such a sample produces a difference of 0.23 %. Since the correction factor is based on measurements that are weak in signal, it is not applied and the difference is added as a component into the overall uncertainty budget.

SPHERE PROJECTION SYSTEM

The second system consists of a 5 cm diameter sphere made from Zenithpolymer, a proprietary material, with two 10 mm diameter entrance ports and an 8 mm diameter exit port. Zenithpolymer is a material of processed PTFE (polytetrafluoroethylene) that functions as a volume reflector. Typical reflectance is 98 % between 300 nm and 1700 nm. It is insoluble in water and its characteristics do not change from –200 ºC to 260 ºC. The light from four 410 W reflector lamps is coupled into the sphere; two lamps per entrance port. The exit port is imaged by an Abbe projection system similar to the system used in the strip lamp system. The sphere system provided similar characteristics to the strip lamp system with more operating complications. The most significant improvement is the uniformity at the retroreflector aperture surface as shown in Figure 14. The sphere source would reduce only one uncertainty component; therefore, it was determined that the additional effort of operating it is not worth the reduction in uncertainty.

The real advantage of the sphere projection system is that any light can be coupled into the sphere without changing any of the projection optics. The high intensity discharge (HID) lamps that are available in cars have a very distinct spectral pattern. The retroreflectance of devices can be calculated if spectral coefficients of retroreflection are measured, but to experimentally verify the results, the sphere projection system is the only option. Additionally, for research purposes a portable tunable laser system can pump the sphere to create a monochromatic source to measure fluorescence bi-spectrally. In this configuration NIST can also determine if a laser beam can be used to measure retroreflection. A laser beam has coherence, which causes diffraction patterns under certain circumstances. By coupling the laser into the sphere through a fiber optic the coherence can be effectively removed. Comparing the results from a laser beam and the monochromatic sphere source can determine if retroreflective devices have issues with coherence.

REFERENCES

(*1*) "Guide to the Expression of Uncertainty in Measurement." International Organization for Standardization, Geneva, Switzerland, First Edition, (1995) 101 pp.

(*2*) "Retroreflection: Definition and Measurement." *Technical Report CIE 54.2-2001*, Commission Internationale De L'Éclairage, Vienna, Austria (2001) 55 pp.

CHAPTER 3

GONIOMETER CHARACTERISTICS

The heart of the new Center for High Accuracy Retroreflection Measurements is a high-precision, six-axis goniometer designed and built by Dynamic Structures and Materials, LLC (DSM) shown schematically in Figure 15 and pictured in Figure 16. The axes shown in Figure 15 are all indicated for movement in the positive direction, and the source and detector lie in the horizontal plane (parallel to the Y axis). The goniometer is attached to a carriage on a precision rail assembly, which allows the illumination distance to be varied from 3 m to 33 m. The X', Y, Z, β_1', β_2', ε axes are all under closed-loop control, while the X axis is positioned manually. The ε axis rotation stage is attached to a short manual translation stage on the Z axis stage to allow adjustment for sample thickness. Samples are attached to a plate with a vacuum mount system on the ε axis rotation stage. Rotation of the β_1' frame allows both signs (diameters up to 1 m) and pavement markings to be accommodated on the goniometer, as well as the detector. The goniometer is rated to hold 25 kg and remain in tolerance. The specifications for wide range of motion, high angular resolution, and accuracy resulted from the desire to use the equipment as a research instrument as well as a calibration device. The goniometer system requirements determined from the documentary standards are listed in Table 6 and the final specifications are presented in Table 7.

The NIST goniometer is not a CIE goniometer as described in CIE Publication 54.2 "Retroreflection: Definition and Measurement." The CIE goniometer is defined as having the first or fixed axis perpendicular to the plane containing the observation axis and the illumination axis. The NIST goniometer was chosen to have the first axis parallel to the observation half-plane because of stability. The observation half-plane in the NIST retroreflectometer is horizontal to the floor instead of vertical. The axis labels for the NIST goniometer are β_1', β_2', and ε. The transformation equations to set the NIST goniometer based on CIE goniometer coordinates are,

$$\beta_1' = \arcsin\left(\cos \beta_2 \sin \beta_1\right) \tag{2}$$

$$\beta_2' = \arctan\left(\frac{\tan \beta_2}{\cos \beta_1}\right) \tag{3}$$

$$\varepsilon' = \varepsilon - \arctan\left(\tan\beta_1 \sin\beta_2\right) \tag{4}$$

GENERAL CONSTRUCTION REQUIREMENTS

All frames and brackets were made of aluminum to keep the weight to a minimum. Square aluminum frames were pinned and bolted together with aluminum epoxy. The cross-section dimensions and other bracing were designed to provide frame stiffness that is consistent with the resolution and accuracy specified for each axis. Steel was used for keyed shaft connections and steel thread inserts were used on aluminum parts where frequent disassembly and re-assembly is expected such as the vacuum mount. Exposed surfaces were painted flat black. Surfaces that could not be painted were covered with black aluminum sheeting that was glued to the surface. All cables and vacuum lines were cleanly routed and bundled with appropriate strain relief for the full range of motion.

GONIOMETER COMMUNICATIONS

A remote PC controls the motion of the system's axes through custom software written under National Instruments' LabWindows. MXI-3 technology, a PCI master/slave system, is used to couple the remote PC via a fiber optic data link running the length of the range to a National Instruments PXI-1002 chassis incorporated into the goniometer's structure. The fiber optic along with a power cable and future cabling are bundled in a cable holder. The cable holder rolls with the goniometer as it moves along the rails. The PXI chassis also houses two NI PXI-7334 stepper motor motion cards and a NI PXI-8420/4 card to provide an interface for RS-232 communication with the system's environmental monitor (temperature and relative humidity) and 3 depth gauges used in the alignment tool. Communication with the 30 m encoder is achieved through a SSI/RS232 interface connected to a COM port on the remote PC. DSM also incorporated an enclosure in the system's structure to protect the stepper motor drives and two NI UMI-7764 Universal Motion Interfaces. The UMI boxes provide connections for step and direction signals from the motion controllers to the stepper motor drives as well as connections for the majority of the position encoders. Emergency-stop switches installed on the goniometer frame in easy reach of any bystander are routed to relays that disable power to the system's motors. A schematic of the communication system is shown in Figure 17.

THREE AXES OF ROTATION

The goniometer consists of a yaw frame sized to rotate just within an external pitch frame. The internal yaw frame is the β_1' axis and is designed so that the frame, bearing mounts, and counterweights do not obscure the frontal view of the specimen through its entire $\pm 95°$ of rotation (with the β_2' axis near zero). The β_2' axis, the external pitch frame, is mounted in a U-frame, which forms the base that sits on the rail system. Attached to the vertical translation axis on the yaw frame is a rotation angle axis, ε', having $\pm 185°$ of rotation shown in Figure 18. Its axis is perpendicular to and intersects with the β_1' and β_2' axes when the Z (vertical) stage is positioned at its zero location.

The accuracy of the goniometer's motion control system over such large motion ranges is made possible through the use of high-end motion components and sensors. Five-phase Vexta Nanostep® CFKII 569 stepping motors were chosen to produce precision motion for the three rotational axes of the goniometer. When set at the smallest step angle, the five-phase Vexta stepper motors have 125,000 steps per revolution. DSM coupled the stepper motors to high accuracy harmonic drives with a 160:1 gear reduction that yielded a potential resolution of greater than 20 million steps per revolution. DSM selected HD Systems harmonic drive gear reducers to couple with the stepping motors. The HD Systems CSF-2UH gearheads have virtually zero backlash and come with built in roller bearings to support the output shaft. The HD harmonic drives provided dramatic increases in stepper motor holding torque to control the rotation of the large goniometer support frame with authority.

Using rotary encoders to provide position feedback, actual "closed-loop" minimum step size for the three rotational axes was less than 0.0002 degrees. Limit switches were incorporated into the frame to protect each axis against overtravel by disabling signals to the respective axis' motor. The encoders selected for the three rotary axes are from the Mercury 2000 family of high precision encoders from MicroE Systems, Inc. The optical encoders use glass-scales with interpolator electronics that enable up to 4.19 million counts per revolution. MicroE Systems precisely mounted the glass scales to DSM's custom-designed encoder hubs. The encoders' small read heads were easily incorporated into the goniometer's structural design, and their robust tolerance to misalignment made adjustments during installation fast and simple.

To determine if the rotary axes met the contract specifications, the goniometer was positioned at 30 m. A mirror was securely mounted to the vacuum mount. A collimated laser

originating near the source aperture was reflected by the mirror to a 20 cm x 25 cm target ruled in millimeters. The position of the laser spot on the target could be measured accurately to < 1 mm vertically and horizontally. Thus, the measurement uncertainty is equal to 0.001° at 60 m; therefore, the β_1' and β_2' movements meet specifications. Initially the epsilon prime axis did not meet specifications. When set up in the pavement marking geometry configuration, rotation of ε' resulted in a significant (>0.02°) deviation of the reflected laser spot from a vertical line. Simultaneously with the sudden deviation, the encoder lost thousands of counts, such that the rotational positioning accuracy of ε' was also out of specification (>0.02°). The ε' harmonic drive was disassembled, cleaned and reassembled by DSM. When tested again, the problems were no longer observed, and the ε' axis could be accurately positioned to within 0.001°, just as β_1' and β_2'.

An additional aspect of the rotary axes is that when an axis rotates, the center point should not move outside of a sphere of confusion. The contract specification stated "The intersection of β_1', β_2' and ε' axes shall not move outside of a sphere that has a diameter of 0.5 mm when all three axes are rotated." A method of locating the depth and height of the β_1', β_2' and ε' axis intersection yielded a measurement of the sphere of confusion, which was within specifications. The method follows:

1. A straightedge was temporarily clamped to the β_2' frame such that the top of the straightedge was coplanar with the β_2' center of rotation. The distance from the straightedge face to the β_2' pivot points was 73.30 mm.
2. The depth stage was set to position the center of the ball tool 73.30 mm from the straightedge face. Figure 19 shows a picture of the ball tool mounted on the goniometer.
3. The Z-axis height was set by visually aligning the ball center to the top of the straightedge, using a spirit level as a guide.
4. Dial indicators were attached to the alignment tool to measure ball run-out in the vertical (Z direction) and horizontal (X direction) plane.
5. With the β_2' frame near vertical and the β_1' frame near $\beta = 0°$, ε' run-out was measured to be 0.00 mm in the vertical plane and ± 0.06 mm in the horizontal plane.

6. The proper position of the depth stage was fine-tuned by iteratively moving the β_1'
   stage throughout its motion range and adjusting the depth to minimize the
   displacement of the ball in the vertical plane. The resultant run-out measured $\pm$
   0.06 mm (vertical) and $\pm$ 0.08 mm (horizontal).

7. Similarly, the optimum Z stage position was found by moving the β_2' frame
   throughout its range of motion and adjusting Z to give minimal displacement in the
   horizontal plane. The resultant run-out measured $\pm$ 0.06 mm (vertical) and $\pm$ 0.17
   mm (horizontal).

In conclusion, for any one-axis move, the sphere of confusion is an ellipsoid having a height in the Z direction of 0.35 mm and a width in the X direction of 0.12 mm. Both dimensions are less than the 0.5 mm maximum specified.

The sphere of confusion specified in the contract with the goniometer designer was the smallest Project 05-16 could afford. The wobble measured in the rotation axis, ε', causes a deviation in setting the β_1' and β_2' axes. Also, the vacuum mount that is affixed to the collet on the rotation drive is not exactly perpendicular to the illumination axis. Therefore, as the rotation axis turns slight corrections are applied to the β_1' and β_2' axes. The correction curve for these corrections is repeatable for the particular vacuum mount and is addressed in the uncertainty calculations of the absolute alignment chapter.

THREE AXES OF TRANSLATION

The accuracy of the goniometer's translation systems is made possible through the use of high-end motion components and sensors. Two-phase Vexta CSK 268MAT stepping motors were chosen to produce precision motion for driving the linear axes of motion. The Z-axis is a linear translation stage mounted directly in the β_1' frame for moving the sample up and down. The X' and Y-axes are linear translation stages incorporated into the goniometer base. The X'-axis moves the goniometer along the illumination axis and the Y-axis moves the goniometer perpendicular to the illumination axis. The Y and Z-axes are operated in closed loop mode with optical encoders to provide positional accuracy of better than 0.05 mm. The X' stage requirements are less stringent. Open loop control provides positional accuracy of 0.25 mm.

Linear movement of Y and Z-axes was validated using a Mitutoyo dial indicator modified to accept various standardized extensions up to 610 mm. In the case of the Z-axis,

accurate readings could not be attained by this method. Therefore motion was measured using the Leica 3000 theodolite positioned 3 m from the sample holder face. Results of the validations are summarized in Table 7.

SAMPLE HOLDER AND DEPTH POSITIONING

A vacuum mount holds the samples in place, as described below. It consists of six 8 cm diameter vacuum cups arranged to hold various shaped signs and road marking material as shown in Figure 20. The vacuum system pulls the specimen against machined rails so that the sample is positively registered to a fixed depth. The vacuum cups are sized to hold about 10 kg. This represents a safety factor of two over the expected maximum sample weight. The vacuum system is designed so that individual or sets of vacuum cups can be selected or deselected quickly by the machine operator. The vacuum source is routed to the sample holder plate as to allow free movement of the full range on all the other axes.

A manually adjustable stage connects the sample holder to the β_1' frame. The purpose of the manual axis is to adjust the depth of the sample holder plate so that the surface of the sample is coplanar with the β_1' and β_2' axes to minimize any offset distance, which would cause errors in the measurement. A precision alignment fixture is used to determine when the surface of the sample is properly positioned (Figure 21) using a four step procedure.

1. A front surface mirror is fixed to the back side of a precision jig plate 30 cm x 30 cm x 1 cm in size, having a flatness and parallelism of 25 μm. This assembly is referred to as the β alignment plate. The β alignment plate is placed in the sample position, and the laser beam that defines the illumination axis is reflected back at the source. The β_1' and β_2' axis are adjusted to center the reflected beam within 0.002° of the source aperture. This step determines the $\beta(0°,0°)$ position of the sample plate.   This alignment procedure is elaborated on in the Absolute Alignment chapter.

2. The alignment fixture is mounted to the goniometer base and the front plane of the β alignment plate is measured using three digital dial indicators in a triangular arrangement.

3. The sample plate is retracted by a translation of the depth stage, the β alignment plate is removed, and a new sample is mounted.

4. The sample front surface is brought up to the dial indicators. Adjustment of the depth and β_1' and β_2' (if necessary) position the retroreflective surface of the sample coplanar with the β_1' and β_2' axes.

The detector system mounts directly onto the vacuum mount using pins and bolts. The detector system is placed at the center of the goniometer for source characterization and calibrations procedures. The X', Y and Z-axes are programmed to automatically center the detector aperture on the illumination axis.

THE RAIL SYSTEM AND DISTANCE DEPENDENCE

The rail system supports the horizontal linear axis and the goniometer. It extends from 3 m to 33 m from the source aperture and is operated manually. The system is composed of two 19 mm diameter chrome plated rails 141 cm apart continuously supported by inverted T-shaped aluminum, which is then supported by posts that are anchored into the concrete floor with epoxy. A sample of the rail section is shown in Figure 22. The goniometer and rail system has a magnetic tape encoder with a resolution of 10 μm and an accuracy of 0.3 mm. Once the goniometer is manually put in a position it is locked into place. Additionally, a linear drive is mounted to the clamping blocks to provide ± 46 cm of automated positioning along the illumination axis.

Installing the rail system was accomplished over several days. Following the center marks and hole outlines previously laid down, a 2.5 cm diameter hole was drilled to a depth of 4 cm to 5 cm at each of the 100 positions. A 12.7 cm diameter hole was cut through the linoleum using a carbide-tipped hole saw. The linoleum was removed using an air chisel. The chisel was also used to remove adhesive and roughen the concrete surface for better adhesion of the epoxy grout. The left rail, as viewed from the source end, was installed first. The rail was tipped on its side, and 6.4 cm studs were installed fully, and then backed out one full turn to allow for height adjustment.

A support consisting of wood blocks and tapered shims was positioned every 60 cm along the rail length. A 10 mm x 10 mm retroreflection target was positioned on a pillow block over the rail center. Using a Leica 1100 total station (a theodolite with electronic distance measuring capabilities) leveled to ± 2 arc seconds, the height of the target at each position was set to 133 mm ± 0.5 mm vs. an arbitrary reference. The longitudinal position of the rail was

adjusted a few millimeters to prevent some of the studs from contacting the sides of the holes. In the lowest part of the floor, 7.6 cm or 8.9 cm bolts with or without heads were used in place of the studs, to ensure that the bolts were at least 1.3 cm below the concrete surface. After positioning the rail side-to-side to within 0.5 mm of $0° \pm 2$ arc seconds and verifying the height, the studs were anchored with Drylock hydraulic cement in five sections of ten holes each.

Position of the rail was verified by two independent methods. A Leica 3000 theodolite was positioned directly over the rail near the longitudinal midpoint. Rail height was measured using a vertical stick placed at 5 m intervals. The rail height was verified to be flat within ± 0.5 mm over the 30 m. The deviations were random, not indicating a slope. The bow of the rail was measured to be less than 1 mm from end to end. In the second method the Leica 1100 was positioned over the rail midpoint, and height of the target on the pillow block was measured. A variation of less than ± 1 mm was observed. Based on these measurements we conclude the rail is straight and level within ± 1 mm over the 30 m distance. Following position verification, the support pads were permanently located by pouring a Five Star rapid epoxy with aggregate foundation.

The second rail was installed in an identical fashion with the following exceptions: The studs were fully screwed in, as no adjustments were necessary in the case of the first rail. The side-to-side variation was held to within 1 mm (not 0.5 mm) of $0° \pm 2$ arc seconds and not verified. This is acceptable as the goniometer base floats on the second rail pillow blocks, allowing up to ± 3.2 mm side-to-side movement. The height was again held to 133 mm ± 0.5 mm.

Before the goniometer was mounted on the rail system, a magnetic tape was installed on angle aluminum that runs the length of the rail system. The magnetic encoder head is mounted on the goniometer and has a resolution of 10 µm and an accuracy of 0.3 mm. An issue with the magnetic tape is applying the proper tension during the application process. The improper amount of tension introduces a systematic error in the magnetic tape. A correction curve was calculated by comparing the Leica 1100 theodolite to the readings of the magnetic encoder. The data is presented in Figure 23. The magnetic tape was stretched 13 mm over the 35 m length. The uncertainty of the calibration curve is dependent on the standard uncertainty of the theodolite, which is ± 2.5 mm.

The overall uncertainty of the distance is a combination of the calibration curve and the initial absolute calibration of the magnetic encoder, which involves the accuracy or reproducibility of the magnetic encoder, the alignment tool uncertainty, the source aperture reference post uncertainty and the uncertainty of the 3 m vernier owned by NIST. Two researchers operate the vernier by one holding the fixed end at the source aperture reference post and the other sliding the adjustment inline with the front surface of the β alignment plate. The machining tolerance in the source reference post is 0.025 mm, which comes from the machine shop capabilities. The electronic dial indicators on the alignment fixture are referenced to this surface. The uncertainty budget for setting the absolute position of the magnetic encoder is presented in Table 8. The total uncertainty budget for the illumination distance of a sample is summarized in Table 9, and the expanded uncertainty is less than the requirement of 10 mm. The sensitivity coefficient for the illumination distance was determined experimentally and is shown in Figure 24. The sensitivity coefficient does not follow the inverse square law because the projection source is not a point source. The overall relative expanded uncertainty for R_L due to the uncertainty in the illumination distance is 0.03 % (k=2).

At the same time the theodolite was used to measure the distance, the vertical and horizontal deviation of the sample holder was determined. The vertical deviation of the goniometer system's center over the 30 m rail length is within ± 0.75 mm, and horizontal deviation of the center is within ± 1.0 mm. The data for these measurements are shown in Figures 25 and 26. Calibration curves were derived from this data. The contribution of uncertainty to the overall uncertainty budget for R_L is presented in the Absolute Alignment Chapter.

The shiny rails caused scattered light depending on the position of the sample. Two baffles were constructed that sit on the rail system. They are positioned at appropriate distances to block scattered light, yet do not interfere with the measurement. The baffles also lift off the rail system. Another significant source of scattered light was the back wall of the facility, especially when the goniometer β_1' frame is rotated to measure pavement marking material. An approximately 3 square meter beam stop was constructed from two glossy black acrylic panels. The panels measure 122 cm x 122 cm each and are attached to movable supports so they can be positioned to completely capture the source beam beyond the end of the rail. The angle of the panels is adjustable to minimize back reflection. With the beam stop in place, the source beam

terminus is nearly invisible under even the darkest room conditions. Additionally, black carpeting was installed between the rails to eliminate reflection from the floor tile. The black carpeting has a visible reflectance value of < 1 % (400 nm to 700 nm) measured by a portable spectrometer.

CHAPTER 4

DETECTOR CHARACTERISTICS

The detector package for the Center for High Accuracy Retroreflection Measurements is a NIST built photometer consisting of an observation aperture, which is the aperture stop for the system, a lens, a holographic transmitting diffuser, a $V(\lambda)$ matching filter and a silicon detector. A schematic of the photometric detection system is presented in Figure 27. The detector package is supported by the observation angle positioner, which is comprised of a 2 m translation stage, a rotation stage and a 20 cm translation stage. Figure 28 is a schematic of the observation angle positioner. The observation distance is maintained equal to the illumination distance using the observation angle positioner. In addition to the photometer, NIST experimented with a spectroradiometer package consisting of an observation aperture, a lens, a holographic transmitting diffuser and an array spectroradiometer employing a back-thinned CCD array. The holographic transmitting diffuser couples the light into a fiber optic bundle that is the input optic for the spectroradiometer. The spectroradiometer package would be used in the future to calculate a spectral mismatch correction for the photometer measurements and to measure spectral coefficient of retroreflection.

THREE AXES DETECTOR STAGES

The observation angle positioner consists of three stages, a 2 m stage, a rotation stage and a 20 cm stage. The purpose of the three stages is to position the observation aperture at the correct observation angle, direct the viewing field toward the retroreflector point of reference, and to maintain the observation distance such that it is equal to the illumination distance. Table 10 summarizes the characteristics of each of the three detector stages.

The 2 m stage is mounted on the optical table perpendicular to the illumination axis. The minimum step size is 0.2 μm and has an optical encoder allowing a positioning accuracy of ± 1 μm. The motor shaft had to be mounted parallel to the stage lead screw due to space, therefore the shafts were coupled using a timing belt and pulley system. The belt drive increases the amount of backlash in the drive system. Following a positive or negative motor move a positional repeatability of 0.9 μm and 0.4 μm respectively, was measured according to the motor driver. However this is irrelevant with the encoder based positioning. The reported encoder

position is maintained within $\pm$ 1 μm of the specified position for a series of bi-directional moves with a deadband window of 3 motor steps. A correction curve for the position of the 2 m stage was determined by measuring the distance between a fixed block on the laser table and a hard point on the detector mounting plate, using a Mitutoyo mechanical micrometer. After several trials, a measurement method was determined which resulted in a minimal standard deviation between measurements. There appears to be a linear deviation from expected position, as the measured error increases from 0 μm gradually to -40 μm $\pm$ 14 μm ($k=2$). This linear deviation has yet to be verified using a laser interferometer, which can measure with an uncertainty of tens of nanometers. A correction curve for the aperture separation is applied based on the current information and will be improved once the laser interferometer is used. This deviation is small compared to the initial alignment of the 2 m stage, which is described in the Chapter 5 – Alignment.

The rotary table has a 180:1 gear ratio; thus 1 motor revolution (25000 steps) corresponds to a 2° table rotation and 1000 encoder steps (0.002° resolution). The minimum move is 1 motor step or 0.00008° thus there are 25 motor steps / encoder step. With 25 motor steps/encoder step, the rotary stage functions properly in encoder step mode. The test was performed as follows: a HeNe laser was securely mounted to the rotary stage, and a white paper target was placed at 15 m. Moves of 4 to 8 encoder steps in both directions were made and the displacement of the laser beam was marked on the target. The first test indicated poor reproducibility and suggested backlash in the drive train. When the Position Maintenance Function (feedback mode) was enabled and the parameters correctly applied, the target moved within 1 mm (0.004°) of the expected position for moves from 0.02° to 0.1° in both directions. If the stage was physically jarred enough to see motor movement (correction), the position also recovered to within 0.004°.

The 20 cm stage is mounted on the optical table directly over the rotary stage, which is mounted on the 2 m stage. The 20 cm stage moves along the observation axis. The minimum step size is 0.2 μm and has an optical encoder allowing a positioning accuracy of $\pm$ 1 μm. The 20 cm stage uses the encoder based positioning. The reported encoder position is maintained within $\pm$ 1 μm of the specified position for a series of bi-directional moves. A correction curve for the position of the 20 cm stage was determined by measuring the distance between a fixed block on the laser table and a hard point on the detector mounting plate, using a Mitutoyo mechanical micrometer. There appears to be a curved deviation from expected position, as the measured

error gradually increases to -10 μm $\pm$ 14 μm ($k=2$) and then to less then –5 μm. This deviation has yet to be verified using a laser interferometer, which can measure with an uncertainty of tens of nanometers. A correction curve for the 20 cm stage was not applied until a better measurement method is used. This deviation is small compared to the initial alignment of the 20 cm stage, which is described in the Chapter 5 –

Alignment.

On top of the 20 cm translation stage is a mounting plate that the detection system is securely attached to. The mounting plate bolts onto the translation stage but is aligned with tool pins. The entire mounting plate is bolted on the goniometer for making the illuminance measurement and for scanning the projected source beam to analyze for uniformity. The reproducibility of the mounting plate is within 0.001°.

PHOTOMETRIC DETECTION

The photometric detector system consisting of an observation aperture, which is the aperture stop for the system, a lens, a holographic transmitting diffuser, a $V(\lambda)$ matching filter and a detector. The detector consists basically of a silicon photodiode, a thermoelectric temperature control, and an electronic assembly containing a current-to-voltage converter circuit having a high sensitivity and a wide dynamic range mounted directly behind the photodiode to minimize noise. The circuit has a computer controllable gain setting from 10^4 V/A to 10^{10} V/A. The system is linear to 0.02 % without correction factors. An input equivalent noise of ~1 fA is achieved at the gain setting of 10^{10} V/A with an integration time of 1.67 s, and a bandwidth of 0.3 Hz.

The spectral responsivity of the photometric detection system, $s(\lambda)$, which includes the focusing optic and transmitting diffuser was measured at the NIST Spectral Comparator Facility (SCF). The absolute spectral responsivity curve is presented in Figure 29. The f_1' calculated for the system is 1.61 %, which is excellent. The absolute illuminance responsivity is 0.10577 nA/lx for the 26 mm aperture. This is a factor of ten less than expected because of the addition of the transmitting diffuser. By knowing the absolute illuminance responsivity, the coefficient of retroreflection can be measured using the absolute method, in addition to the relative method cited in CIE 54.2 - 2001. The absolute method directly ties the retroreflectance scale to SI units. The photometric system will be calibrated at the NIST Spectral Irradiance and Radiance

Response Calibrations with a Uniform Source (SIRCUS) facility. This laser-based facility has many advantages over the SCF. First, the wavelength uncertainty of SIRCUS is smaller by a factor of 100 due to the fact that SCF produces monochromatic light with a bandwidth of 5 nm where SIRCUS produces laser light with a bandwidth of 0.001 nm. Second, the flux from SIRCUS is 100 times larger than SCF, and finally, the SIRCUS facility over illuminates the detector system instead of under filling it. By overfilling the detector system no uniformity or geometric corrections are required. The relative expanded uncertainty for the absolute illuminance responsivity is 0.40 % ($k=2$) when calibrated by SIRCUS. The NIST Photometry project has a reference luminance meter that has a relative expanded uncertainty of 0.50% ($k=2$) for luminance responsivity. By using the ratio methods in CIE 54.2 – 2001, these scale uncertainties are not included because the same detector system is used and the uncertainties cancel. The overall uncertainty budgets for both methods are presented in Chapter 6 – Overall Uncertainty Budget.

The transmitting diffuser is required in the detection system to remove the pointing sensitivity. Figure 30 shows the dependence of the coefficient of retroreflection on the positioning of the 2 m stage. Without the transmitting diffuser this dependence was larger than acceptable. Figure 31 shows the dependence of the coefficient of retroreflection on the positioning of the rotary stage and Figure 32 shows the dependence with respect to positioning the 20 cm stage. The dependence on the 20 cm stage is significantly less since its movement is along the observation axis. The uncertainty contributions of these components will be determined in Chapter 5 – Alignment. The disadvantage of having the transmitting diffuser is that it absorbs and scatters more than 50 % of the light. Another effect is that the uniformity of the detector is altered. Without the transmitting diffuser the uniformity of the detection system is a couple of percent. Figure 33 shows the measured uniformity of the detection system with the transmitting diffuser. With the 26 mm observation aperture in place the uniformity changes by 20 % from the center to the edges. Initially, 20 % appears to be an unacceptable change in uniformity. However, geometrical modeling, as was done with the source aperture, shows that the uncertainty due to this is 0.005 % for prismatic material. The reason for the small uncertainty is the symmetry of the non-uniformity caused by the transmitting diffuser. The transmitting diffuser disperses the light into a 20° cone. The transmitting diffuser is larger than the silicon detector as shown in Figure 27. The light entering the side of the diffuser will not cause as large

a signal as the same flux of light entering the center of the diffuser. The diffuser causes a steeper gradient in the uniformity of the detector but makes the response smooth and centered, which is more important as shown by geometrical modeling using the synthesis of apertures. The initial angle values used in the simulation were $\alpha = 0.33°$, $\beta_1 = -5°$, $\beta_2 = 0°$, and $\varepsilon = 0°$. When these values were changed, no large changes in the relative standard uncertainties were observed. Using the ratio method eliminates the need for signal normalization.

Since most retroreflective devices do not have a spectrally flat reflectance factors, spectral mismatch correction factors will need to be calculated. The spectral mismatch correction factor is given by,

$$smcf(S_t(\lambda)) = \frac{\int_\lambda S_A(\lambda)s_{rel}(\lambda)d\lambda \int_\lambda S_t(\lambda)V(\lambda)d\lambda}{\int_\lambda S_A(\lambda)V(\lambda)d\lambda \int_\lambda S_t(\lambda)s_{rel}(\lambda)d\lambda},$$

(5)

where $S_t(\lambda)$ is the relative retroreflected spectral power distribution, $S_A(\lambda)$ is the relative spectral power distribution of CIE Illuminant A, and $s_{rel}(\lambda)$ is the relative response of the photometric system. The relative response of the photometric system is the same as $s(\lambda)$. Therefore, to make a corrected photometric measurement, the relative retroreflected spectral power distribution, $S_t(\lambda)$, needs to be measured. The quality of the spectrum required can be realized on a diode array system with reasonable stray light rejection as described in the next section. The magnitude of spectral mismatch correction factors can be as high as 5 %, but the uncertainty due to the correction factor is typically less than 0.10 %.

SPECTRORADIOMETRIC DETECTION

The spectroradiometer required for the Center for High Accuracy Retroreflection Measurements has to measure the retroreflected spectral power distribution, $S_t(\lambda)$, as quick as possible with appropriate signal to noise. The $S_t(\lambda)$ is used to calculate a spectral mismatch correction factor for the photopic measurements. Except for white materials, every photopic measurement requires a quick relative $S_t(\lambda)$ to maintain the level of uncertainty. The second use of the spectroradiometer is to measure the coefficient of spectral retroreflection. The measurement of the coefficient of spectral retroreflection requires the absolute measurement of the $S_t(\lambda)$. Three types of spectroradiometers are available to meet the requirements.

The first type is a double grating spectroradiometer with a photomultiplier for the detector. The double grating spectroradiometer measures the retroreflected spectral power

distribution with a stray light rejection of 10^7. A high stray light rejection allows measurement of the chromaticity coordinates with the lowest uncertainty capable. However, the double grating spectroradiometer is a scanning instrument and the signal is low. Collection of a typical spectrum requires about one half hour. Additionally, the use of a photomultiplier introduces uncertainty because they are extremely temperature dependent and do not have a stable responsivity. A high accuracy silicon detector does not produce a large enough photocurrent to meet this need. A double grating spectroradiometer is not the appropriate choice.

The second type is a single grating scanning spectroradiometer with a silicon detector. The single grating scanning spectroradiometer measures the $S_t(\lambda)$ with a stray light rejection of 10^4. This level of stray light rejection allows measurement of chromaticity coordinates with a standard uncertainty of roughly 0.005. Collection of a typical spectrum requires about 15 minutes. Initially, the NIST researchers thought this would be the appropriate choice. However, NIST researchers have made significant progress in the third type of spectroradiometer.

The third type is a single grating spectroradiometer with a back-thinned CCD array. Typical CCD array spectroradiometer of this type have a stray light rejection of 10^3. This level of stray light rejection allows measurements of chromaticity coordinates with a standard uncertainty of roughly 0.015. An uncertainty of 0.015 is entirely too large to be useful to the retroreflection community. Researchers at NIST have developed a correction matrix for CCD array spectroradiometers that eliminates the stray light from the signal[1], therefore, increasing the stray light rejection to at least 10^5. This level of stray light rejection allows measurement of chromaticity coordinates with a standard uncertainty of roughly 0.002. Another significant advantage of the CCD array system is the reduction in acquisition times. The typical acquisition times for retroreflective materials is 15 s – 20 s, which is the acquisition time required for the photometric measurements.

The particular instrument chosen to validate these conclusions has been characterized by the staff at NIST and compared to other instruments of the CCD array type. The input optics consists of an observer aperture, a lens, a transmitting diffuser and a fiber optic bundle that directly attaches to the instrument. The first test is to measure BCRA tiles that have been measured by the Spectral Tri-function Automated Reference Reflectometer (STARR) instrument. The STARR instrument is the national reference instrument for spectral reflection measurements.[2] The STARR instrument can measure samples with a 0 degree incident angle

and a minimum detection angle of 5 degrees. Figure 34 shows sample spectra from the STARR instrument compared to the CAS system used in the CHARM facility. The BCRA tiles were mounted 3 m away from the source aperture and detected at a detection angle of 5 degrees in both STARR and the CHARM facility. The reflectance factor was determined by dividing the spectrum measured at the observer aperture by the source spectrum. The agreement is quite good. The only difference is the magnitude of the signal in the blue region for the red tile. NIST is currently assessing both STARR and CHARM to determine the cause of this difference. The difference in the chromaticity coordinates for the two measurements are shown in Table 11. The acquisition time is 100 s for the BCRA tiles. The BCRA tiles are diffuse reflectors; therefore, they reflect significantly less light than retroreflective material.

The second set of measurements made is on retroreflection signage material. The acquisition times were 30 s at a distance of 5 m and 100 s at a distance of 15 m. The signal to noise level is sufficient such that it is not the largest source of uncertainty when measuring the spectral coefficient of retroreflection. The third set of measurements made is on yellow pavement marking material. Figure 35 shows the sample set of spectra. The acquisition times were 100 s. The three spectra were taken at 30 m geometry at a distance of 5 m illuminated by Illuminant A. The difference in the three materials is the beads were clear, yellow, or a mix. By employing the stray light corrected CCD system NIST facility will have the capability in the future of measuring the spectral coefficient of retroreflection.

(*1*) Zong, Y., Brown, S.W., Lykke, K.R., and Ohno, Y., "A Simple Stray Light Correction Method for Array Spectrometers." Submitted to *Applied Optics*.

(*2*) Barnes, P.Y., Early, E.A., and Parr, A.C., "NIST Measurement Services: Spectral Reflectance." NIST Special Publication 250-48, U.S. Department of Commerce/National Institute of Standards and Technology, Washington D.C. (1998) 157 pp.

CHAPTER 5

ABSOLUTE ALIGNMENT

The most critical aspect of the NIST Reference Retroreflectometer is the alignment of the three components: the source optical system, the goniometer and the detection system. The following sections describe the methods for aligning the components and the effect on the four angles used for defining the retroreflective geometry. The expected uncertainty from these alignment procedures is calculated.

SETTING THE ILLUMINATION AXIS

The first axis that must be defined is the illumination axis. The illumination axis is defined as the axis from the retroreflector point of reference pointing to the source point of reference. The points of reference are defined as the center of the goniometer and the source aperture. Unique to the NIST retroreflectometer is the capability to move the goniometer along a rail system, varying the source to sample distance from 3 to 32 m. The left rail (when looking at the sample face) is the reference rail and determines the horizontal position of the goniometer center. As discussed in Chapter 3, the goniometer center is preserved within $\pm$ 1 mm upon translation along the 30 m rail system. Our goal is therefore to set the illumination axis collinear with the goniometer center path.

A variable diameter iris is placed on the goniometer sample holder and centered on the goniometer center. The goniometer is positioned at the minimum source-sample distance, and the source light is centered on the iris by adjusting the vertical table height and the horizontal position of the source rail. The goniometer is then moved to the maximum distance and the adjustment process repeated. This process is repeated iteratively until no further adjustments to the source position are required.

ABSOLUTE NIST ENTRANCE ANGLE COMPONENTS ALIGNMENT

The absolute alignment of the NIST entrance angle components, β_1' and β_2', relies on the light source that defines the illumination axis described previously. A 30.48 cm square precision flat ($\pm$ 0.0173 mm, uncertainty in parallelism) aluminum plate with a small hole is mounted against the hard stops on the goniometer sample holder, using tooling pins to locate the center of the hole at the center of the goniometer. A front surface mirror is pressed against the flat back of

the aluminum plate. Thus the mirror is plane parallel with the goniometer sample-mounting surface. The reflected source beam can be centered on the source aperture within 1 mm by adjusting the pitch and yaw of the goniometer in fine increments. The alignment tool is then mounted and the micrometers are set to zero.

The uncertainty for the NIST entrance angle components is reduced to the items used to calibrate not procedural transfers or measured quantities. The following equation,

$$A = C + L + G + M \tag{6}$$

is used to model the absolute calibration of the alignment tool, where C is the uncertainty comparing the front surface of the mirror to the front surface of the precision flat aluminum plate, L is the angular contribution of the source alignment procedure, G is the angular contribution due to the goniometer, and M is the uncertainty of the micrometer readings. The standard uncertainty of the micrometers is 0.0115 mm across a typical sample distance of 210 mm, which works out to be a standard uncertainty of 0.0063°. Table 12 shows the uncertainty budget for setting the alignment tool. The uncertainty of setting arbitrary NIST entrance angle components is composed of the alignment tool uncertainty, A, the uncertainty of mounting a sample, S, and the resolution of the goniometer, $\Delta\beta$, as shown in the following model and Table 13,

$$\beta_{\#}^{'} = A + S + \Delta\beta . \tag{7}$$

Therefore, for any arbitrary NIST entrance angle components the absolute uncertainty will be $\pm 0.020°$ ($k=2$). To convert the NIST entrance angle components to the CIE goniometer system entrance angle components the following equations are used,

$$\beta_1 = \arctan\left(\frac{\tan \beta_1^{'}}{\cos \beta_2^{'}}\right), \text{ and} \tag{8}$$

$$\beta_2 = \arcsin\left(\cos \beta_1^{'} \sin \beta_2^{'}\right) \tag{9}$$

when $-90° < \beta_1' < 90°$ and $-90° < \beta_2' < 90°$. The uncertainty for this conversion is presented in Table 14 and Table 15. The uncertainty varies for the chosen angles but is on the order of $\pm 0.020°$ ($k=2$) for angles that are not at the extreme of the goniometer motion.

To set the absolute entrance angle for pavement marking samples, a precision 90° ($\pm 0.00278°$) reflective alignment cube is mounted against the sample hard stops. The reflected source beam is positioned on the source aperture as described above to set the absolute entrance

angle to 90°. The uncertainty of the alignment cube is 0.001604° and the type of evaluation is B(R), which stands for a Type B evaluation derived from a rectangular distribution. The specification on the alignment cube is 0.00278°, which is a tolerance following a rectangular distribution. To approximate a rectangular distribution as a normal distribution, the tolerance is divided by the square root of three, as shown in the *GUM*. The other difference between setting signage versus pavement marking material is the distance between the micrometers on the alignment tool. The standard uncertainty of the micrometers is 0.0115 mm across a typical sample distance of 145 mm for β_2' and 600 mm for β_1', which works out to be a standard uncertainty of 0.0091º and 0.0022º, respectively. By substituting these uncertainty values into the tables, the expanded uncertainties for the CIE goniometer parameters are determined to be 0.0069° (*k=2*) for β_1 and 0.0006° (*k=2*) for β_2.

ABSOLUTE OBSERVATION ANGLE ALIGNMENT

The next parameter to set is the position of the observer aperture. Ideally, if the observer aperture could be positioned in the same physical space as the source aperture, the encoders for the observation angle positioner could be read and the observation angle equal to zero ($\alpha = 0$) would be determined. Since this is not physically possible, the observer aperture must be positioned in a known location and measured to determine its exact location. Figure 36 shows a drawing of the source and observer aperture holders. We presently use either 26 mm or 43 mm diameter apertures. A variety of apertures sizes can be constructed to match the customers' requests. The important aspects of the aperture designs are the reference pins at the top of the holders, which are machined to position the outside edge of the pin at the center of the aperture (to within 0.025 mm) and in the aperture plane (shown in the top view of Figure 36).

The first stage to be set absolutely is the rotation stage. A collimated laser is positioned at the goniometer center, or reflected from the center of the β alignment mirror. The laser originates along the illumination axis, at the sample point of reference. The laser or reflected beam is aimed at the detector by a defined movement of the goniometer yaw axis. The detector mounting plate is fitted with a 4 mm pinhole in place of the detector aperture. An aluminum cylinder, having the same diameter as the photopic detector package and equipped with a quadrature detector at its axis, is mounted in place of the photopic detector. A computer code positions the rotation stage such that the output of the quadrant detector is balanced. The

rotation stage is thus aligned with the observation axis to within a standard uncertainty of ± 0.008°.

To calibrate the small stage, the observer aperture is positioned 1 cm behind the source aperture. To approximately zero the long stage a simple photodiode is positioned toward the goniometer viewing the aperture source such that only half the photodiode is illuminated. The edge of the source aperture is imaged on the photodiode. The long stage is moved across the source aperture until the signal on the photodiode becomes constant. At the apex of the curve the observer aperture is directly behind the source aperture. A micrometer measures the distance between the aperture faces. With this measurement, the small stage is absolutely calibrated for position to the uncertainty of its encoder (± 0.014 mm) and the uncertainty of the reference pins (± 0.014 mm) for an expanded uncertainty of ± 0.050 mm ($k=2$). Another issue is that since the observer aperture is not positioned at the center of the rotation stage, the rotational movement causes a change in the position not just the viewing angle. To decouple this movement the position of the rotation center must be determined. To determine the center of rotation, the observer aperture is moved roughly to the center. A computer read micrometer is positioned against the reference pin. The 20 cm stage is moved until the micrometer reading does not change when the rotation stage is moved. By knowing the distance the reference pin is away from the center of rotation, the position change due just to rotation can be calculated. To calibrate the long stage, the long stage moves the observer aperture 5 cm away from the source aperture and the small stage positions the observer aperture reference pin at the center of rotation. A micrometer measures the distance between the reference pins. With this measurement the long stage is absolutely calibrated for position to an expanded uncertainty of ± 0.050 mm ($k=2$).

The illumination distance is measured by a magnetic tape that is mounted to the goniometer and the rail system. The observation distance is initially set by the magnetic tape and the absolute position of the small stage. The observation distance is then calculated by the movement of the small, long, and rotation stages. By knowing the illumination distance, the observation distance and the aperture separation, the absolute observation angle can be calculated by the law of cosines. The aperture separation is calculated using the equation,

$$c = \sqrt{y^2 + x^2 - 2xy\cos(\pi/2 - r)} \,, \tag{10}$$

and Table 16 shows a typical uncertainty budget. The observation distance is calculated using the equation,

$$d = x\sin(r) - y + \sqrt{s^2 - x^2\cos^2(r)} \,, \tag{11}$$

and Table 17 shows a typical uncertainty budget. This equation comes from solving the law of cosines,

$$s^2 = (d + y)^2 + x^2 - 2x(d + y)\cos(\pi/2 - r) \tag{12}$$

for the observation distance, d. In this case, the observation distance cannot be solved using a right triangle because the 90° angle formed by the illumination axis and the long stage has uncertainty that is not accounted for in an equation using $d = x/\sin(r) - y$. The arbitrary setting of the observation angle is calculated using the equation,

$$\alpha = \cos^{-1}\left(\frac{s^2 + d^2 - c^2}{2sd}\right), \tag{13}$$

and Table 18 shows a typical uncertainty budget. The observation angle is set to an expanded uncertainty of $\pm 0.00037°$ ($k=2$).

ABSOLUTE ROTATION ANGLE ALIGNMENT

The procedure reported here for setting the absolute rotation angle (ε) differs significantly from that described in the Phase I report. We acquired a theodolite, which allows the use of a method that is significantly easier, less prone to operator error, and still retains an acceptable uncertainty.

The rotation angle is the angle of the datum axis relative to the observation half-plane. We use the earth's gravitation field as our point of reference to set the observation half plane and also to measure the datum axis thus determining the absolute rotation angle. The procedure follows: First a theodolite is positioned approximately 15 m from the detector stage and set level versus gravity to $\pm 0.00055°$. The vertical position of the source aperture is determined. The detector aperture at the minimum observation angle is set equal to the source aperture in the vertical plane. The detector is moved to the maximum observation angle and the vertical position determined. The source table legs are adjusted to minimize the vertical difference. A limiting uncertainty of ± 0.48 mm in setting the detector aperture is the alignment of the theodolite crosshair on the detector aperture target. This represents an angular uncertainty in the

observation half-plane of 0.014°. Leveling of the table did not significantly affect the position of the illumination axis because at α_{min} the detector aperture is directly over the fixed legs of the table, and only a 1 mm adjustment in the legs under the aperture near α_{max} was required. This part of the procedure is only required once, unless the source table is moved.

The second step in this alignment procedure is to measure the sample datum axis rotation relative to the gravitational point of reference. The theodolite is now conveniently mounted near the operator station. It is again set level versus gravity to $\pm\,0.00055°$. The sample is mounted on the goniometer and the ε axis is simply rotated to line up the datum axis with the optical crosshairs in the theodolite. A schematic of this procedure is shown in Figure 37. This optical alignment can be performed to a standard uncertainty level of 0.18°. The dominating component of the 0.18° is the width of the sample. A wider sample can be set with a smaller uncertainty. The expanded combined uncertainty for setting the rotation angle is $\pm\,0.36°$ (k=2).

Since the NIST goniometer is not the same as a CIE goniometer, a correction is required for the rotation angle. The correction is calculated using the equation,

$$\Delta\varepsilon = \tan^{-1}\left(\tan\beta_1'\sin\beta_2'\right). \tag{14}$$

The uncertainty due to this correction is significantly smaller than the uncertainty of ε.

CHAPTER 6

OVERALL UNCERTAINTY BUDGET

The final uncertainty budget summarizes all of the details presented in Chapters 2 – 5. CIE 54.2 defines three coefficients that are analyzed in this chapter. The coefficient of luminous intensity is calculated using the following equation,

$$R_{\mathrm{I}} = \frac{(m_{\mathrm{T}} - m_{\mathrm{D}}) \cdot d^2}{m_{\mathrm{S}}} \tag{15}$$

where m_{T} is the photometer reading of the specimen, m_{D} is the photometer reading of a non-retroreflecting specimen, d is the observation distance, and m_{S} is the photometer reading of the light source perpendicular to the source at the illumination distance. The uncertainty budget for the equation 15 is shown in Table 19. However, Table 19 does not include a correction factor that is composed of all the topics discussed in Chapters 2 – 5. Table 20 is a summary of all these components for an actual white encapsulated lens piece of signage material. Items 12 through 15 depend on the uncertainty of the four CIE goniometer system angles and the material under test. For each sample to be calibrated these dependency curves have to be determined. Figures 38, 39, 40, and 41 show the dependency curves for the sample piece of signage material. Including the additional uncertainty components, the best measurement capability for the CHARM facility is 0.55 % (*k=2*)

The sample piece of signage material represents an almost ideal sample. Table 21 summarizes the components for a red microprismatic piece of signage material. The uncertainty in the spectral mismatch correction factor increases and the uncertainty due to the rotational angle dependence can become dominant. Depending on the rotational angle chosen the uncertainty can be from 0.09 % to 1.32 %. Therefore the overall relative expanded uncertainty for the best measurement capabilities for microprismatic material is from 0.70 % to 2.7 % (*k=2*).

Table 22 summarizes the components for a yellow beaded sample of pavement marking material. The pavement marking material samples are typically very non-uniform, increasing that component of uncertainty. Pavement marking material also has a significant component of uncertainty due to the dark signal measurement. Since the signal level is small, the scattered light from the front edge of the pavement marking material and off of the equipment causes a standard uncertainty contribution of 0.35 %. The overall expanded uncertainty for the best measurement capability of pavement marking material is1.02 % (*k=2*).

Equation 15 describes a ratio method for the determination of the coefficient of luminous intensity. Another method is the direct luminous intensity method where the illuminance is measured with a photometer calibrated for illuminance responsivity and the luminance is measured with a calibrated luminance meter. The relative expanded uncertainty for the illuminance responsivity is 0.40 % and for the luminance responsivity is 0.50 %. These additional uncertainty components among others bring the total relative expanded uncertainty for a direct luminous intensity calibration of ideal material to 1.0 % ($k=2$).

The coefficient of retroreflection is calculated using the following equation,

$$R_A = \frac{(m_T - m_D) \cdot d^2}{A \cdot m_S} \tag{16}$$

and the coefficient of retroreflected luminance is calculated using the equation,

$$R_L = \frac{(m_T - m_D) \cdot d^2}{A \cdot m_S \cdot \cos(\alpha - \beta_1) \cos \beta_2} \tag{17}$$

where A is the area of the sample. Currently, the procedure written in many standards requires that physical measurement of the sample area. Without preparing a special sample that has a well-defined mask, the area will be difficult to measure with a small uncertainty. Table 23 shows an example uncertainty budget for the measurement of the area of a 20 cm x 20 cm sample with an uncertainty of 0.5 mm on the length and width. The area measurement becomes the primary uncertainty component, 1.77 %, which makes the overall relative expanded uncertainty 3.6 % ($k=2$) for an ideal material. NIST staff is working on writing measurement procedures that do not require the physical measurement of the sample area. Simply the sample area crosses out; therefore, the measurement is not dependent on the sample area.

CHAPTER 7

CALIBRATION SERVICES AND TRACEABILITY TO NIST

The mission of NIST is to develop and promote measurement, standards, and technology to enhance productivity, facilitate trade, and improve the quality of life. To help meet the measurement and standards needs of retroreflective materials manufacturers and users, NIST provides calibrations, test methods, proficiency evaluation materials, measurement quality assurance programs, and laboratory accreditation services that assist a customer in establishing traceability of results of measurements or values of standards describe in the next sections.

TRACEABILITY TO NIST

Traceability requires the establishment of an unbroken chain of comparisons to stated references. NIST assures the traceability of results of measurements or values of standards that NIST itself provides, either directly or through an official NIST program or collaboration. Other organizations are responsible for establishing the traceability of their own results or values to those of NIST or other stated references. The specific NIST statement of policy follows.

To support the conduct of its mission and to ensure that the use of its name, products, and services is consistent with its authority and responsibility, NIST:

1.   Adopts for its own use and recommends for use by others the definition of traceability provided in the most recent version of the *International Vocabulary of Basic and General Terms in Metrology*: "property of the result of a measurement or the value of a standard whereby it can be related to stated references, usually national or international standards, through an unbroken chain of comparisons all having stated uncertainties."

2.   Establishes traceability of the results of its own measurements and values of its own standards and of results and values provided to customers in NIST calibration and measurement certificates, operating in accordance with the *NIST System for Assuring Quality in the Results of Measurements Delivered to Customers in Calibration and Measurement Certificates.*

3.   Asserts that providing support for a claim of traceability of the result of a measurement or value of a standard is the responsibility of the provider of that result or value, whether that provider is NIST or another organization; and that assessing the validity of such a claim is the responsibility of the user of that result or value.

4.	Communicates, especially where claims expressing or implying the contrary are made, that NIST does not define, specify, assure, or certify traceability of the results of measurements or values of standards except those that NIST itself provides, either directly or through an official NIST program or collaboration.

5.	Collaborates on development of standard definitions, interpretations, and recommended practices with organizations that have authority and responsibility for variously defining, specifying, assuring, or certifying traceability.

6.	Develops and disseminates technical information on traceability and conducts coordinated outreach programs on issues of traceability and related requirements. Assigns responsibility for oversight of implementation of the NIST policy on traceability to the NIST Measurement Services Advisory Group.

Traceability is established through "an unbroken chain of comparisons all having stated uncertainties." In practical terms, for each link in the chain the following must be in place,

- A clear definition of the particular quantity that has been measured, in this case examples are coefficient of retroreflection or coefficient of luminous intensity
- A complete description of the measurement system used to perform the measurement
- A stated measurement result or value, with a documented uncertainty
- A complete specification of the stated reference at the time the measurement system was compared to it, whether the calibrated artifact came directly from NIST or was supplied by another vendor that is traceable to NIST
- An 'internal measurement assurance' program for establishing the status of the measurement system at all times pertinent to the claim of traceability
- An 'internal measurement assurance' program for establishing the status of the stated reference at the time that the measurement system was compared to it.

Therefore, as an example, a NIST calibration report gives a brief description of the quantity measured, the description of the instrument used to measure the quantity, the value of the quantity measured along with a stated uncertainty and uncertainty budget, and a time frame of when the measurement device was last calibrated or the scale realized that it transfers. The full descriptions are published in a journal and are referenced in the calibration report. Also, behind the report is the NIST System for Assuring Quality in the Results of Measurements Delivered to Customers in Calibration and Measurement Certificates. The quality system provides a written

set of documents to ensure a consistent methodology of calibration, which must exist and be reviewed regularly by NIST management.

The user of the result of a measurement or value of a standard is responsible for assessing the validity of a claim of traceability. The provider of the result of a measurement or value of a standard is responsible for supporting its claim of the traceability of that result or value. Thus, if a customer asks a provider for a complete chain of traceability, it is the provider who is responsible for providing the necessary information that the user assesses.

With the project NIST has developed a calibration program where submitted artifacts are calibrated for requested quantities, such as coefficient of retroreflection, coefficient of luminous intensity, or coefficient of retroreflected luminance. This calibration program provides documentation of calibration, which includes the measurement value and the uncertainty associated with the measurement. The uncertainty is determined by an uncertainty budget, which is derived from characterizing the artifact. This calibration report begins the chain of traceability to NIST.

It is important to note that 'NIST traceable,' in and of itself, does not guarantee the lowest uncertainty. If the calibration is too long or the intermediate calibrations are not of high quality, the uncertainty may become significantly large, much larger than that of the NIST scale. However, as long as an unbroken chain of comparisons with stated uncertainties is made, the measurement is considered traceable to NIST. For example, a calibration facility has a piece of white non-exposed glass bead retroreflective sheeting calibrated by NIST at four sets of angles, ($\alpha = 0.2°$ and $0.5°$, $\beta = -4°$ and $30°$, specifications from ASTM D4956).(*1*) The uncertainty for this artifact is 1.0 % (*k*=2), which is the basis for the calibration facilities scale. The calibration facility uses this artifact to calibrate the instrument, which requires measuring the artifact introducing uncertainty. The calibrated instrument has an uncertainty of 1.4 % (*k*=2), half attributed to the calibration standard and half to the transfer of the calibration standard value to the instrument. When the calibration facility measures a test sample that is white glass bead sheeting at one of these four sets of angles, the total uncertainty is 1.7 % (*k*=2). However, if a test sample is measured that is red or prismatic material, the uncertainty budget must account for these contributions. An important aspect is if a second facility follows these same procedures but the equipment is not as good and the uncertainty budget is 5.0 % (*k*=2), both calibrations are still traceable to NIST.

CALIBRATION SERVICES

The specific calibration service procedures at NIST are expanded upon in a series of documents labeled Special Publications. A Special Publication in the 250 series is to be published in the Spring of 2005 on the calibration of retroreflective material. The publication provides a general description and then describes the scale realization, appropriate artifacts for calibration, equipment for calibration, calibration procedures, and the uncertainty budget of the calibration.

The scale realization describes internal calibrations done at NIST that provide internal traceability to fundamental units. Included in this section of the SP250 is a verification and maintenance schedule. On a regular daily, monthly and annual schedule certain components need to be revalidated to maintain the level of quoted uncertainty. This list is always expanding and changing as time passes and data is collected on the stability of items. For example, on a daily basis the alignment tool is calibrated and the reference check standard is validated. The color temperature of the light source is validated every 50 lamp hours, the illuminance uniformity of the source is scanned every 100 lamp hours, the spectrometer is calibrated for spectral responsivity on a monthly basis, and the photometer response is measured against a calibrated FEL using a 0/45 measurement of a diffuse reflectance plaque on a monthly basis. On an annual basis, the photometer is calibrated for absolute spectral responsivity to monitor changes in the $V(\lambda)$ filter, the goniometer magnetic encoder correction curve, the detection stage correction curves and the observation angle is re-calibrated.

SP250 provides a discussion on what samples are appropriate for standards. Suggestions on tests that can be performed before submission are stated. The equipment for calibration and uncertainty budget of the calibration are very brief statements of the material presented in this report.

The calibration procedures are based on ASTM standards and CIE recommendations. This section in the SP250 provides more specific details to enable the customer to reproduce the measurement. For example the following procedure is provided. Before calibration the light source is turned on and set to the current which provides 2856 K at the sample, typically 17.6 A. A 30-minute warm-up period is required. The goniometer is positioned at the specified distance from the source aperture. The absolute entrance angles are set to 0° using the reflective alignment plate. The goniometer yaw axis is rotated 90°. The detector package is mounted on

the goniometer sample plate and the aperture is centered on the illumination axis. The illuminance at the sample is measured at nine points. The mean and standard deviation are calculated and recorded. The detector is removed and position of the sample plate restored to the observation positioner. A reference check standard is mounted and the system is validated. The test sample is mounted and the absolute rotation angle is set by viewing through the theodolite. The angles to be measured are entered into the controlling program. The retroreflected light is measured at each required angle and the coefficient of retroreflectance is calculated and recorded. At each angle, sensitivity curves are automatically measured and used to calculate the uncertainty of the measurement. Additionally, at each angle a retroreflection spectral power distribution is measured, which is used to calculate the spectral mismatch correction factor. The measurements are repeated two more times to determine the repeatability of the sample. The ambient temperature at the sample and the relative humidity are recorded. After the measurements are completed, the results are analyzed and a calibration report is generated.

The cost of the calibration service changes with time depending on factors determine by the NIST management. All of these factors are based on the number of hours required to perform the calibration. A time budget for the calibration of retroreflective samples has been prepared. With the basic automation of the equipment and the complete uncertainty analysis, an estimate of the time required for calibration has been determined:

Number of hours = [n * (m + 0.3) + 2] (18)

where n is the number of test samples and m is number of angle combinations per sample. At current hourly rates and factors 1 test sample with 1 angle combination would have a price of $921. A test sample with 4 angle combinations would have a price of $1758. Two test samples with 6 angle combinations would have a price of $4075. History has shown that the factors determine by the NIST management will continue to increase; however, as the system becomes more automated, the required hours of measurement for multiple angle sets will decrease the price.

Another service under investigation is a test. A test is different from a calibration because the determine quantity does not have an uncertainty associated with it. The test sample is tested to determine if it meets a specification significantly reducing the number of hours measurement required. A testing service is for determining compliance only.

MEASUREMENT ASSURANCE PROGRAM

The purpose of the Measurement Assurance Program (MAP) is to determine the capabilities of a given laboratory and tie it to the National Standardization Program. This is achieved in a method that will simultaneously check measurements and procedures of the given laboratory by means of a package of various items to be measured. NIST in the past has provided a MAP service document in NBS Special Publication 671, "Retroreflectance MAP Service for Coefficient of Luminous Intensity."(2) The original MAP package contained several types of retroreflectors that are chosen as diagnostic tools for certain aspects of a retroreflectometer, shown in Figure 42. The aspects range from geometrical capabilities to detection limits. Included were a white bead sheeting retroreflector, a second type of white bead sheeting retrorelfector, a white prismatic retroreflector and a flat black mat. Also, included were seven colored glass filters shown in Figure 43. The luminous transmittance of the seven colored glass filters were measured by two methods, a direct line of sight and an indirect line of sight using a white diffusing plaque. The luminous transmittance provides spectral information on the source and detector capabilities. As part of the measurement the test laboratory completed a questionnaire that asks about specific details of the measurement such as the distance and uncertainty characteristics of the measurement.

The final product of the MAP comparison is a report of calibration that is property of the given laboratory. Included in Appendix D is a sample MAP service report from NBS SP671. The report contains: the Purpose of the report, the Materials used in the comparison, the Measurement Procedures of NIST and Instrument Description of the NIST reference retroreflectometer, the Results which show the measurements at NIST before and after the laboratory made its measurements, and the Conclusions derived from these measurements. Through the MAP service a given laboratory can receive more assistance and interaction than by obtaining a calibrated artifact from NIST. As part of this project, the artifacts from the original MAP service are being tested for stability. Additional artifacts are under development to provide the test laboratory more diagnostic tools. Once a few sets of artifacts are characterized and have passed, SP671 will be rewritten to include the updated information due to the capabilities of the new facility. The cost for this service has not been determined.

NATIONAL VOLUNTARY LABORATORY ACCREDITATION PROGRAM

The National Voluntary Laboratory Accreditation Program (NVLAP) is an accreditation body operated by NIST. Laboratory accreditation is a finding of a laboratory's competence and capability to provide scientifically sound and appropriate measurement services within their scope of accreditation. Embedded in the process is an evaluation of the lab's ability to achieve and maintain traceability for the accredited services. Accreditation to ISO/IEC 17025: General requirements for the competence of testing and calibration laboratories (*3*) determines that a laboratory has all of the necessary facilities, equipment, standards, procedures, uncertainty analyses, personnel, etc., which make it capable of providing traceable measurement results. Laboratory accreditation does not speak to the specifics of any individual measurement result but to the overall capability of a lab to provide the service.

As part of this project, NIST investigated and began to develop an accreditation program with NVLAP. With the development of the CIPM Mutual Recognition Arrangement (MRA) that was drawn up by the International Committee of Weights and Measures (CIPM) under the authority given to it in the Metre Convention, the need for a NVLAP program will become necessary for any international trade. The principal objectives of the MRA are to establish through measurement comparisons the degree of equivalence of national measurement standards maintained by National Metrology Institutes (NMIs), to provide for the mutual recognition of calibration and measurement certificates issued by NMIs, and to provide a secure technical foundation for wider agreements related to international trade, commerce, and regulatory affairs.

In developing a program the following items must be accomplished:

Identify laboratory community

The laboratory community consists of federal and state department of transportation laboratories, manufacturers, and secondary laboratories that typically are instrument producers. The number of potential laboratories that would apply for NVLAP accreditation is not large, but it is not required to be a certain size.

Identify laboratory user community

The laboratory user community consists of federal and state department of transportation laboratories and a significant number of manufacturers including manufacturers of materials and instruments.

Identify standards writing bodies

The standards writing bodies have been identified in this report, ASTM International and Commission Internationale De L'Éclairage. Soon the International Organization for Standardization will be included in this list.

Identify test methods and standards

Many of the documents are provided in the Bibliography of this report.

Identify product certification/validation programs

This aspect needs to be identified.

Identify regulatory bodies both domestic and foreign

This aspect needs to be identified.

Identify other stakeholders

This aspect needs to be identified.

Identify sources of technical expertise and assistance – domestic and foreign

The product of this report has established technical expertise at NIST. Through interactions with the CIE Technical Committee 2-56 on developing an ISO/CIE standard for retroreflection measurement, information on foreign technical expertise and assistance is being collected.

Identify number of labs and amount of calibrations

This aspect needs to be identified.

Select the "units" of the Scope of Accreditation

The units for Scope of Accreditation will depend on the requests from customers. Most likely the units will be limited to Coefficient of Luminous Intensity, Coefficient of Retroreflection, and Coefficient of Retroreflected Luminance.

Establish specific technical requirements

The specific technical requirements are currently be developed as part of working in CIE Technical Committee 2-56.

Establish laboratory staff qualifications and certifications

This aspect needs to be established.

Establish components of a laboratory: equipment, facilities, …

The components of the laboratory need to be established and will depend on the determination of the specific technical requirements.

Establish accreditation process sequence

This aspect needs to be identified.

Develop the assessment techniques for on-sites, demonstrations, …

The assessment techniques need to be developed and listed.

Design proficiency testing programs

The proficiency testing programs will be almost exactly like the programs finalized in the MAP service.

Set on-site team size and skill set

This aspect needs to be determined, but mostly like will include two individuals: a quality assessor and a technical assessor.

Create NVLAP program-specific checklists

This aspect needs to be identified.

Establish evaluation criteria for granting of accreditation

The evaluation criteria are based on ISO 17025 and the ISO and ASTM standards associated with the measurement of the identified units for scope of accreditation.

Establish fee schedule

A fee schedule needs to be determined. The NVLAP headquarters can be contact to provide rough estimates of the initial assessment and then continuing assessments in years following the initial assessment.

Determine contents of the NVLAP application package

This aspect needs to be identified.

Publish Federal Register announcement

This aspect needs to be completed.

Set time window for accepting initial applications, then no restrictions.

This aspect needs to be identified.

The accreditation program with NVLAP will be completed and instituted once a few customers provide written requests of interest for this service to the NVLAP headquarters.

(*1*) "Standard Specification for Retroreflective Sheeting for Traffic Control." *ASTM D4956-04*, ASTM International, (2003) 12 pp.

(*2*) Eckerle, K.L., and Hsia, J.J., "Retroreflectance MAP Service for Coefficient of Luminous Intensity." *NBS Special Publication 671,* U.S. Department of Commerce/National Bureau of Standards, Washington D.C. (1984) 49 pp.

(*3*) "General requirements for the competence of testing and calibration laboratories," *ISO/IEC 17025*, International Organization for Standardization, Geneva, Switzerland, First Edition, (1999) 34 pp.

REFERENCES

([1]) "Guide to the Expression of Uncertainty in Measurement." International Organization for Standardization, Geneva, Switzerland, First Edition, (1995) 101 pp.

([2]) "Retroreflection: Definition and Measurement." *Technical Report CIE 54.2-2001*, Commission Internationale De L'Éclairage, Vienna, Austria (2001) 55 pp.

([1]) Zong, Y., Brown, S.W., Lykke, K.R., and Ohno, Y., "A Simple Stray Light Correction Method for Array Spectrometers." Submitted to *Applied Optics*.

([1]) Barnes, P.Y., Early, E.A., and Parr, A.C., "NIST Measurement Services: Spectral Reflectance." NIST Special Publication 250-48, U.S. Department of Commerce/National Institute of Standards and Technology, Washington D.C. (1998) 157 pp.

([1]) "Standard Specification for Retroreflective Sheeting for Traffic Control." *ASTM D4956-04*, ASTM International, (2003) 12 pp.

([1]) Eckerle, K.L., and Hsia, J.J., "Retroreflectance MAP Service for Coefficient of Luminous Intensity." *NBS Special Publication 671,* U.S. Department of Commerce/National Bureau of Standards, Washington D.C. (1984) 49 pp.

([1]) "General requirements for the competence of testing and calibration laboratories," *ISO/IEC 17025*, International Organization for Standardization, Geneva, Switzerland, First Edition, (1999) 34 pp.

APPENDIX A

BIBLIOGRAPHY OF DOCUMENTARY RETROREFLECTION

Document No.	Title
A-A-251	Retroreflective Tape and Retroreflective Sheeting
AASHTO T257	Standard Method of Test for Instrumental Photometric Measurement
AASHTO M268	Standard Specification for Retroreflective Sheeting for Traffic Control
ASTM D 4061	Test Method for Retroreflectance of Horizontal Coatings
ASTM D 4280	Specification for Extended Life Type, Non-plowable, Prismatic, Raised Retroreflective Pavement Markers
ASTM D 4383	Specification for Plowable, Raised Retroreflective Pavement Markers
ASTM D 4956	Standard Specification for Retroreflective Sheeting for Traffic Control
ASTM D 6359	Standard Specification for Minimum Retroreflectance of Newly Applied Pavement Marking Using Portable Hand-Operated Instruments
ASTM E 808	Standard Practice for Describing Retroreflection
ASTM E 809	Standard Practice for Measuring Photometric Characteristics of Retroreflectors
ASTM E 810	Standard Test Method of Coefficient of Retroreflection of Retroreflective Sheeting
ASTM E 811	Standard Practice for Measuring Colorimetric Characteristics of Retroreflectors Under Nighttime Conditions
ASTM E 1501	Standard Specification for Nighttime Photometric Performance of Retroreflective Pedestrian Markings for Visibility Enhancement
ASTM E 1696	Standard Test Method for Field Measurement of Raised Retroreflective Pavement Markers Using a Portable Retroreflectometer
ASTM E 1709	Standard Test Method for Measurement of Retroreflective Signs Using a Portable Retroreflectometer
ASTM E 1710	Standard Test Method for Measurement of Retroreflective Pavement Marking Materials
ASTM E 1743	Standard Practice for Selection and Use of Portable Retroreflectometers for the Measurement of Pavement Marking Materials
ASTM E 1809	Standard Test Method for Measurement of High-visibility Retroreflective Clothing Marking Material Using a Portable Retroreflectometer
BS AU 145D	Retroreflecting Number Plates
CIE 54.2-2001	Retroreflection Definition and Measurement
CNS Z 8015	Method of Test for Retroreflective Sheeting and Tape
DIN 67520-1	Retroreflecting Materials for Traffic Safety
EN 1463-1	Road Marking Materials – Retroreflecting Road Studs – Part 1. Initial Performance Requirements
EN 1463-2	Road Marking Materials – Retroreflecting Road Studs – Part 1. Road Test Performance Specifications

FAA AC 150/5345-39   Spec/L-853 Runway and Taxiway Retroreflective Markers
FED-STD-370   Instrumental Photometric Measurements/Retroreflection
FED-STD-373   Instrumental Color Measurements of Retroreflective Materials and Devices Under Nighttime Illumination

JIS Z8714   Retroreflectors – Optical Properties – Measuring Method
JIS Z9117   Retroreflective Sheeting and Tape for Safety
SAA AS 1906.1   Retroreflective Materials and Devices for Road Traffic Control Purposes
SAA AS 1906.2   Retroreflective Devices (Non-pavement Application)
SAA AS 1906.3   Raised Pavement Markers (Retroreflective and Non-retroreflective)
SAA AS/NZS 1906.4 Retroreflective Materials and Devices for Road Traffic Control Purposes – High Visibility Materials for Safety Garments

SAE J1967   Retroreflective Materials for Vehicle Conspicuity

APPENDIX B

UNCERTAINTY OF ADDITIONAL RETROREFLECTION ANGLES

ORIENTATION ANGLE, ω_s

The orientation angle is the angle in a plane perpendicular to the retroreflector axis from the entrance half-plane to the datum axis. The orientation angle is used in the Intrinsic and the Application Systems. It is dependent on the rotation angle and the entrance angle components as shown in the equation,

$$\omega_s = \varepsilon + \tan^{-1}\left(\frac{\sin\beta_2}{\tan\beta_1}\right) + 90°[1 - \mathrm{sgn}(\beta_1)] \tag{B1}$$

Table B-1 shows a representative uncertainty budget for the orientation angle and the equations for the sensitivity coefficients. The orientation angle is not uniquely defined by three individual parameters. Figure B-1 shows the dependence of the uncertainty on the entrance angle component, β_1, where β_2 is equal to 0°. The orientation angle is set equal to zero by changing the rotation angle. The absolute uncertainty in the orientation angle varies from $\pm 0.36°$ ($k=2$) to infinity as β_1 approaches 0°. When β approaches zero, the illumination axis and the retroreflector axis coincide; therefore the entrance half-plane is ill defined. This is a special case; by convention, $\omega_s = 0°$. Another special case is when $\beta_1 = 0 \neq \beta_2$. In this case the following equation applies,

$$\omega_s = \varepsilon + 90°\,\mathrm{sgn}(\beta_2). \tag{B2}$$

The uncertainty for the orientation angle seems to be the same as the rotation angle, which is $\pm 0.36°$ ($k=2$); however, β_1 always has some uncertainty and can never be exactly equal to 0. Therefore, the uncertainty of the orientation angle when β_1 approaches 0 is always infinite or since it is an angle 360°.

PRESENTATION ANGLE, γ

The presentation angle is the dihedral angle from the entrance half-plane to the observation half-plane measured counter-clockwise from the viewpoint of the light source. The orientation angle is used in the Intrinsic System. It is dependent on the entrance angle components as shown in the equation,

$$\gamma = \tan^{-1}\left(\frac{\tan\beta_2}{\sin\beta_1}\right). \tag{B3}$$

Table B-2 shows a representative uncertainty budget for the presentation angle and the equations for the sensitivity coefficients. The absolute uncertainty in the presentation angle varies from ± 0.05° (*k=2*) to infinity. When β approaches zero, the illumination axis and the retroreflector axis coincide causing the uncertainty to go to infinity. Therefore, special cases exist. When $\beta_1 = 0 \neq \beta_2$ the presentation angle reduces to,

$$\gamma = 90°\,\text{sgn}(\beta_2) \tag{B4}$$

and when $\beta_1 = 0 = \beta_2$,

$$\gamma = -\rho = -\varepsilon\,. \tag{B5}$$

Equation B4 implies that the presentation angle has no uncertainty in this special case, and eq. B5 shows that the uncertainty is equal to the uncertainty of the rotation angle, which is $\pm 0.36°$ (*k=2*). In the first special case the uncertainty does not explode and can be determined using eq. B3. Much like the orientation angle, when β approaches 0 as in the second special case the uncertainty of the presentation angle is always infinite or since it is an angle 360°.

OBSERVATION-ELEVATION ANGLE, *a*

The observation-elevation angle is the complement of the angle between the retroreflector axis and the observation axis. The observation-elevation angle is used in the Road Marking System. For horizontal road markings, the retroreflector axis is considered to be normal to the road surface. Therefore, the observation-elevation angle is the angle the observation axis makes with the road surface. It is dependent on the entrance angle components and the observation angle as shown in the equation,

$$a = \sin^{-1}\left(\cos(\beta_1 - \alpha)\cos\beta_2\right). \tag{B6}$$

Table B-3 shows the uncertainty budget for the observation-elevation angle and the equations for the sensitivity coefficients. The chosen entrance angle components and observation angles are equivalent to the CEN 30 m geometry. The absolute uncertainty in the observation-elevation angle is $\pm 0.017°$ (*k=2*).

ROAD MARKING FIRST AZIMUTHAL ANGLE, *b*

The road marking first azimuthal angle is the dihedral angle from the half-plane originating on the line of the retroreflector axis and containing the obverse of the illumination axis to the half-plane originating on the line of the retroreflector axis and containing the observation axis, measured clockwise from a viewpoint on the retroreflector axis. It is dependent on the entrance angle components and the observation angle as shown in the equation,

$$b = 180° + \text{sgn}(\beta_2)\cos^{-1}\left[\frac{\sin^2\beta_2\cos\beta_1\cos(\beta_1-\alpha)+\sin\beta_1\sin(\beta_1-\alpha)}{\cos a\sqrt{1-\cos^2\beta_1\cos^2\beta_2}}\right]. \tag{B7}$$

Table B-4 shows the uncertainty budget for the road marking first azimuthal angle and the equations for the sensitivity coefficients. The chosen entrance angle components and observation angles are equivalent to the CEN 30 m geometry. The absolute uncertainty in the road marking first azimuthal angle will be ± 0.025° (*k=2*).

ILLUMINATION-ELEVATION ANGLE, *e*

The illumination-elevation angle is the complement of the angle from the illumination axis to the retroreflector axis. The illumination-elevation angle is used in the Road Marking System. For horizontal road markings, the retroreflector axis is considered to be normal to the road surface. Therefore, the illumination-elevation angle is the angle the illumination axis makes with the road surface. It is dependent on the entrance angle components and the observation angle as shown in the equation,

$$e = \sin^{-1}\left(\cos\beta_1\cos\beta_2\right). \tag{B8}$$

Table B-5 shows the uncertainty budget for the illumination-elevation angle and the equations for the sensitivity coefficients. The chosen entrance angle components are equivalent to the CEN 30 m geometry. The absolute uncertainty in the observation-elevation angle will be ± 0.017° (*k=2*).

ROAD MARKING SECOND AZIMUTHAL ANGLE, *d*

The road marking second azimuthal angle is the angle in the plane perpendicular to the retroreflector axis from the half-plane that originates on the line of the retroreflector axis and contains the observation axis, to the obverse of the datum axis, measured clockwise from a

viewpoint on the retroreflector axis. It is dependent on the orientation angle and the road marking second azimuthal angle as shown in the equation,

$$d = \omega_s + b - 180°.$$
(B9)

Table B-6 shows the uncertainty budget for the road marking second azimuthal angle and the equations for the sensitivity coefficients. The chosen orientation angle and road marking first azimuthal angles are equivalent to the CEN 30 m geometry. The absolute uncertainty in the road marking second azimuthal angle will be $\pm 0.361°$ (*k=2*).

APPENDIX C

SAMPLE CALIBRATION REPORT

REPORT OF CALIBRATION
Special Photometric Tests for Submitted Retroreflective Sheeting 37100S

for

a white prismatic retroreflective sample
with S/N: NIST20001

Submitted by:

Company ABC
Attn.: John Doe
100 1st Avenue
Hometown, MD 10000

(See your Purchase Order No. XYZ, dated December 32, 2000)

1. Calibration Item

A white prismatic retroreflective sample manufactured by Company ABC was calibrated for coefficient of retroreflected luminance. The sample designation number scribed on the back of the sample is NIST20001.

2. Description of the Calibration

The first paragraph describes the calibration and what NIST scale it is based. Also stated is when the NIST scale was last realized and what international definition it is based. The details of the NIST coefficient of retroreflected luminance unit are described in reference [1].

The second paragraph states briefly the procedure used to calibrate the item and any particular details. The room temperature, instrument ambient temperature and relative humidity are stated for when the calibration was performed.

Calibration of coefficient of retroreflected luminance
Company ABC

3. Results of the Calibration

The results of the calibration are shown in Table 1. The relative expanded uncertainty (with coverage factor k=2) is stated. The uncertainty budget is shown in Table 2. The NIST policy on uncertainty statements is described in reference [2].

Table 1. Results of Calibration

Item Designation	Observation Angle [°]	Entrance Angle 1 [°]	Entrance Angle 2 [°]	Rotation Angle [°]	Coeff. of Retroreflected Luminance [cd/lx/m^2]
NIST20001	0.200	-4.00	0.00	0.00	4.0854

4. General Information

More specific details are added in this section.

The Calibration Report shall not be reproduced except in full, without the written approval of NIST.

Prepared by:

C. Cameron Miller
Optical Technology Division
Physics Laboratory
(301) 975-4713

Approved by:

Yoshihiro Ohno
For the Director,
National Institute of Standards and Technology
(301) 975-2321

References:

[1] C. Miller, NIST Special Publication 250-XX "Retroreflection Calibration" (2005).
[2] B. N. Taylor and C. E. Kuyatt, "Guidelines for Evaluating and Expressing the Uncertainty of NIST Measurement Results," NIST Technical Note 1297 (1993).

Calibration Date: December 33, 2005
NIST Test No.: 844/222333-05   Page 2 of 3

Calibration of coefficient of retroreflected luminance
Company ABC

Table 2. Uncertainty budget for this calibration

Uncertainty Component	Type	Rel. Standard Uncertainty (%)
Various Items	B	0.18
Various Items	B	0.08
Various Items	B	0.01
Various Items	A	0.04
Various Items	B	0.11
Various Items	A	0.30
Relative combined standard uncertainty		0.XX
Relative expanded uncertainty (k=2)		**0.XX**

APPENDIX D

SAMPLE MAP REPORT

REPORT OF CALIBRATION

for the

Retroreflectance MAP Service for
Coefficient of Retroreflected Luminance

Reported to:

Company ABC
Attn.: John Doe
100 1st Avenue
Hometown, MD 10000

(See your Purchase Order No. XYZ, dated December 32, 2000)

1. Purpose of Measurements

The purpose of this test is to determine the coefficient of retroreflected luminance for two white bead sheeting retroreflectors and a white prismatic cube-corner retroreflector. Also, the luminous transmittance of seven colored glass filters is determined. The NIST and the participating laboratory have accomplished these determinations. Conclusions for these determinations are presented.

2. Materials

The retroreflectors and colored filters contained in the MAP package are described in detail in reference [1]. The serial numbers for the retroreflectors is MAP-R11, MAP-R12, and MAP-R13 and are scribed on the back of the retroreflector. The serial numbers for the colored filters is MAP-F11, MAP-F12, MAP-F13, MAP-F14, MAP-F15, MAP-F16, and MAP-F17.

3. Measurement Methods
Measurements made by the NIST are described in reference [2]. Measurements made by the participating laboratory were performed using its normal operating procedures.

4. Results of Measurement

The results of the MAP comparison are shown in Tables 1 and 2 for the retroreflectors and Table 3 for the colored glass filters. Since NIST measured the MAP package before and after the participating laboratory made its measurements, three values are reported for each condition.

A. Retroreflectors

In addition to the angular parameters α, β_1, β_2, and ε we define some quantities relevant to data analysis in Tables 4 and 5.

(1) The quantity $100\dfrac{\Delta R}{R}$ is the upper bound of the uncertainty in R predicted by the

uncertainties of the angular parameters expressed as a percent and estimated from data supplied by the participant.

(2) The quantity $100\dfrac{3\times\delta R_P}{R_P}$ is three times the standard deviation of the mean R obtained

from repeated measurements by the participant expressed in percent.

(3) The quantity L is the uncertainty in R due to aperture centroid (source and receiver), linearity, and color temperature of the source and photopic response of the receiver expressed in percent.

(4) The quantity P_{LAB} is the sum of (1), (2) and (3). It is an upper bound of the uncertainty in R due to the participating laboratory and is expressed in percent.

(5) The quantity U is the sum of PLAB, PNIST (the upper bound on the uncertainty due to NIST [1]), and a third component which estimates changes in the retroreflectance of the MAP sample due to possible temperature and pressure changes in its environment.

(6) The quantity B is the percent change in the measurements made by NIST before and after the measurements performed by the participating laboratory.

(7) The quantity D is the percent difference between the NIST average of before and after measurements and the value obtained by the participating laboratory.

B. Colored Filters

The bounds on the uncertainties of the luminous transmittance values for the colored glass filters are listed in Table 6.

(1) The quantity $3\times\delta Y_P$ is three times the standard deviation of the mean.

(2) The quantity C is the difference between the Y values obtained by NIST before and after the participating laboratory.

(3) The quantity U is the sum of items (1) and (2) and bounds on the uncertainties due to NIST [1].

(4) The quantity D is the difference between the participant values and the NIST values.

5. Conclusion

If D>U; then there is a bias.

A. *Retroreflectors*

Since D<U in Tables 1 and 2 for both the bead sheeting retroreflectors and the prismatic retroreflector, we conclude that the estimates given by the participant used to obtain M are valid. Therefore, the quantities M are realistic bounds on the participant's measurement process.

B. *Colored Glass Filters*

Since D>U in Table 4 in some cases, we conclude that there exists a bias in three cases. It is necessary for the participant to decide if these biases are of an acceptable level. In the other cases, we conclude that the bias of the participating laboratory is equal to or less than U.

Prepared by:

C. Cameron Miller
Optical Technology Division
Physics Laboratory
(301) 975-4713

Approved by:

Yoshihiro Ohno
For the Director,
National Institute of Standards and Technology
(301) 975-2321

References:

[1] C.Miller, NIST Special Publication XXX "Retroreflectance MAP Service for Coefficient of Retroreflected Luminance" (2005).

[2] C. Miller, NIST Special Publication 250-XX "Retroreflection Calibration" (2005).

Table 1 – Results of the pilot intercomparison with Laboratory XX - Beaded.

α [°]	β_1 [°]	NIST R before	R Laboratory XX	NIST R after
High Intensity White				
0.200	-4.00	4.0854	4.110	4.0048
0.200	20.00	3.8072	3.817	3.7393
0.200	40.00	2.4309	2.407	2.4065
1.500	-4.00	0.1991	0.203	0.1960
1.500	20.00	0.1914	0.196	0.1904
1.500	40.00	0.1371	0.139	0.1342
Engineering White				
0.200	-4.00	1.6180	1.626	1.5572
0.200	20.00	1.2014	1.230	1.1522
0.200	40.00	0.3491	0.362	0.3317
1.500	-4.00	0.1340	0.133	0.1291
1.500	20.00	0.1245	0.125	0.1195
1.500	40.00	0.0776	0.0787	0.0744

Table 2 – Results of the pilot intercomparison with Laboratory XX - Prismatic ($\varepsilon = 0°$)

α [°]	β_1 [°]	β_2 [°]	NIST R before	R Laboratory XX	NIST R after
			Prismatic Reflector		
0.500	0.00	0.00	0.9042	0.915	0.9163
0.500	-10.00	0.00	0.8820	0.873	0.8870
0.500	10.00	0.00	0.8548	0.864	0.8585
0.200	0.00	0.00	5.5970	5.704	5.5657
0.200	-10.00	0.00	4.7419	4.930	4.7694
0.200	10.00	0.00	4.7238	4.786	4.6381
0.500	0.00	-20.00	0.3690	0.421	0.3311
0.500	-10.00	-20.00	0.2949	0.333	0.2825
0.500	10.00	-20.00	0.3080	0.325	0.2813
0.200	0.00	-20.00	2.1500	2.408	1.9783
0.200	-10.00	-20.00	1.9689	2.196	1.8271
0.200	10.00	-20.00	2.0741	2.196	1.8842
0.500	0.00	20.00	0.4284	0.425	0.3766
0.500	-10.00	20.00	0.3114	0.300	0.3044
0.500	10.00	20.00	0.3717	0.362	0.3167
0.200	0.00	20.00	2.8327	2.814	2.4938
0.200	-10.00	20.00	2.0371	1.960	1.9794
0.200	10.00	20.00	2.5243	2.504	2.2998

Table 3 - Results of the pilot intercomparison with Laboratory XX – Filters

Filter	NIST Y before	Y Laboratory XX	NIST Y after
MAP-F11	0.01300	0.01338	0.01317
MAP-F11	0.06384	0.06270	0.06419
MAP-F11	0.67456	0.68900	0.67611
MAP-F11	0.79876	0.80600	0.78694
MAP-F11	0.35934	0.36800	0.35723
MAP-F11	0.19549	0.19750	0.19438
MAP-F11	0.00000	0.00001	0.00000

Table 4 – Uncertainty analysis for results with Laboratory XX - Beaded.

α [°]	β_1 [°]	$\Delta R/R$ [%]	$3 \times \delta R_P/R_P$ [%]	L [%]	P_{LAB} [%]	U [%]	B [%]	D [%]
			High Intensity White					
0.200	-4.00	0.86	0.421	2.3	3.581	8.751	0.997	-1.604
0.200	20.00	0.89	0.272	2.3	3.462	8.642	0.900	-1.159
0.200	40.00	1.05	0.432	2.3	3.784	9.004	0.505	0.484
1.500	-4.00	0.95	0.085	2.3	3.335	8.655	0.785	-2.759
1.500	20.00	0.98	0.530	2.3	3.810	9.130	0.262	-2.672
1.500	40.00	0.97	0.124	2.3	3.394	8.534	1.069	-2.470
			Engineering White					
0.200	-4.00	0.72	0.320	2.2	3.240	8.060	1.915	-2.419
0.200	20.00	0.88	0.422	2.2	3.502	8.422	2.091	-4.521
0.200	40.00	0.90	0.478	2.2	3.578	8.178	2.556	-6.345
1.500	-4.00	0.68	0.130	2.2	3.010	7.750	1.863	-1.102
1.500	20.00	0.74	0.139	2.2	3.079	7.899	2.049	-2.459
1.500	40.00	0.89	1.320	2.2	4.410	9.270	2.106	-3.553

Table 5 – Uncertainty analysis for results with Laboratory XX - Beaded.

α [°]	β_1 [°]	β_2 [°]	$\Delta R/R$ [%]	$3 \times \delta R_P/R_P$ [%]	L [%]	P_{LAB} [%]	U [%]	B [%]	D [%]
0.500	0.00	0.00	3.109	1.760	2.6	7.469	14.85	-0.665	-0.522
0.500	-10.00	0.00	2.530	0.461	2.6	5.591	13.02	-0.283	1.300
0.500	10.00	0.00	3.772	0.776	2.6	7.148	15.11	-0.216	-0.858
0.200	0.00	0.00	3.200	0.212	2.6	6.012	13.64	0.281	-2.197
0.200	-10.00	0.00	3.918	0.381	2.6	6.899	15.03	-0.289	-3.666
0.200	10.00	0.00	4.199	0.308	2.6	7.107	15.43	0.916	-2.244
0.500	0.00	-20.00	2.899	1.578	2.6	7.077	22.98	5.413	-20.27
0.500	-10.00	-20.00	4.637	2.683	2.6	9.920	26.62	2.148	-15.35
0.500	10.00	-20.00	3.579	2.594	2.6	8.773	23.07	4.531	-10.30
0.200	0.00	-20.00	5.327	1.049	2.6	8.976	22.88	4.159	-16.66
0.200	-10.00	-20.00	11.24	2.738	2.6	16.58	32.88	3.736	-15.70
0.200	10.00	-20.00	9.527	1.447	2.6	13.57	28.47	4.793	-10.96
0.500	0.00	20.00	2.646	3.505	2.6	8.751	20.19	6.435	-5.590
0.500	-10.00	20.00	3.206	3.626	2.6	9.432	22.03	1.137	2.566
0.500	10.00	20.00	2.982	1.651	2.6	7.233	19.03	7.990	-5.171
0.200	0.00	20.00	2.565	2.452	2.6	7.617	16.94	6.363	-5.660
0.200	-10.00	20.00	6.625	2.322	2.6	11.55	23.65	1.437	2.403
0.200	10.00	20.00	5.065	2.383	2.6	10.05	19.89	4.654	-3.812

Table 6 - Uncertainty analysis for results with Laboratory XX - Filters

| Filter	$3 \times \delta Y_P$	C	U	D	D>U
MAP-F11	0.0001	0.0001	0.0010	0.0003	No
MAP-F11	0.0010	0.0002	0.0022	0.0013	No
MAP-F11	0.0035	0.0008	0.0050	0.0137	Yes
MAP-F11	0.0035	0.0009	0.0050	0.0082	Yes
MAP-F11	0.0052	0.0011	0.0071	0.0097	Yes
MAP-F11	0.0048	0.0006	0.0058	0.0026	No
MAP-F11	0.0000	0.0000	0.0000	0.0000	No
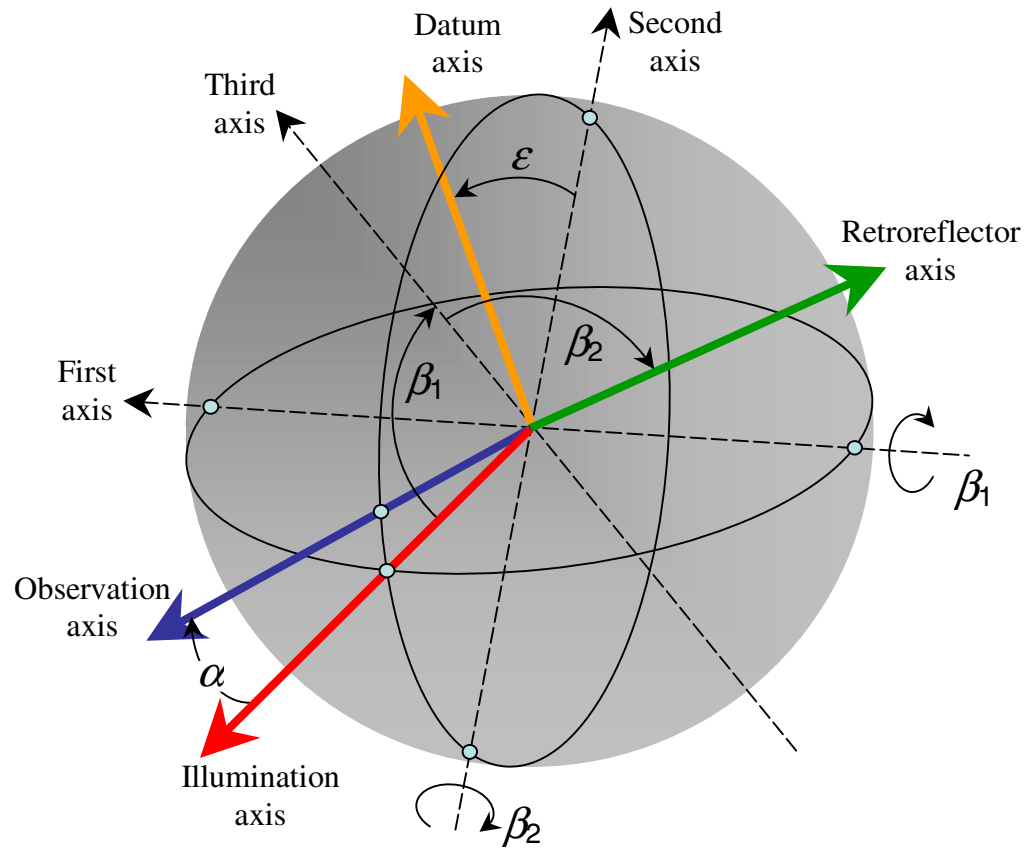
**Figure 1 –** System for specifying and measuring retroreflectors.

**Figure 2** – Conceptual drawing of the CHARM facility
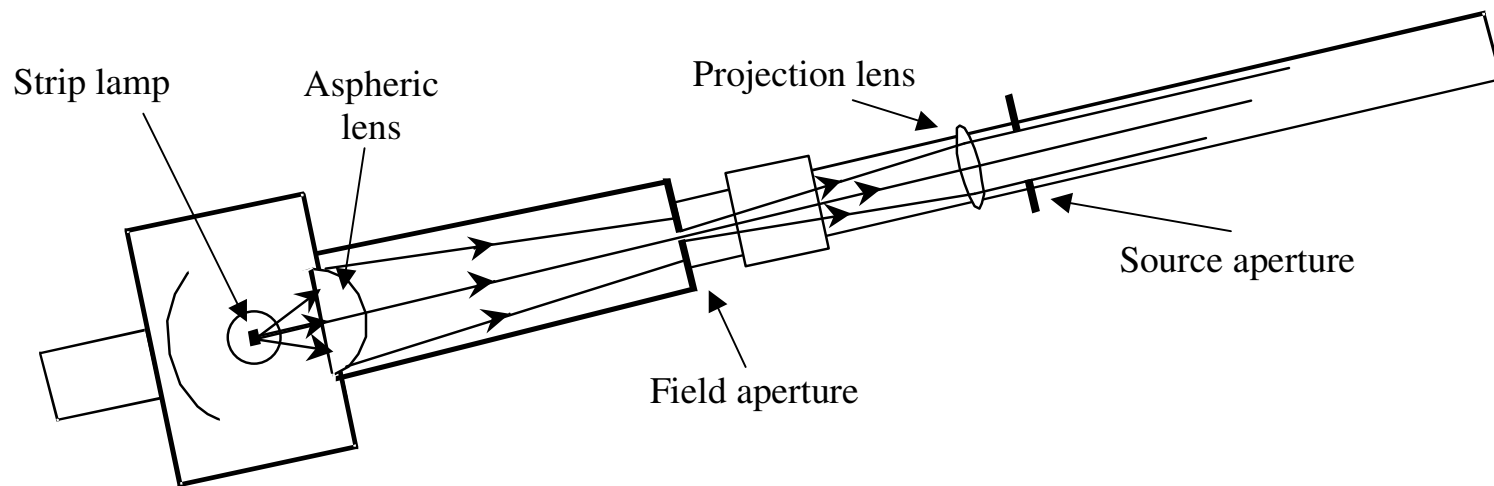
**Figure 3** – Presented is a schematic of the Strip Lamp Projection System
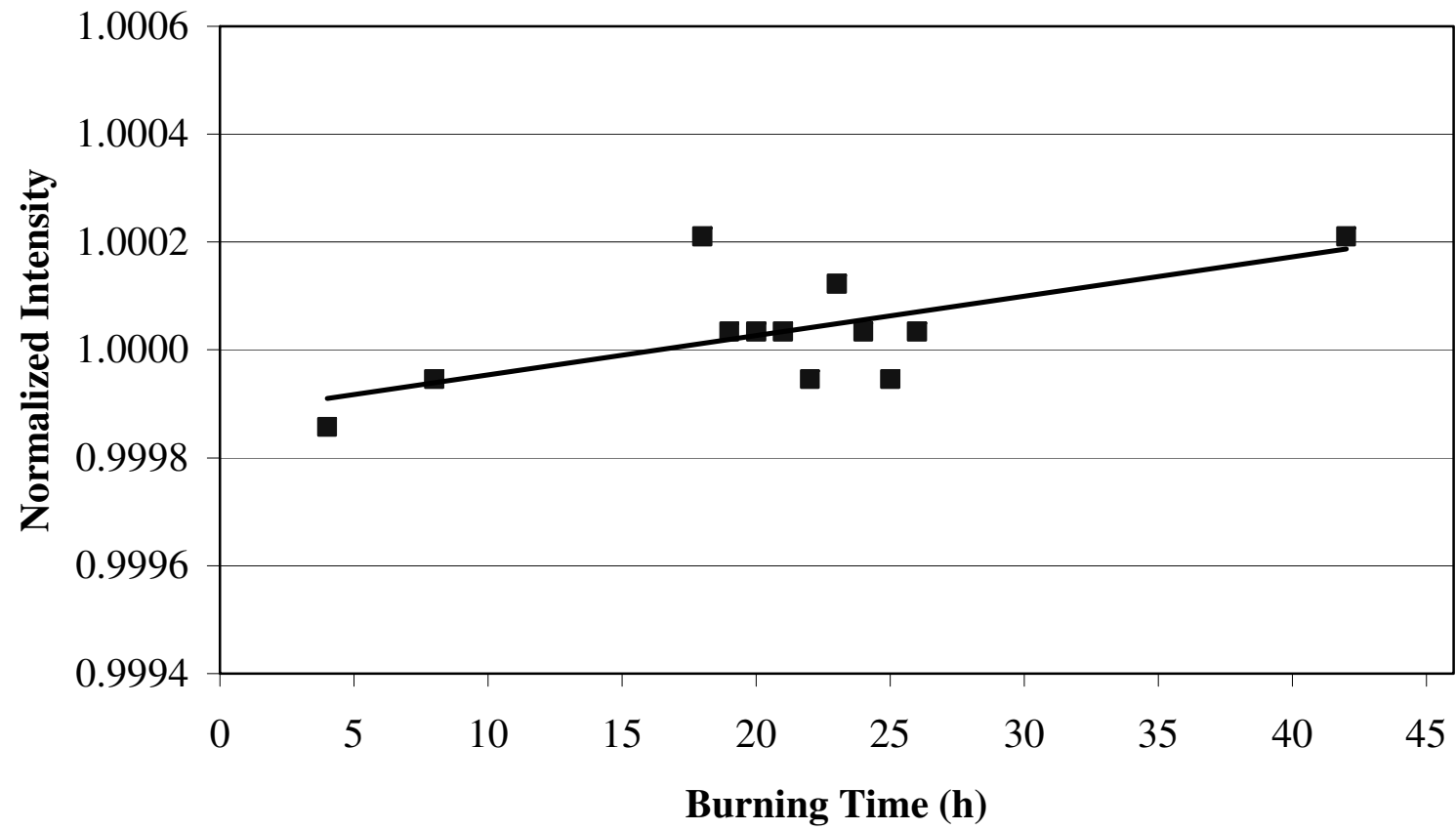
**Figure 4 –** Shown is the normalized luminous intensity of the strip lamp source over a 45 h period.
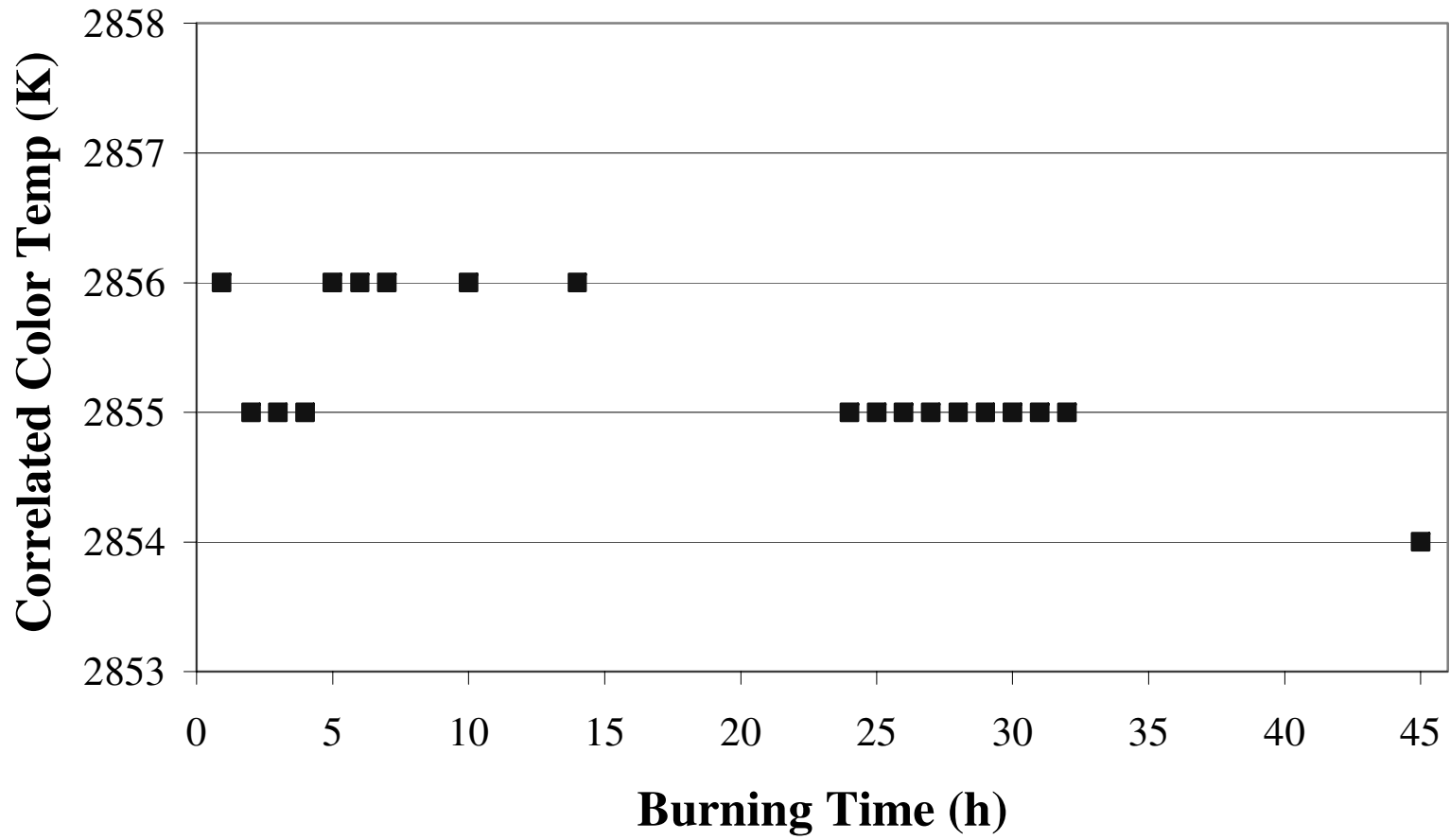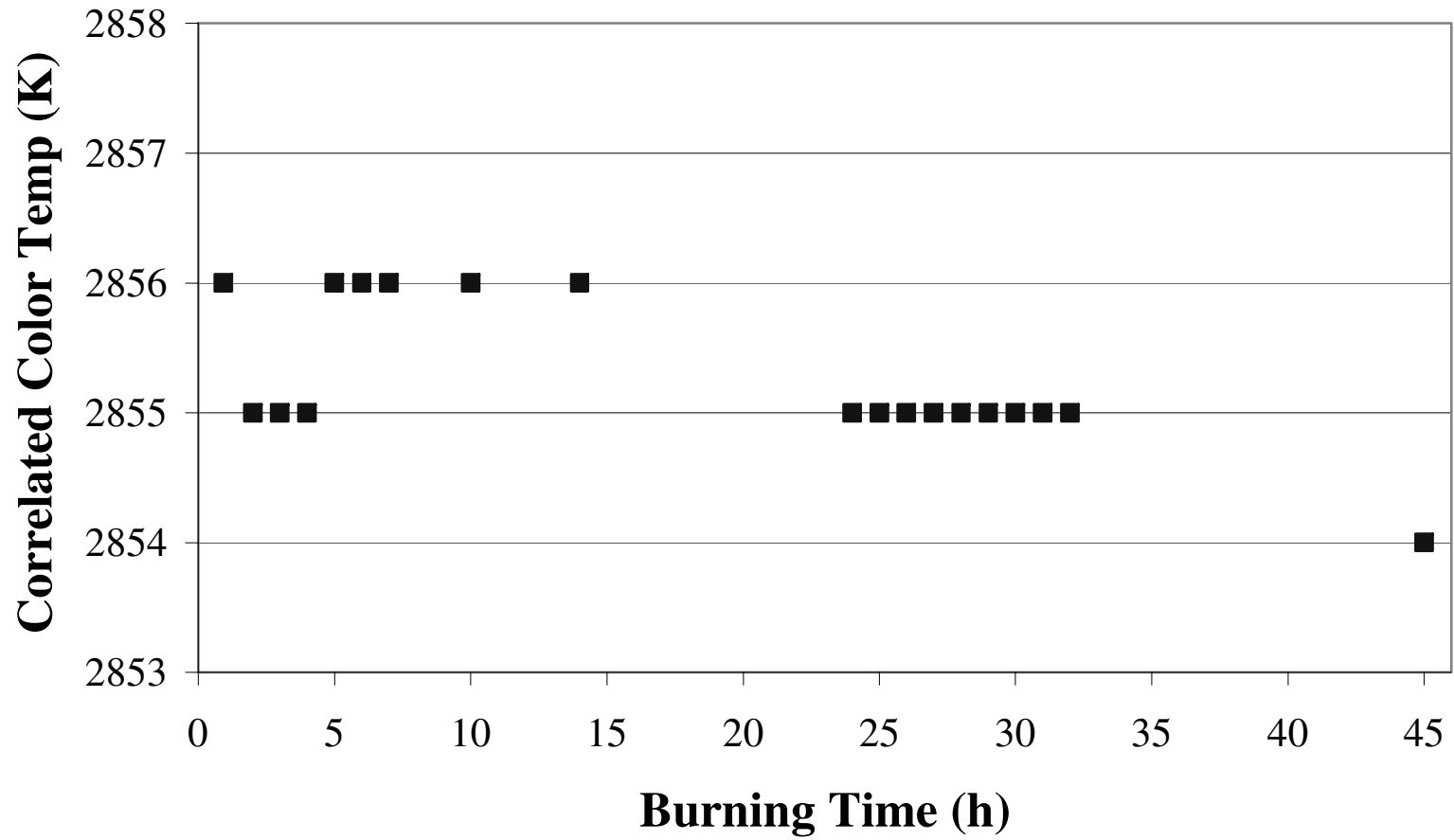
**Figure 5 –** Shown is the correlated color temperature of the strip lamp source over a 45 h period.
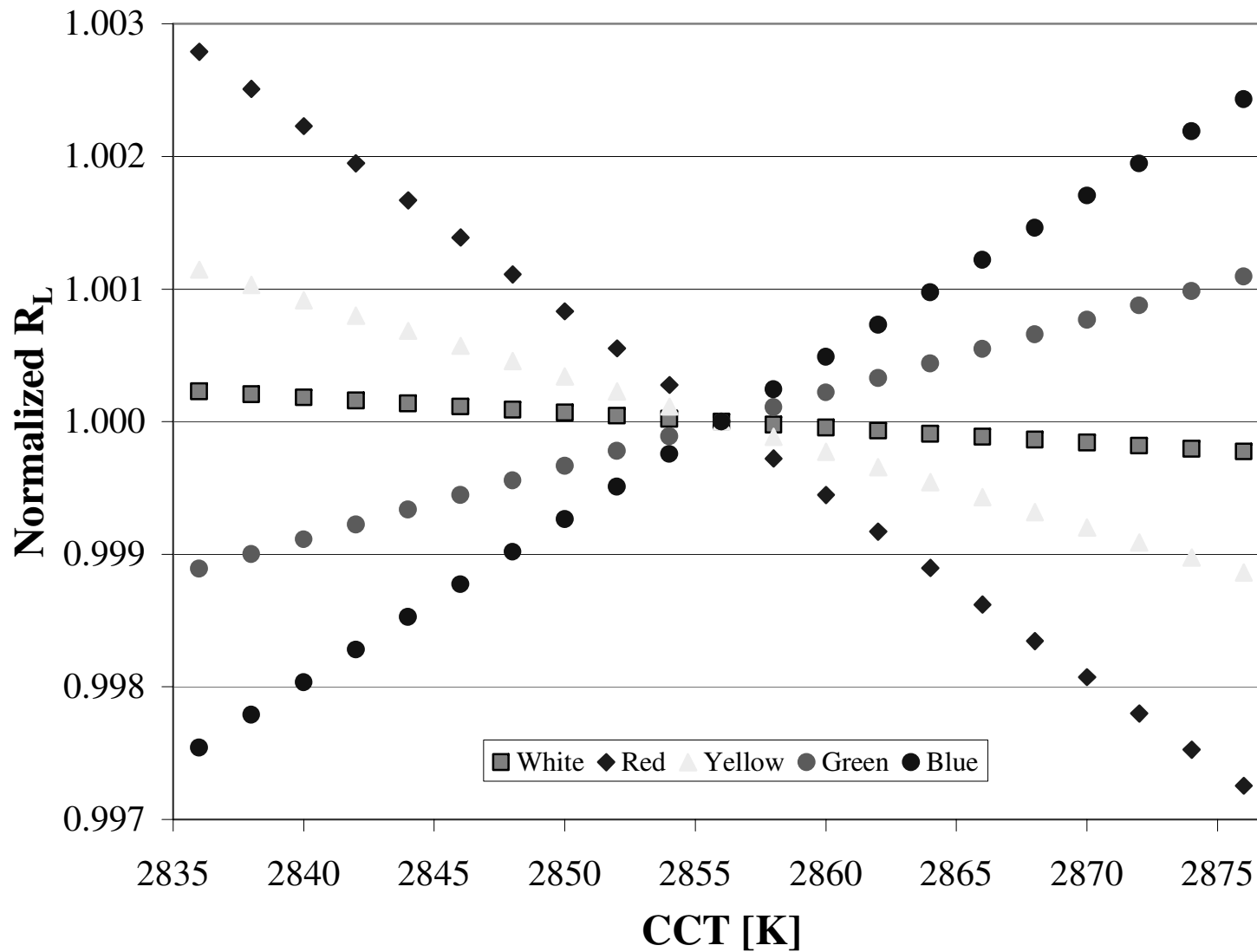
Figure 6 – Shown is the sensitivity curves for different materials with respect to CCT.
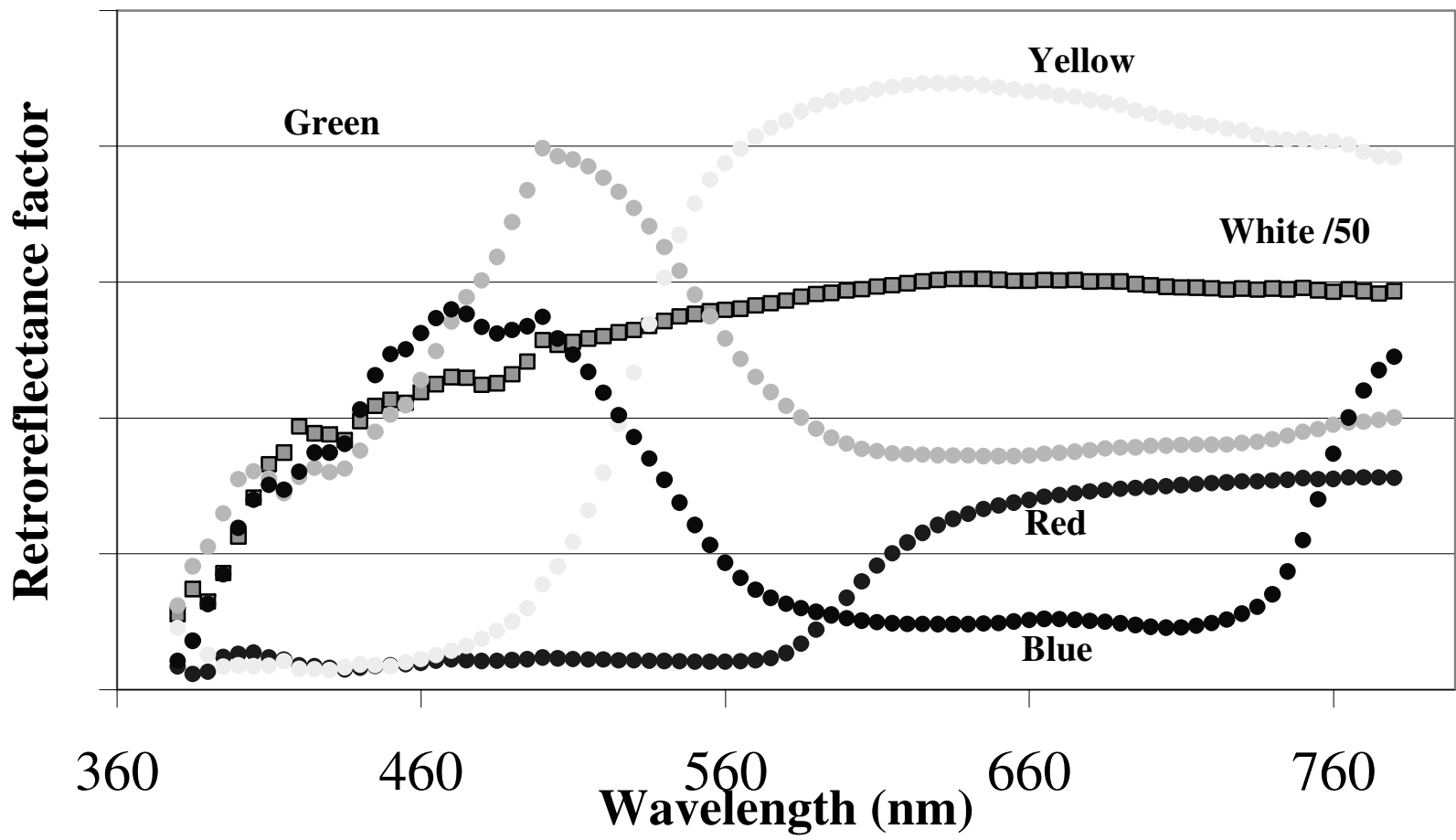
Figure 7 – Shown is the retroreflectance curves used for the CCT sensitivity calculations. The white signal is divided by 50.
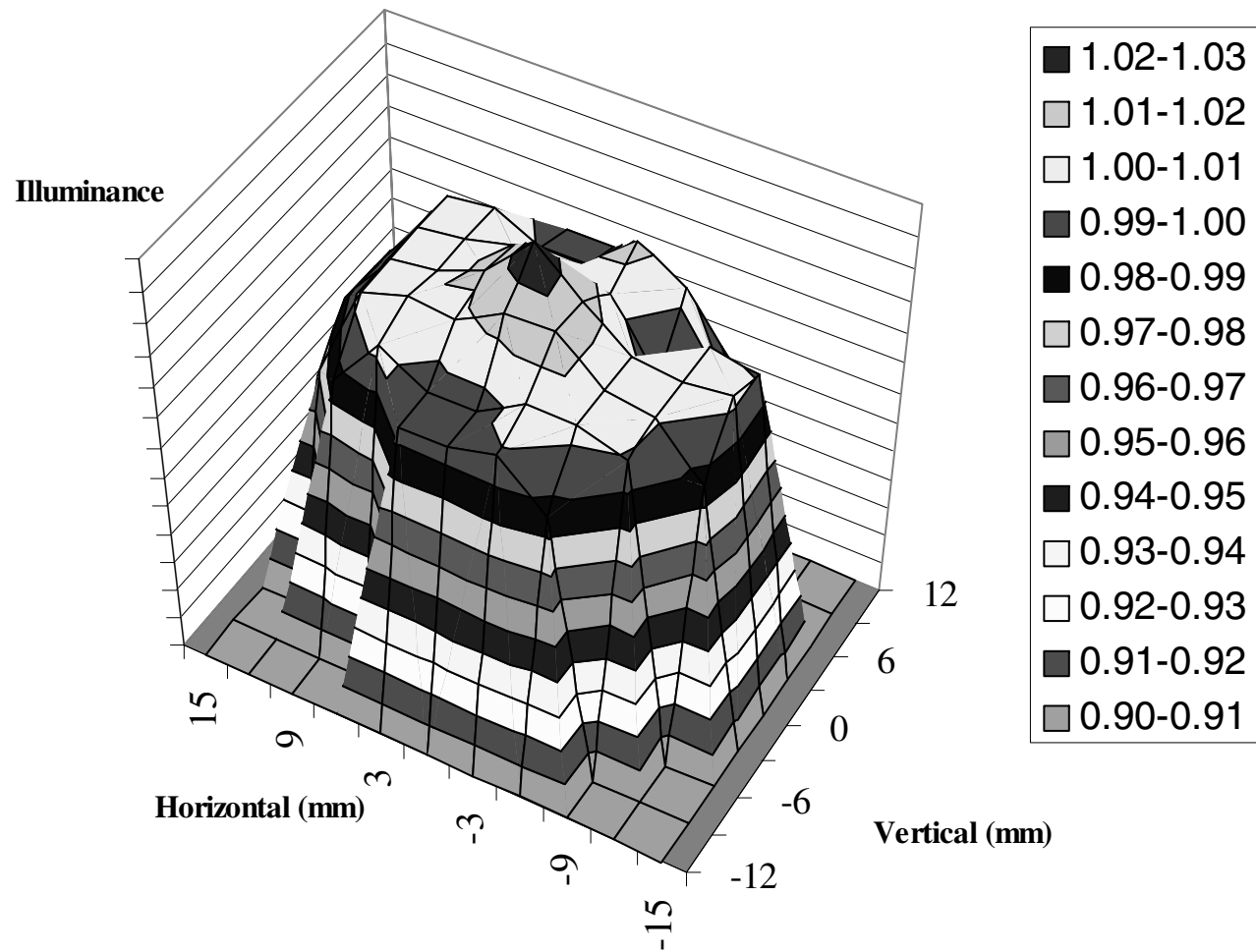
Figure 8 – Shown is the uniformity of the source aperture.
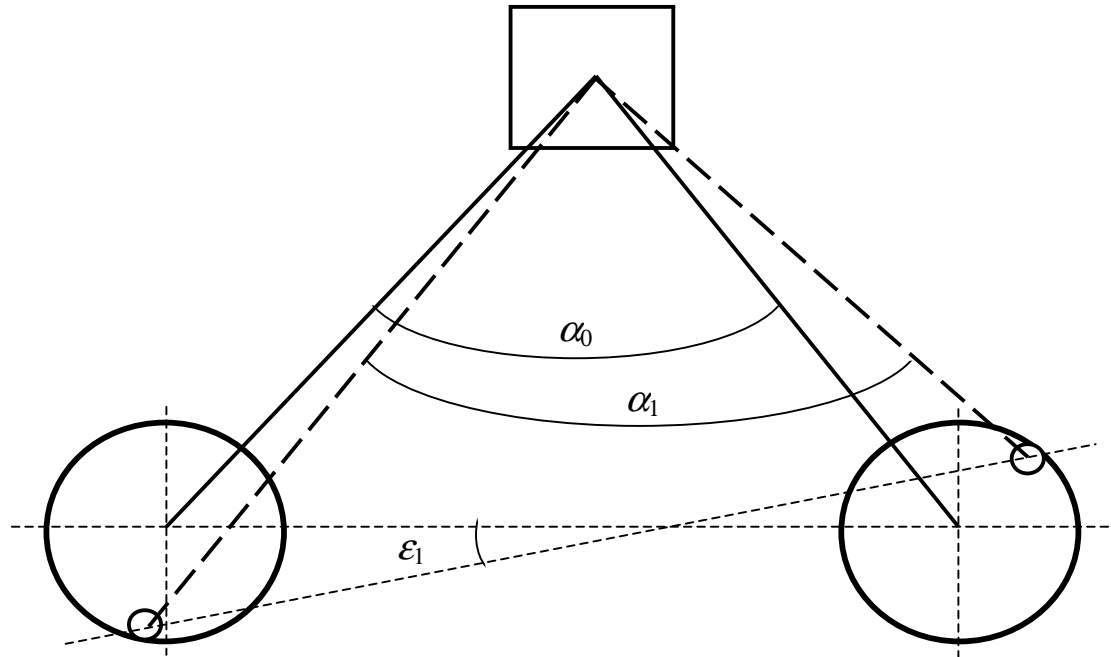
Figure 9 – Shown is a demonstration of the aperture synthesis procedure.
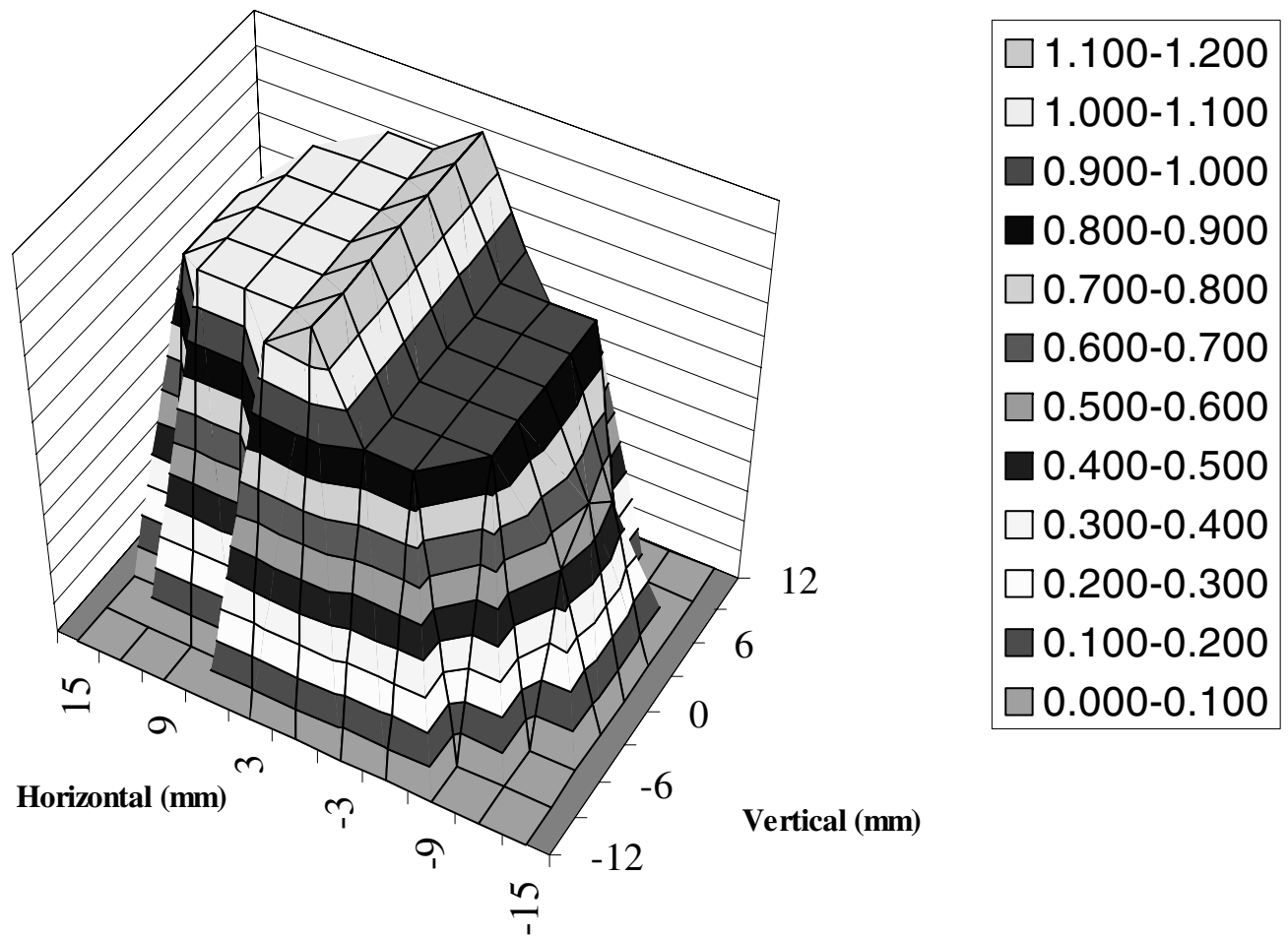
Figure 10 – Shown is the model used in calculating the source aperture uniformity dependence for other systems

.
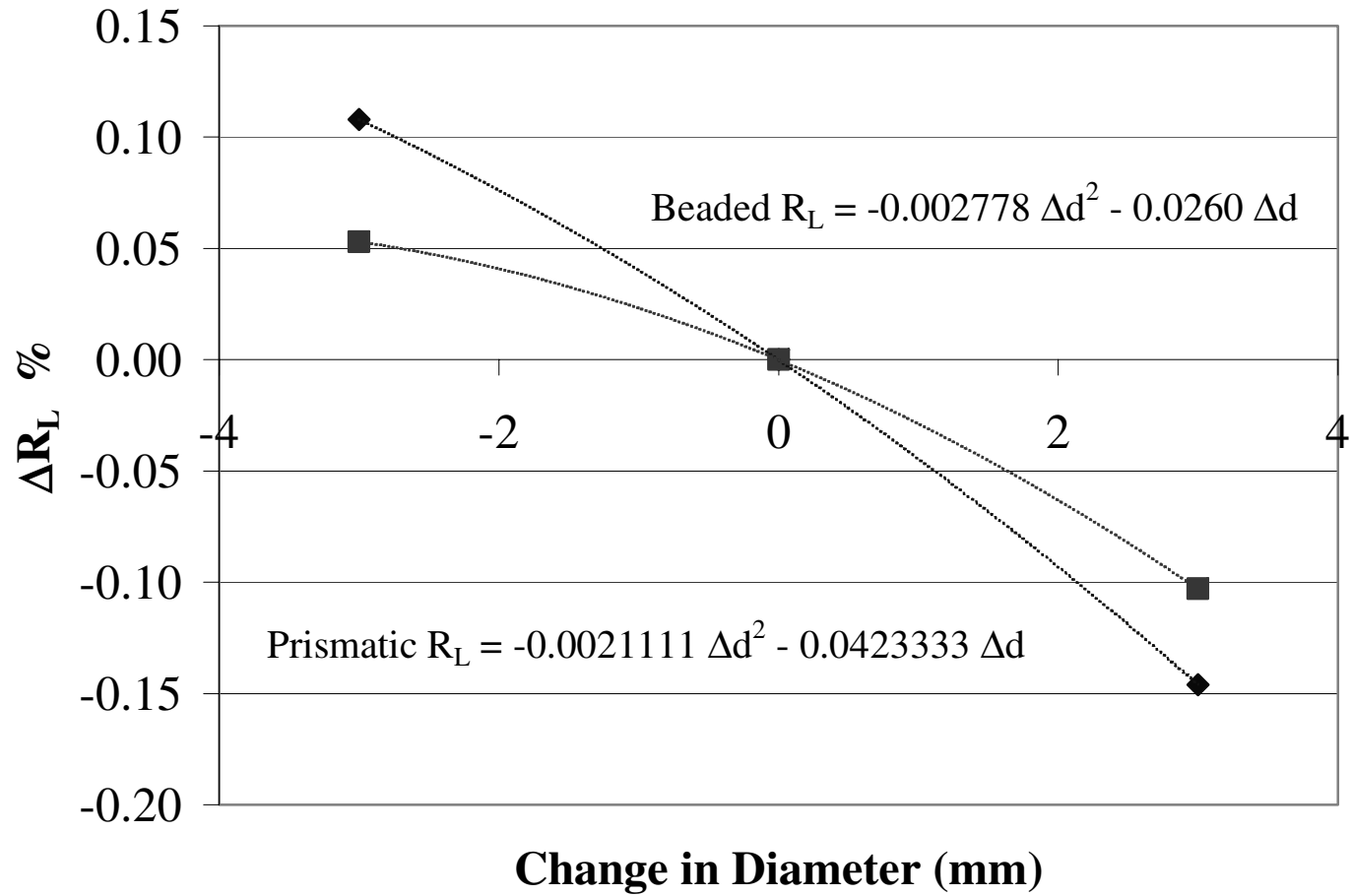
Figure 11 – Presented is the R_L dependence on the source aperture diameter, where the red squares are the beaded material and the blue diamonds are the prismatic material.
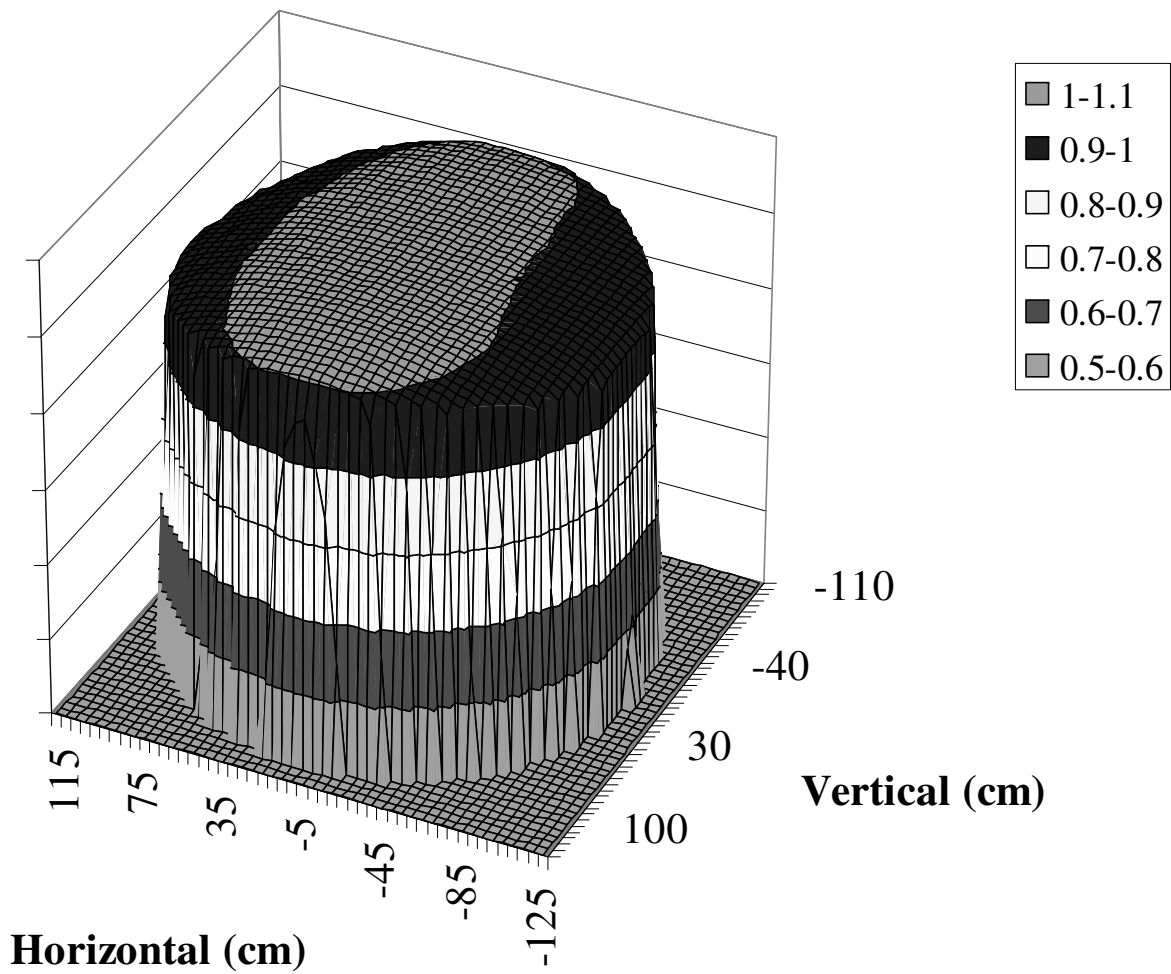
Figure 12 – Shown is the uniformity of the projection system at the retroreflector aperture surface.
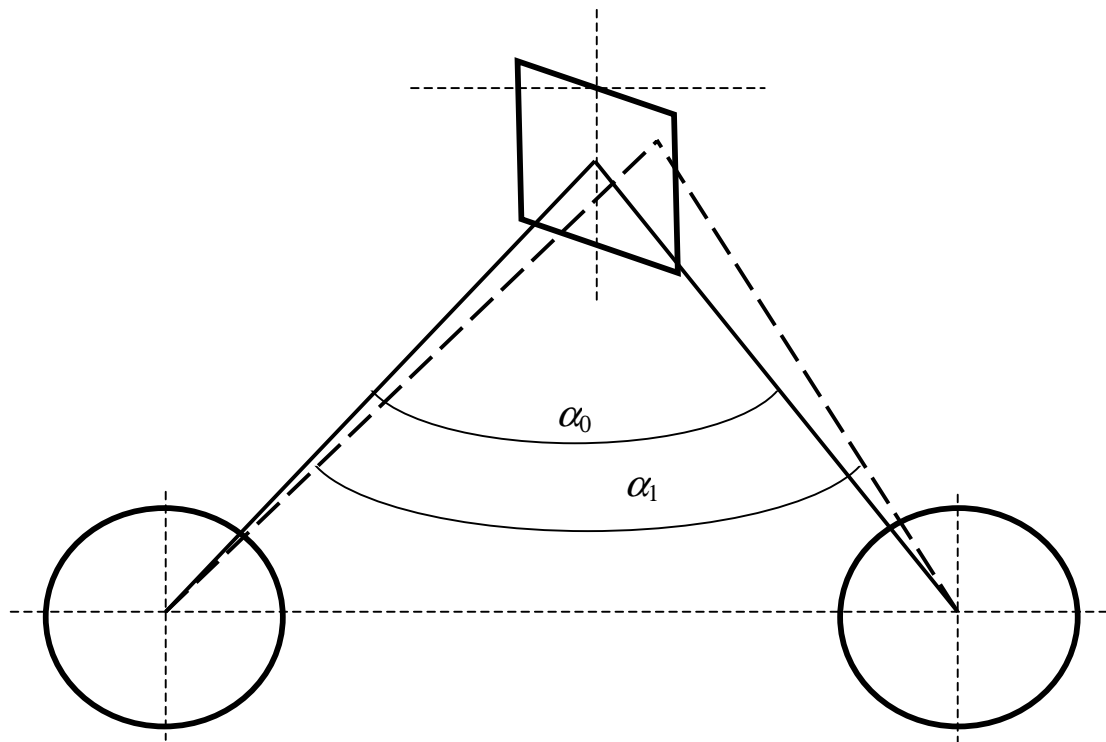
Figure 13 – Shown is a demonstration that the sections of the retroreflective device are illuminated with a different set of angles than the center of the device.
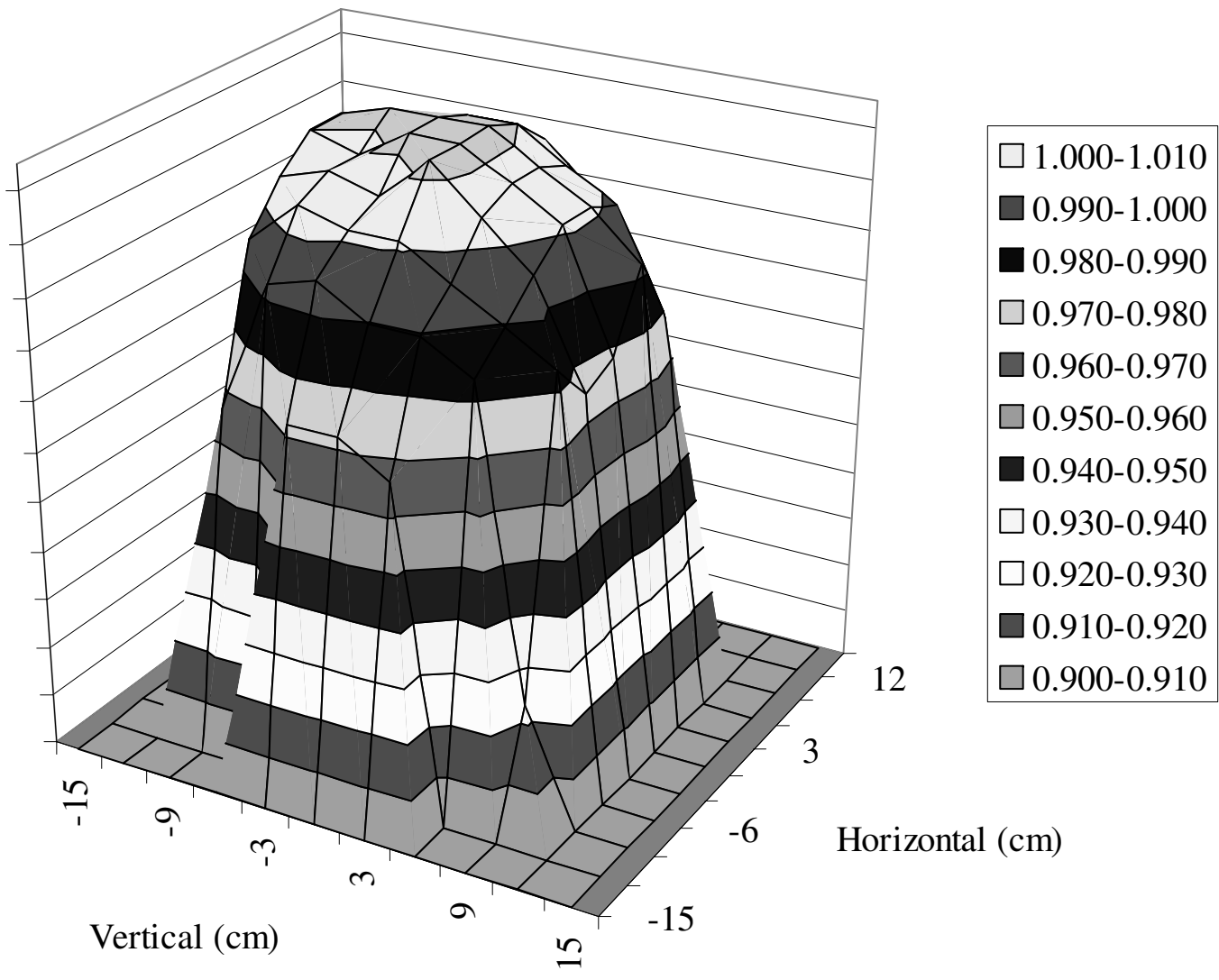
Figure 14 – Shown is the uniformity of the sphere source projection system at the retroreflector aperture surface.

Legend:
- 1.000-1.010
- 0.990-1.000
- 0.980-0.990
- 0.970-0.980
- 0.960-0.970
- 0.950-0.960
- 0.940-0.950
- 0.930-0.940
- 0.920-0.930
- 0.910-0.920
- 0.900-0.910

C. Miller, et. al., Project 05-16
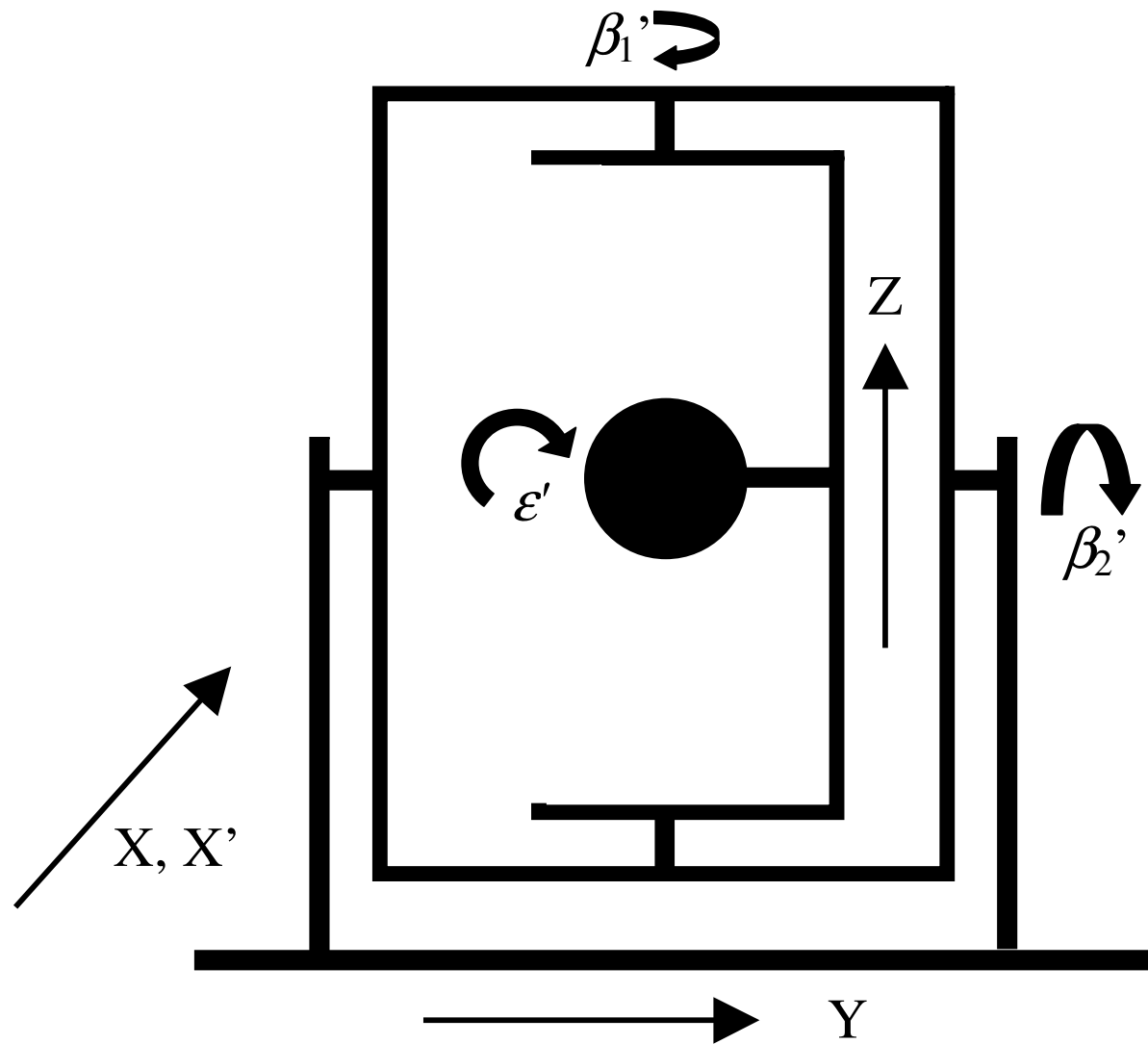
Figure 15 – Shown is a schematic of the goniometer with all the axes labeled.

Figure 16 – Shown is a picture of the goniometer.
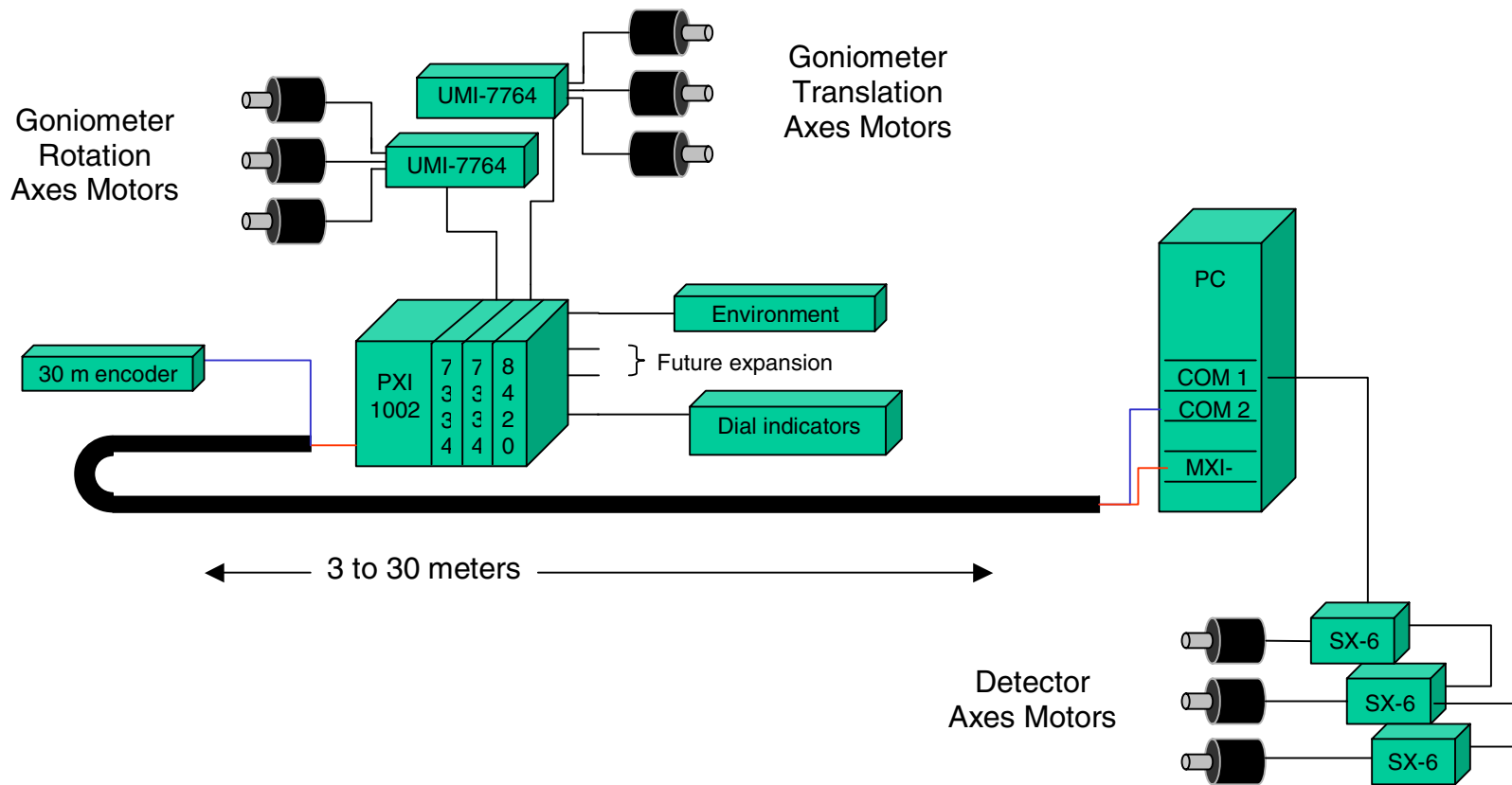
Figure 17 - Shown is a schematic of the goniometer communication system.

C. Miller, et. al., Project 05-16
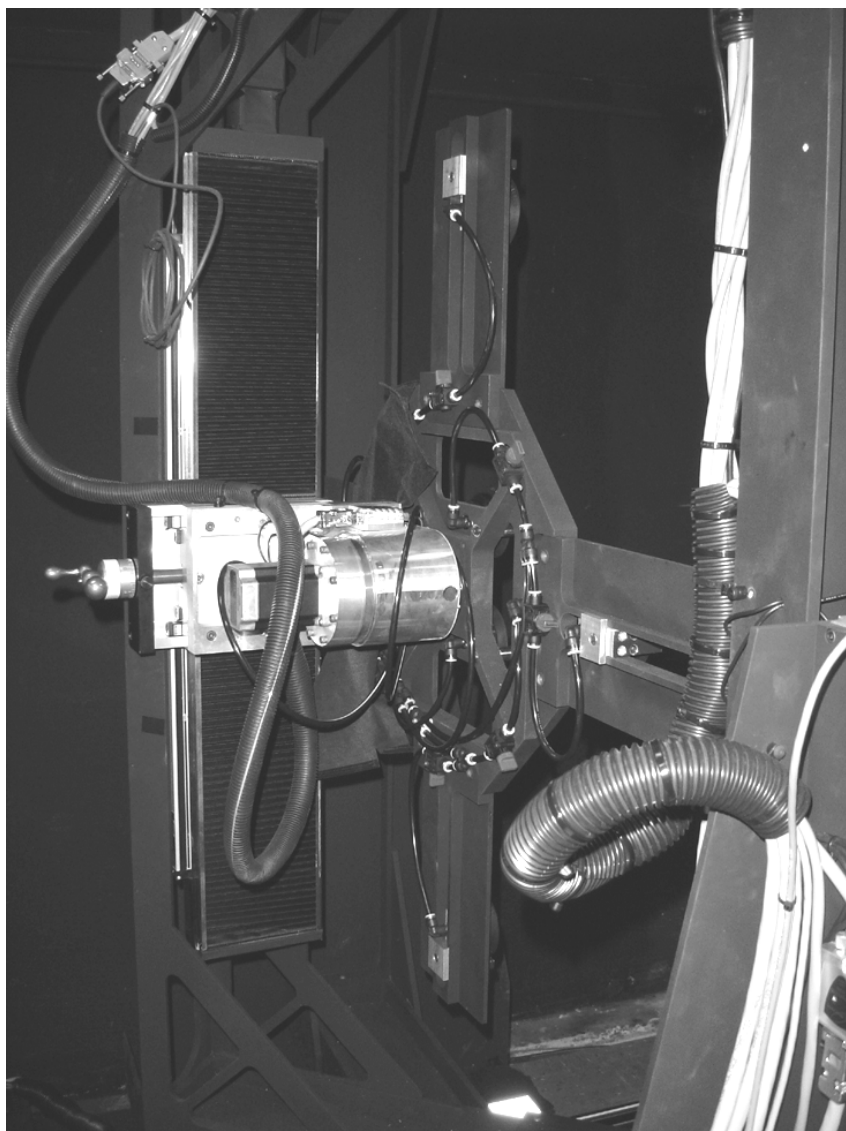
Figure 18 – Shown is the rotation axis of the goniometer.
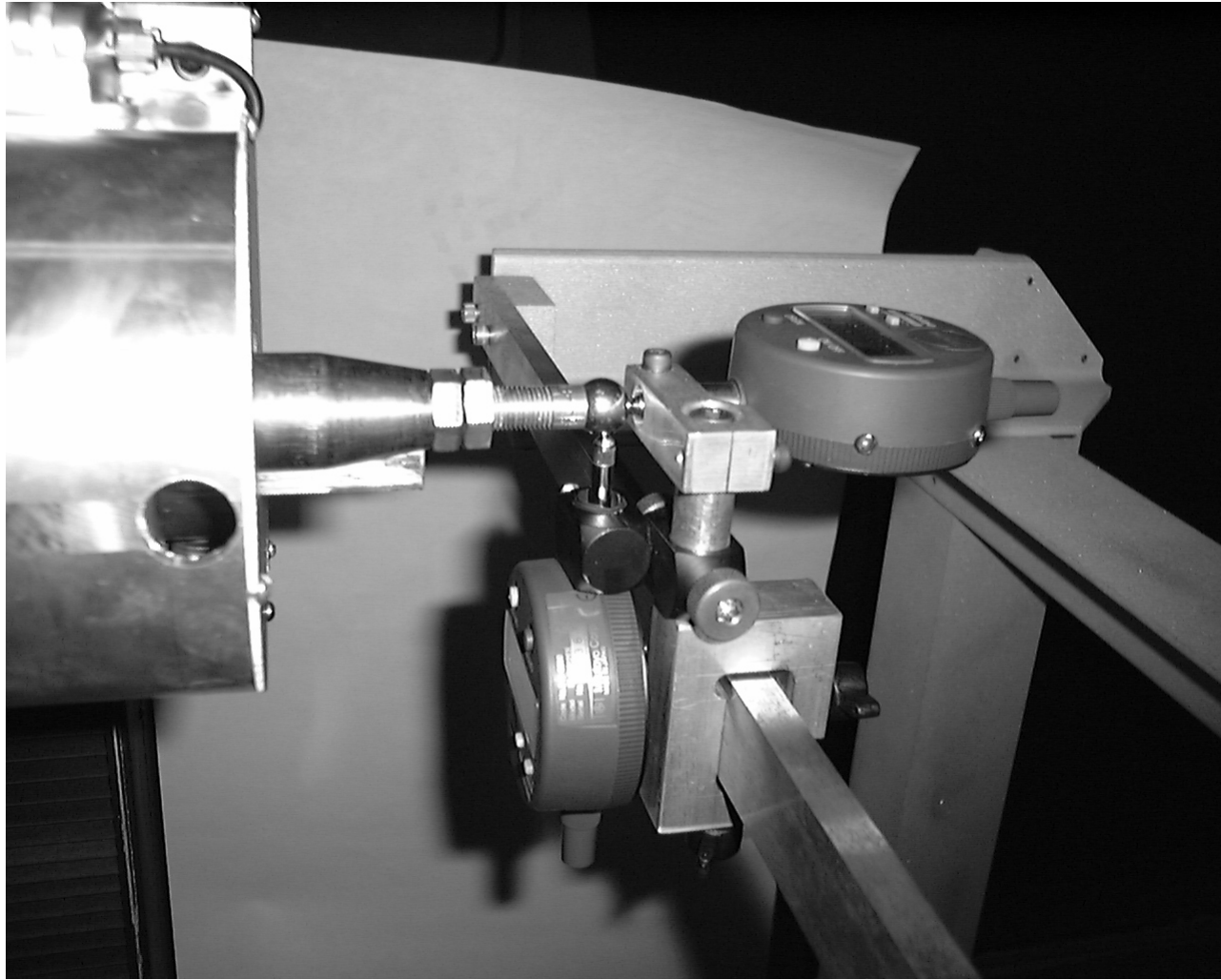
Figure 19 – Shown is the ball tool mounted in the goniometer.
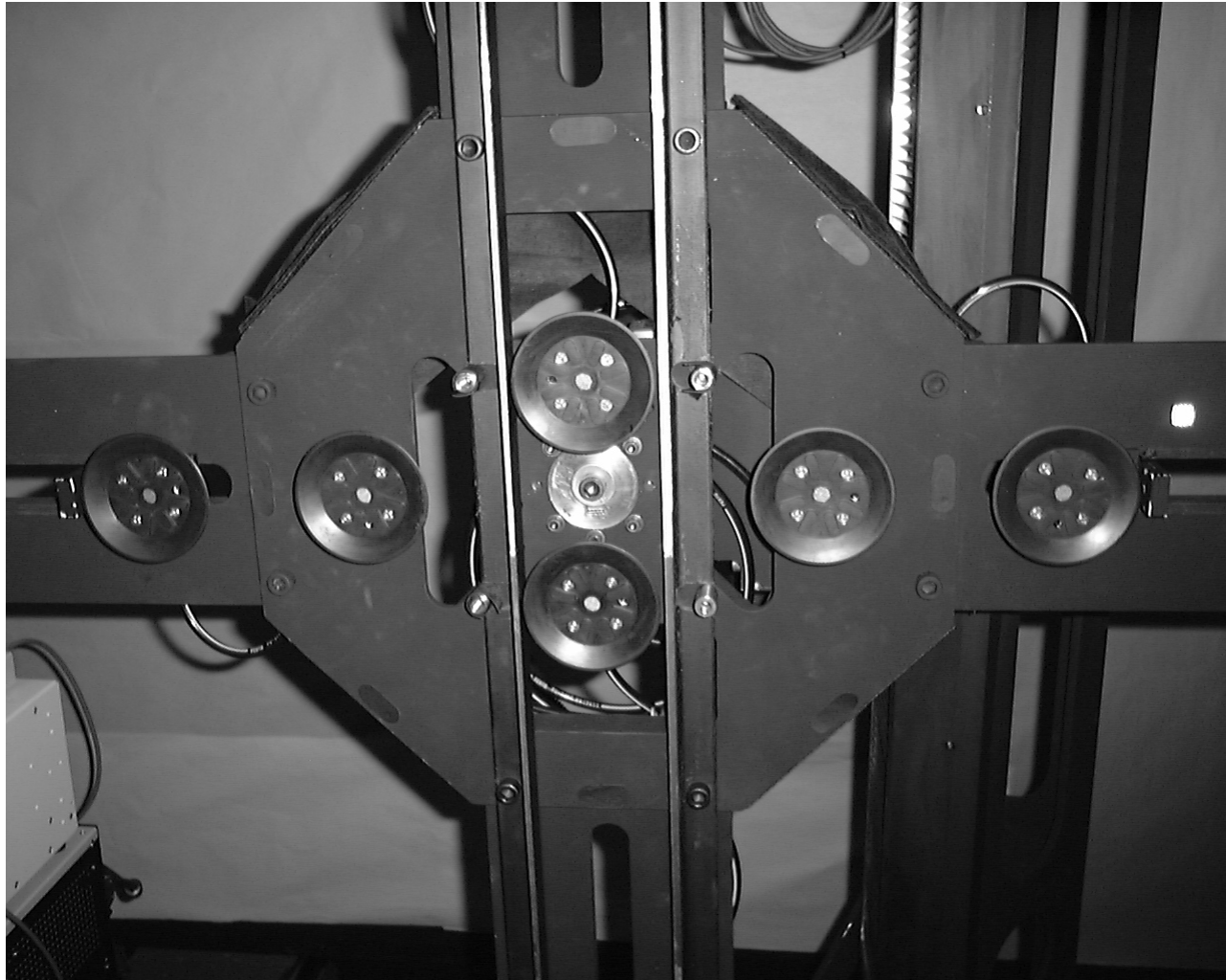
Figure 20 – Shown is the front of the vacuum mount.
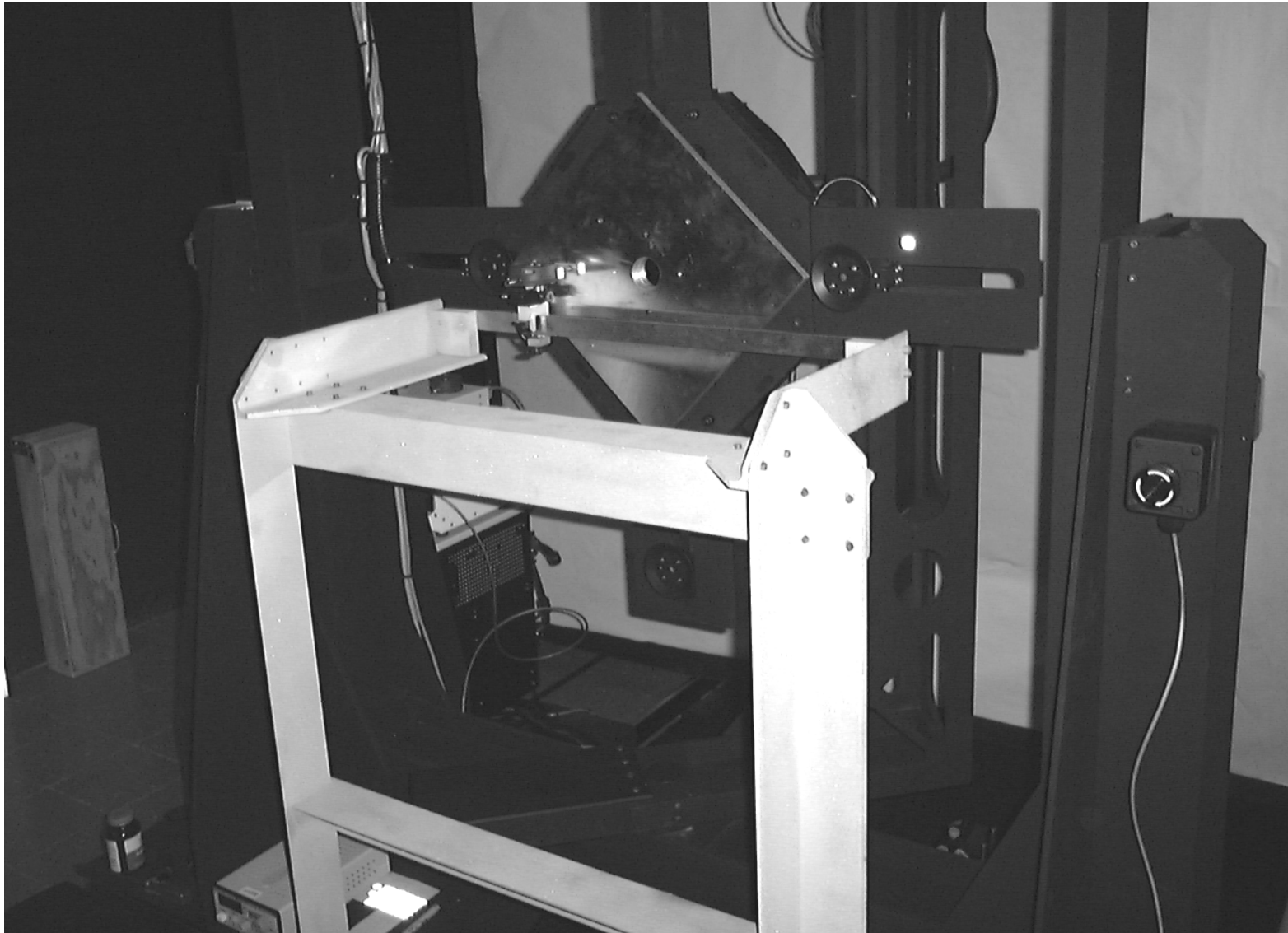
Figure 21 – Shown is the alignment tool in position with a sample mounted.

Figure 22 – Shown is a section of the rail system.
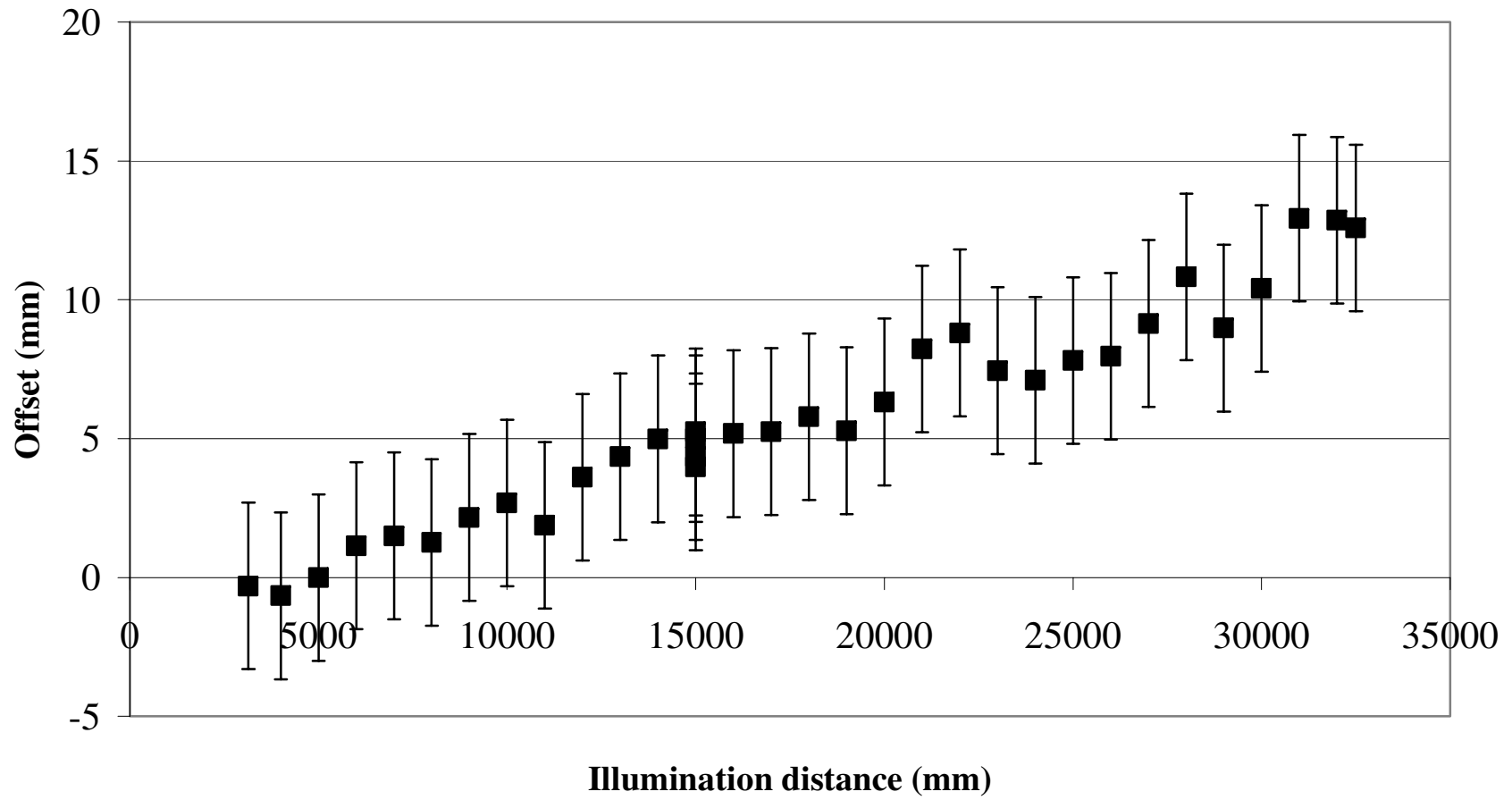
Figure 23 – Shown is the theodolite distance minus the magnetic encoder distance.
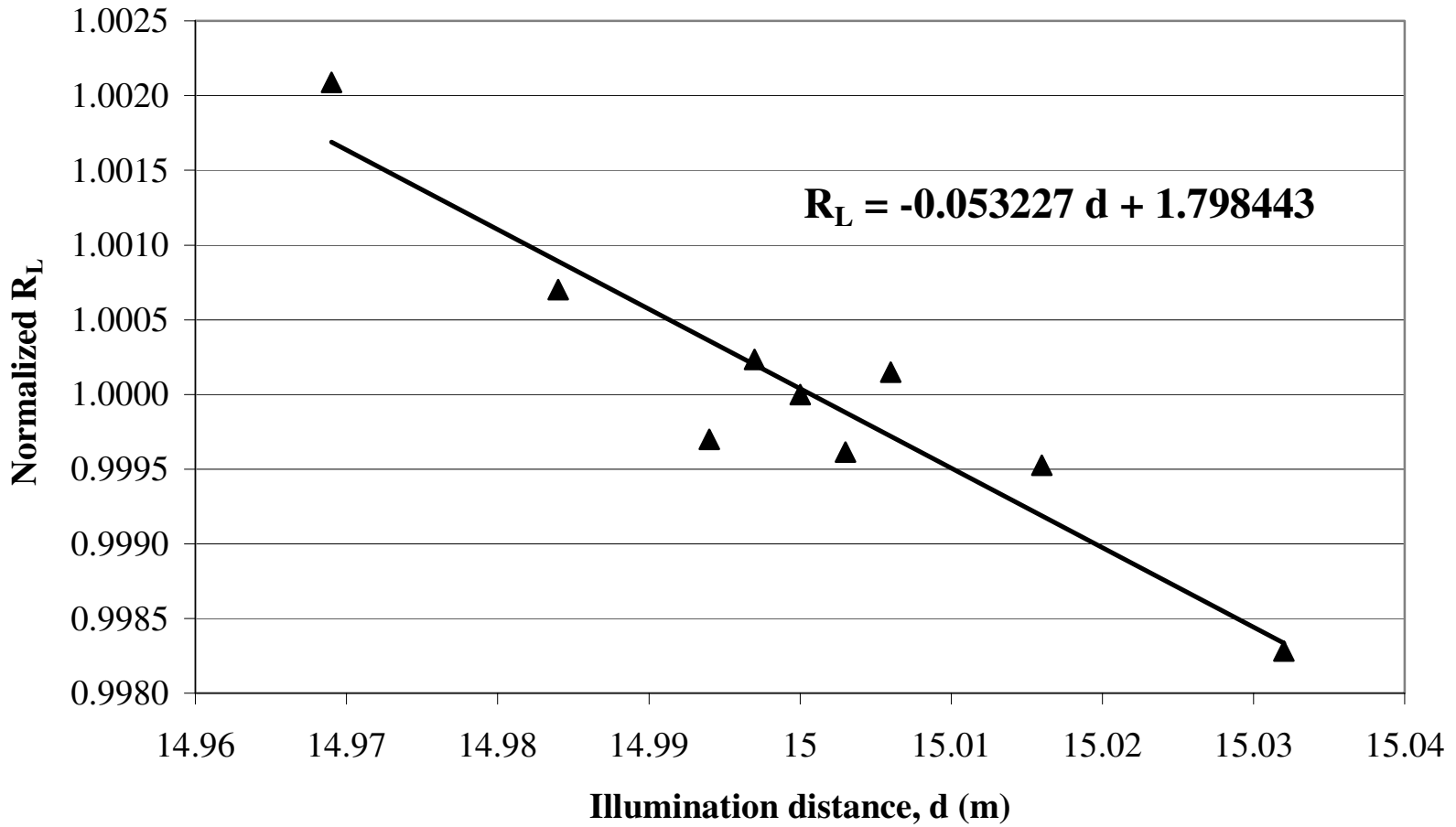
Figure 24 – Shown is the change in R_L dependent on the illumination distance.
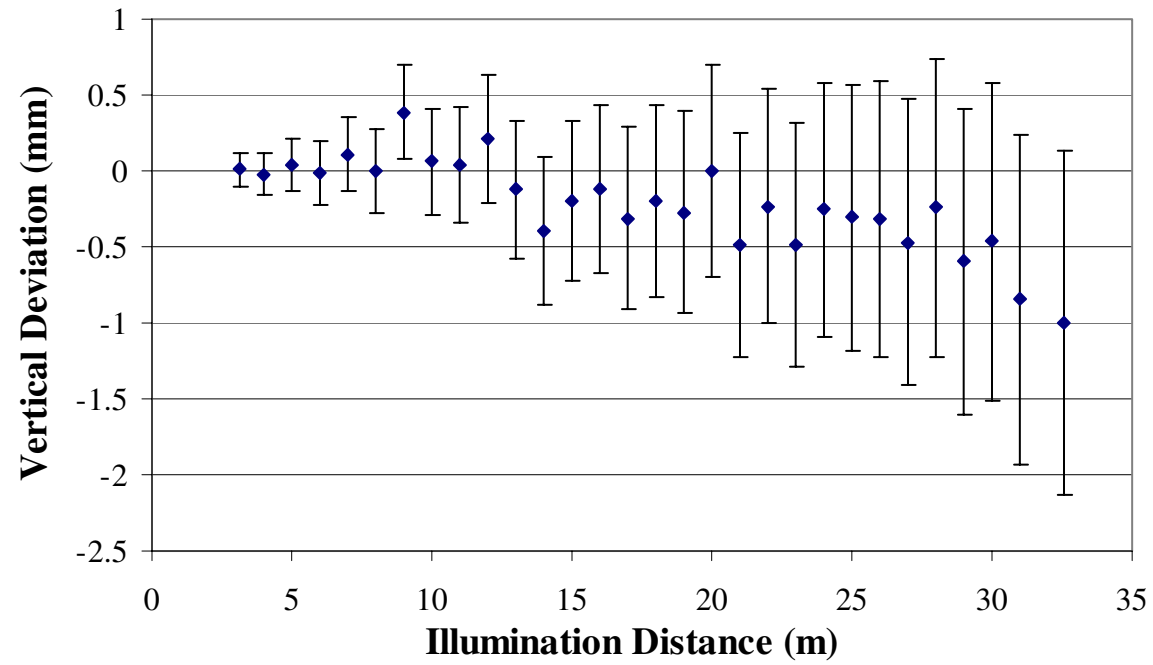
Figure 25 – Shown is the vertical deviation of the sample holder compared to the illumination axis.
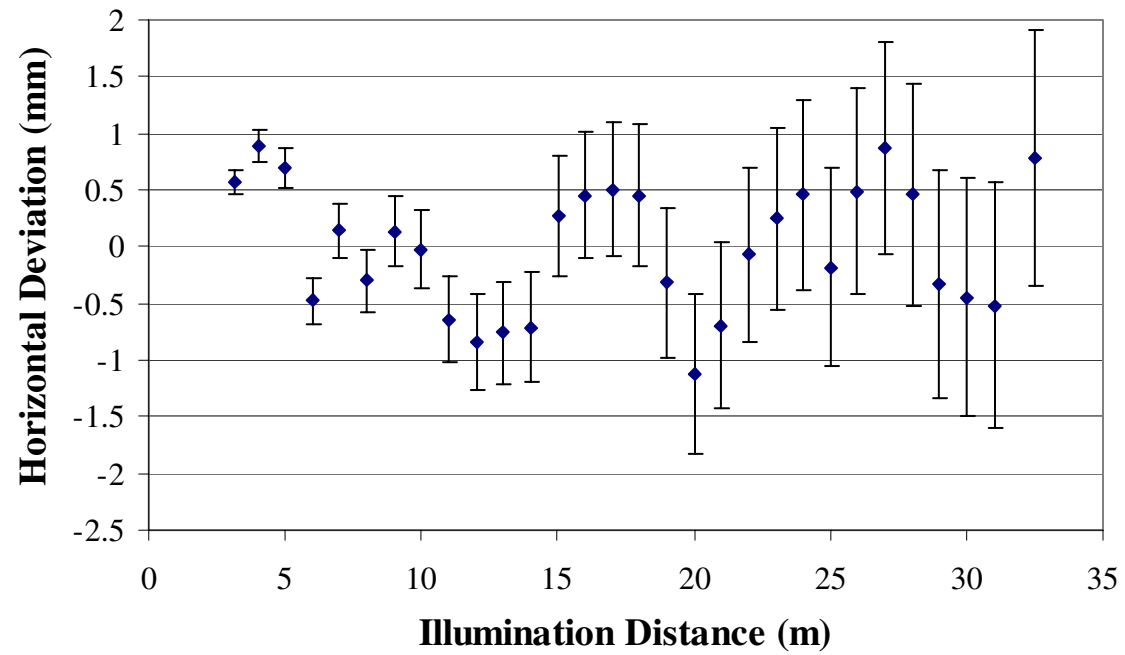
Figure 26 – Shown is the horizontal deviation of the samples holder compared to the illumination axis.
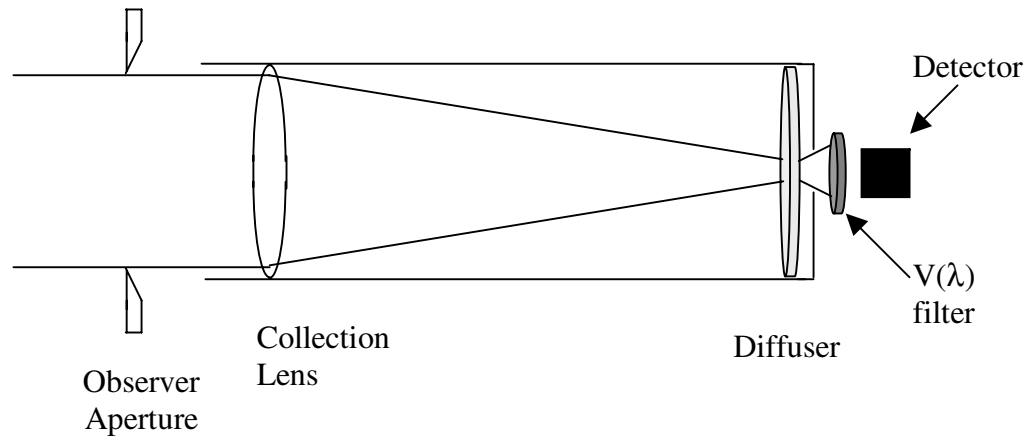
Figure 27 – Presented is a schematic of the photometric detection system.
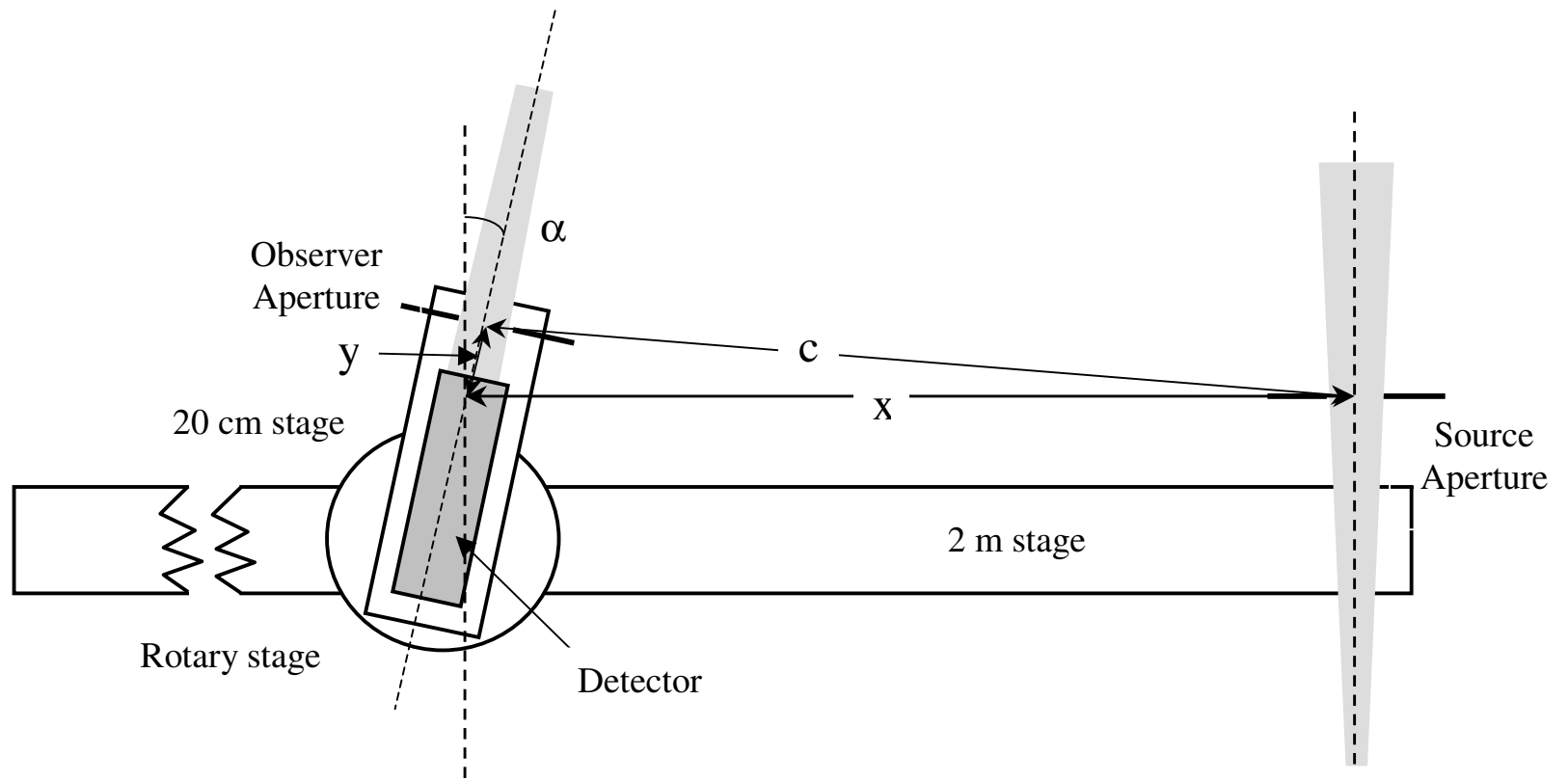
Figure 28 – Presented is a schematic of the observation angle positioner.
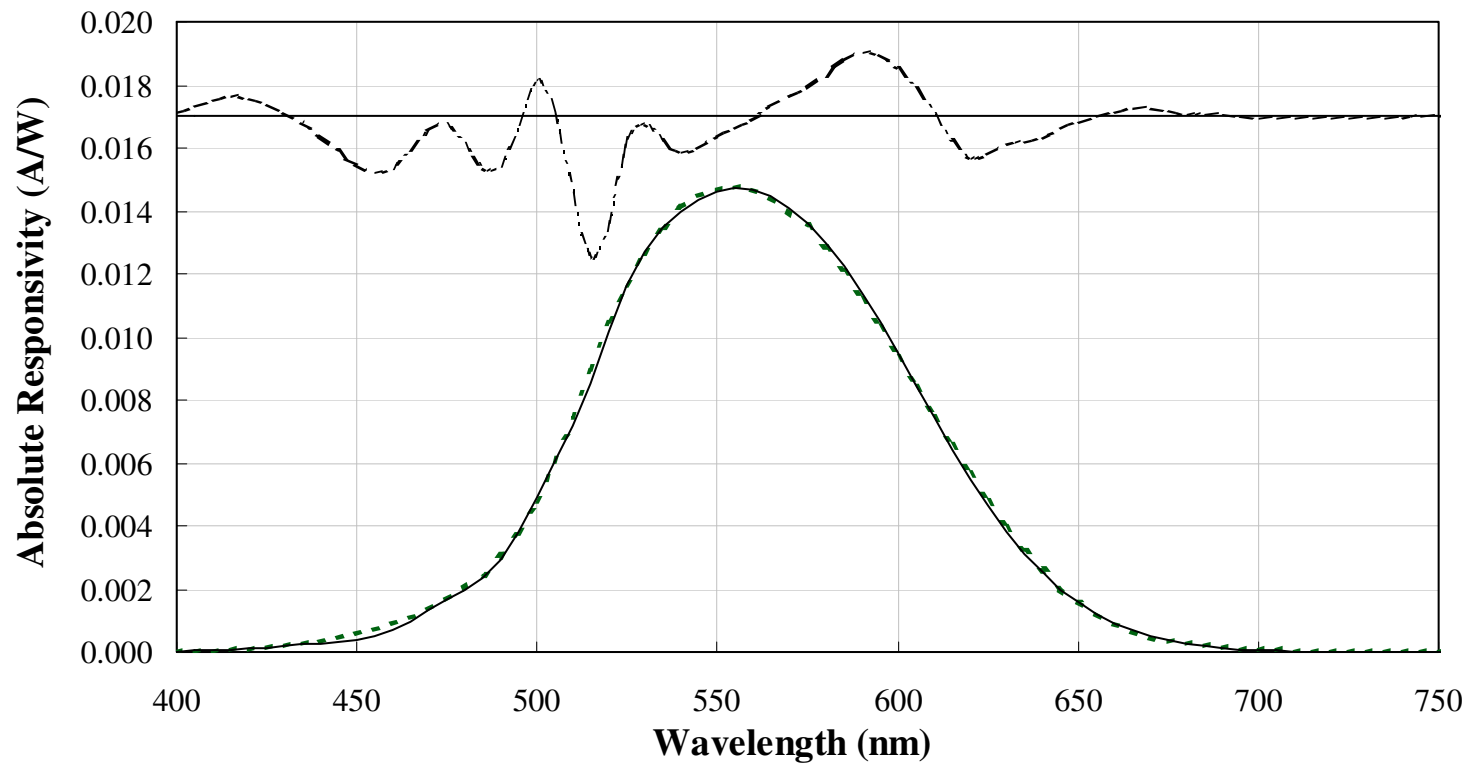
Figure 29 – Shown is the spectral responsivity of the photometric detection system (solid) versus the CIE $V(\lambda)$ function (dotted). The dashed line at the top shows the difference between the two curves multiplied by 10.
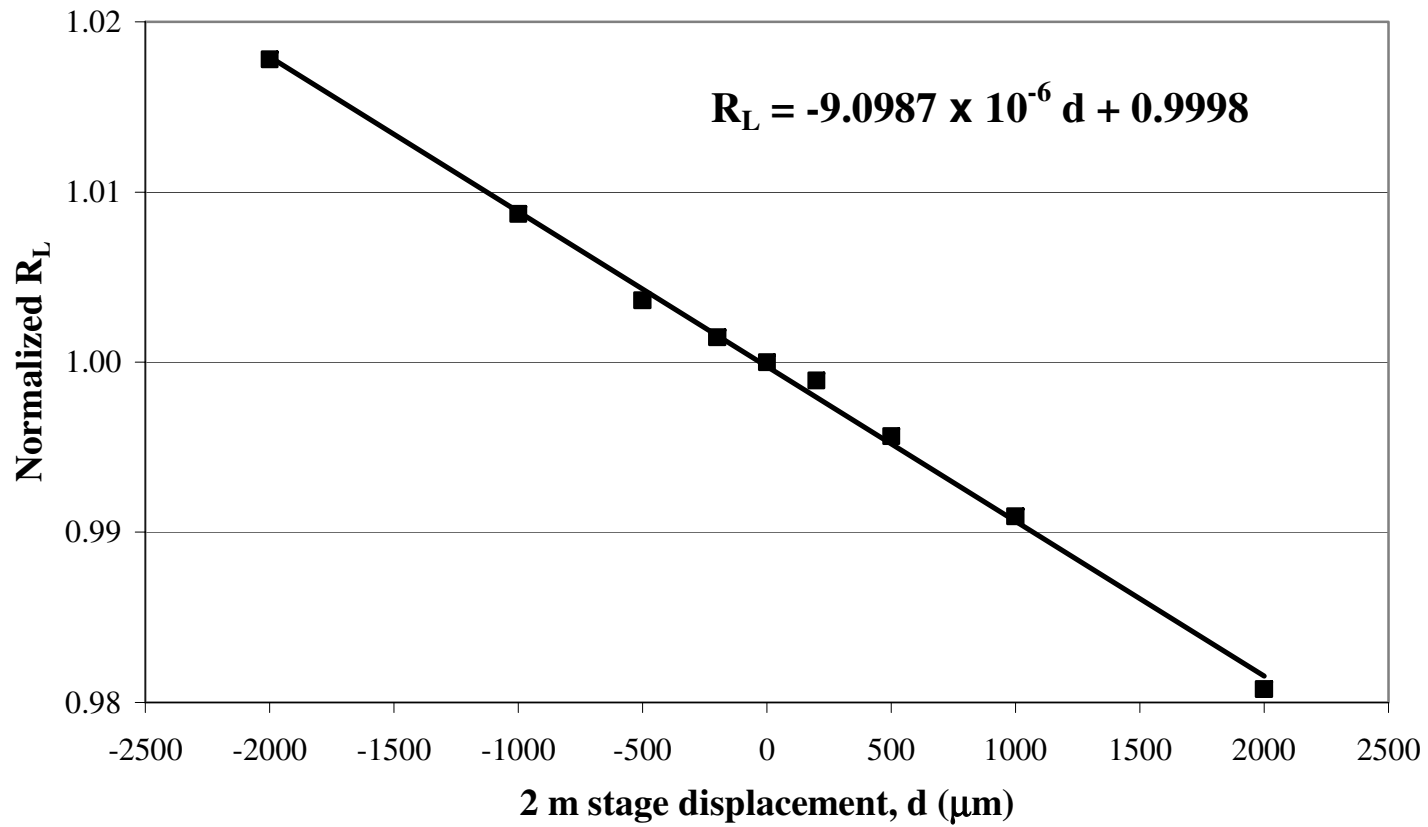
Figure 30 – Shown is the change in R_L dependent on the 2 m axis positioning.
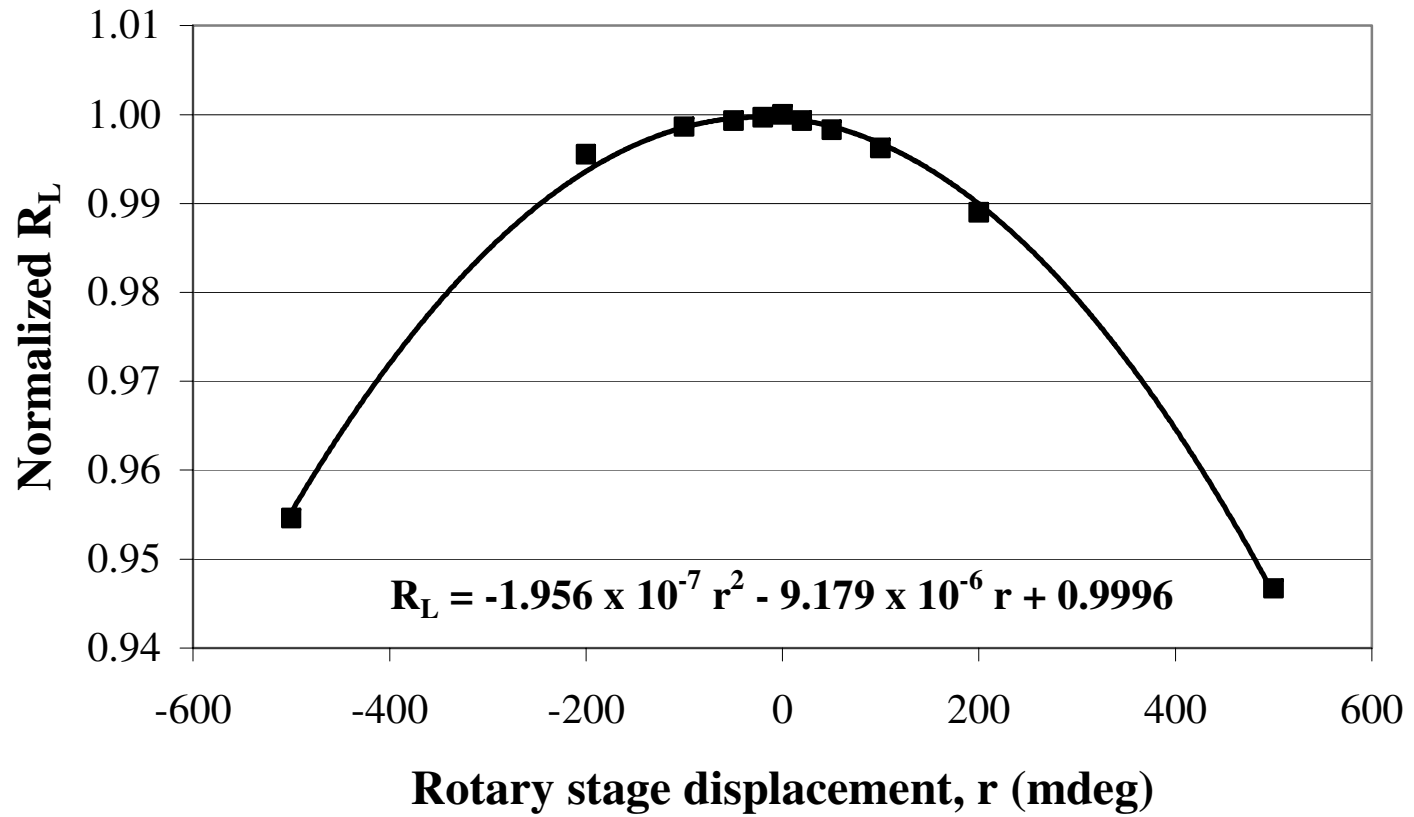
Figure 31 – Shown is the change in R_L dependent on the rotary stage positioning.

$$R_L = -1.956 \times 10^{-7} \, r^2 - 9.179 \times 10^{-6} \, r + 0.9996$$
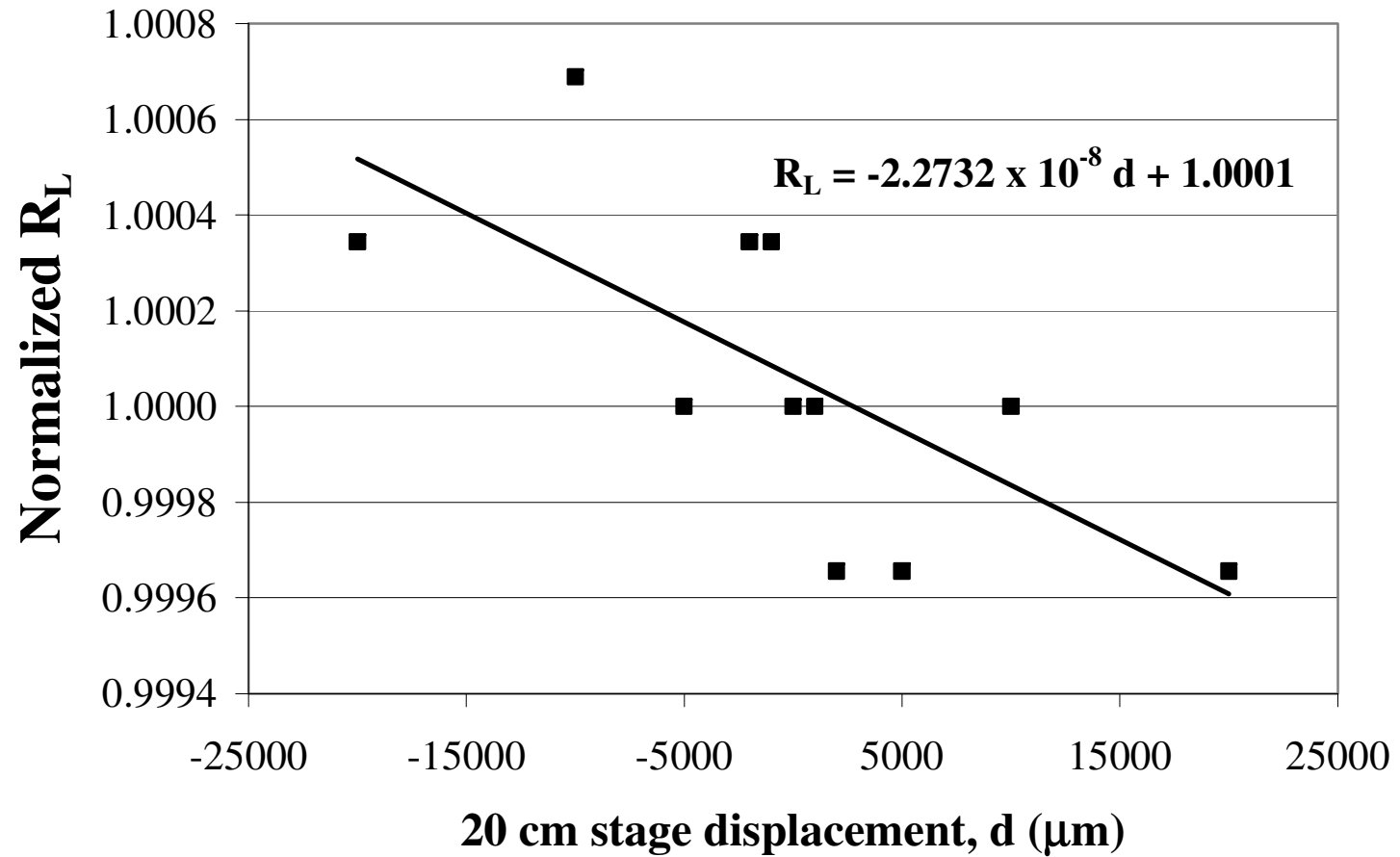
Figure 32 – Shown is the change in R_L dependent on the 20 cm axis positioning.
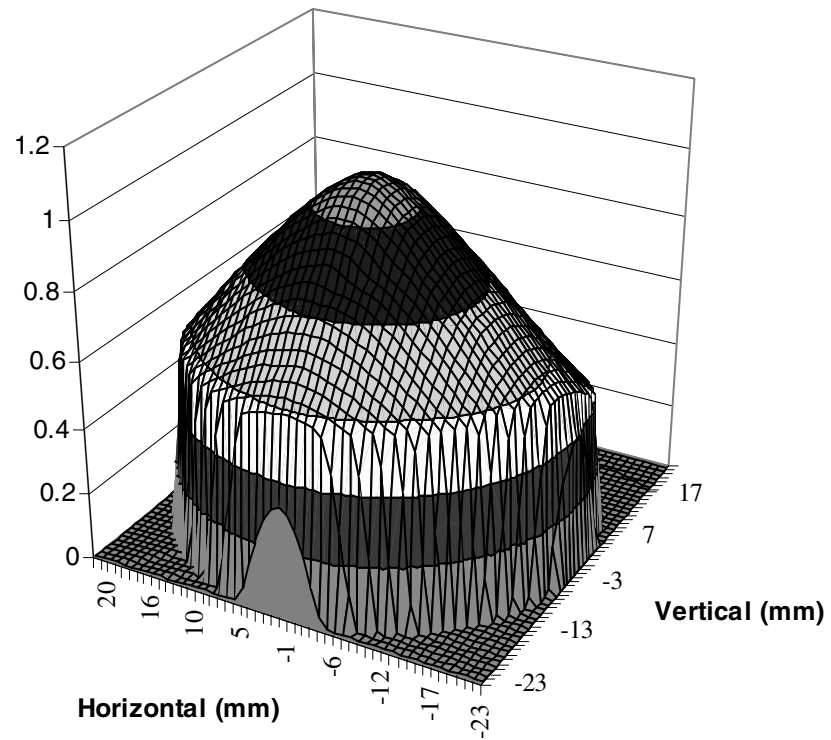
Figure 33 – Presented is the response uniformity of the photometric detection system.
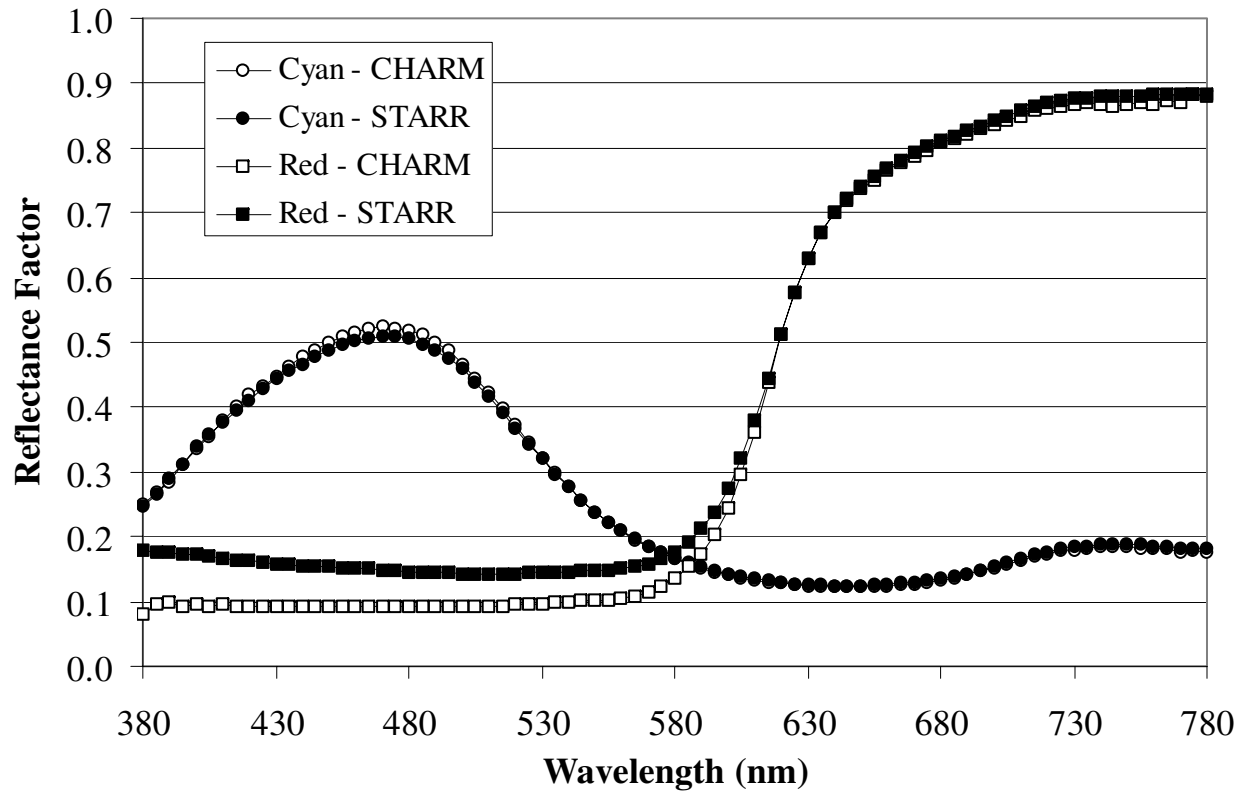
Figure 34 – Sample CHARM and STARR spectra for BCRA tiles.
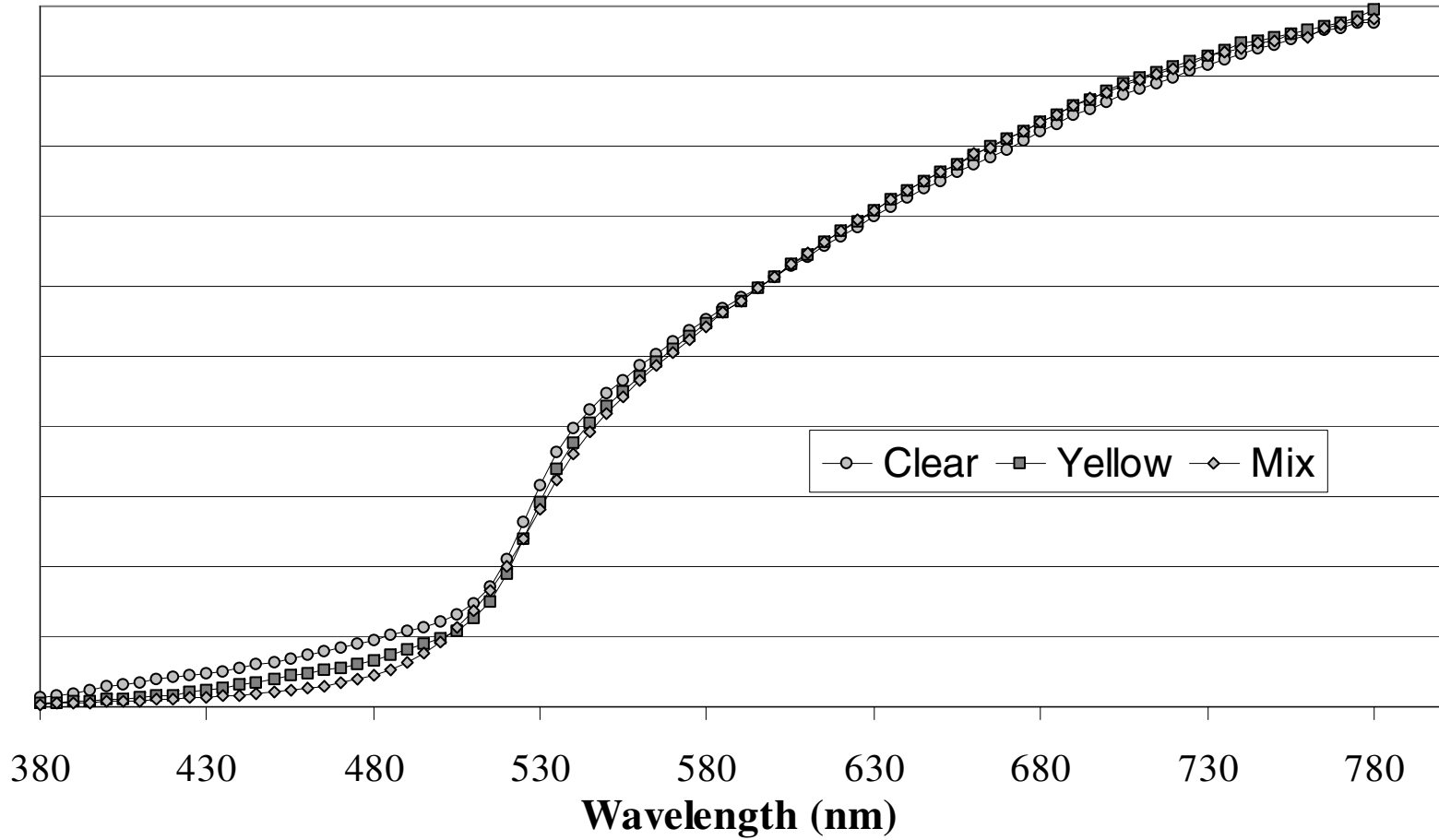
Figure 35 – Shown is three spectra using the corrected diode array system.
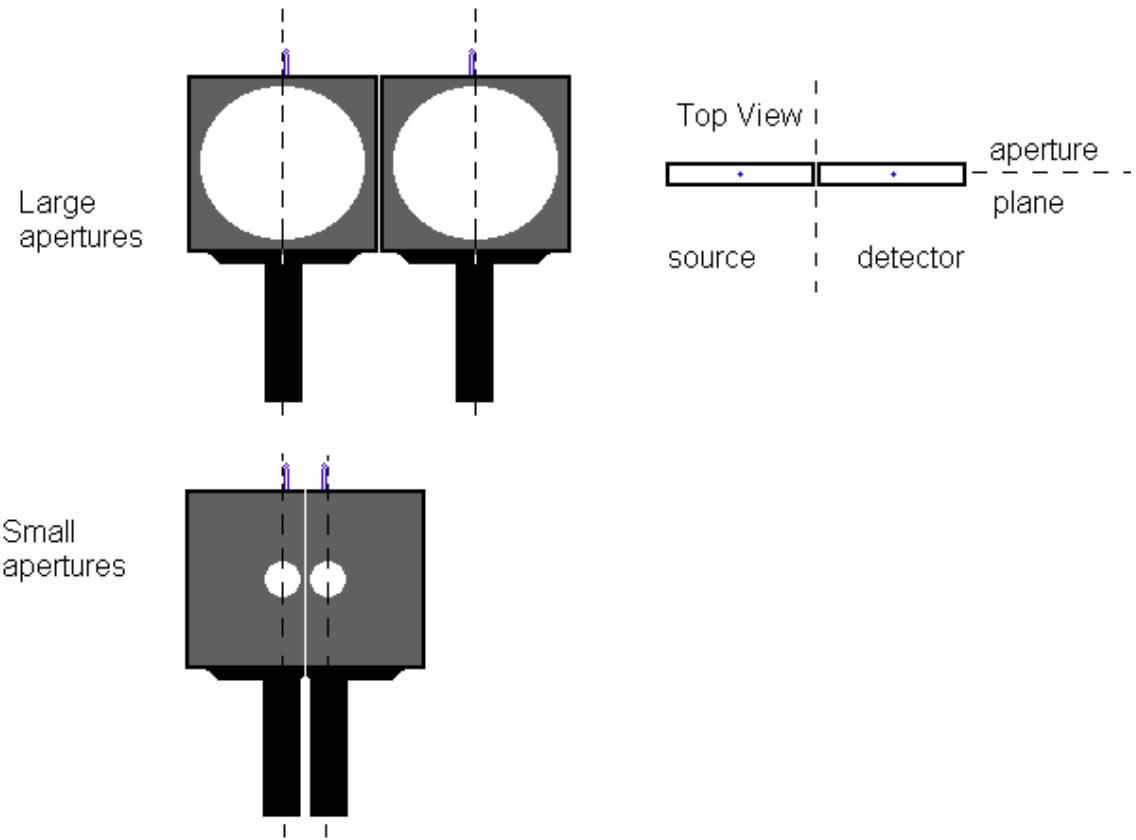
Figure 36 – Aperture holders with large and small apertures

sample

detector aperture at αmax

detector aperture at αmin

source table

theodolite

ε

image of sample through theodolite
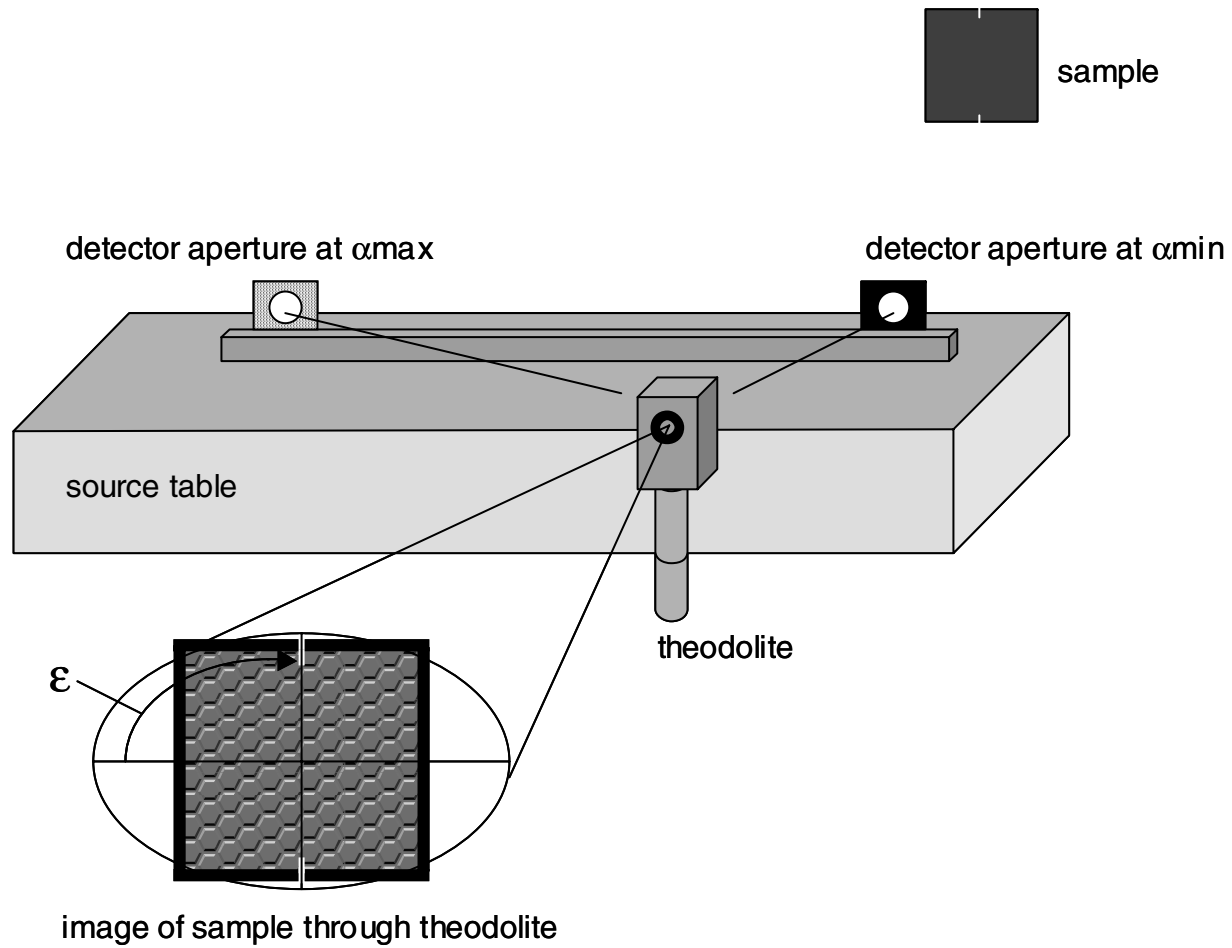
Figure 37 – Alignment of rotation angle
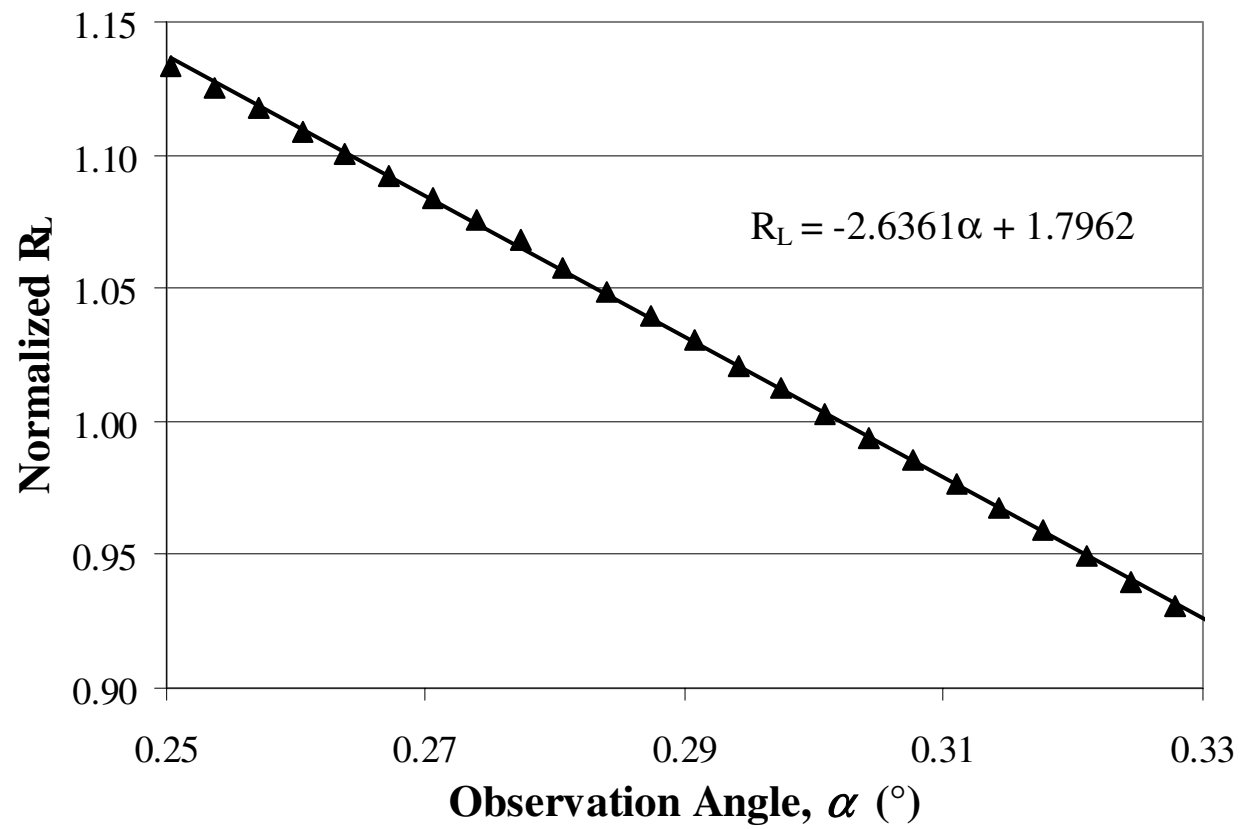
Figure 38 – Shown is the change in R_L dependent on the observation angle for a white encapsulated lens signage material.

The plotted equation is:

$$R_L = -2.6361\alpha + 1.7962$$
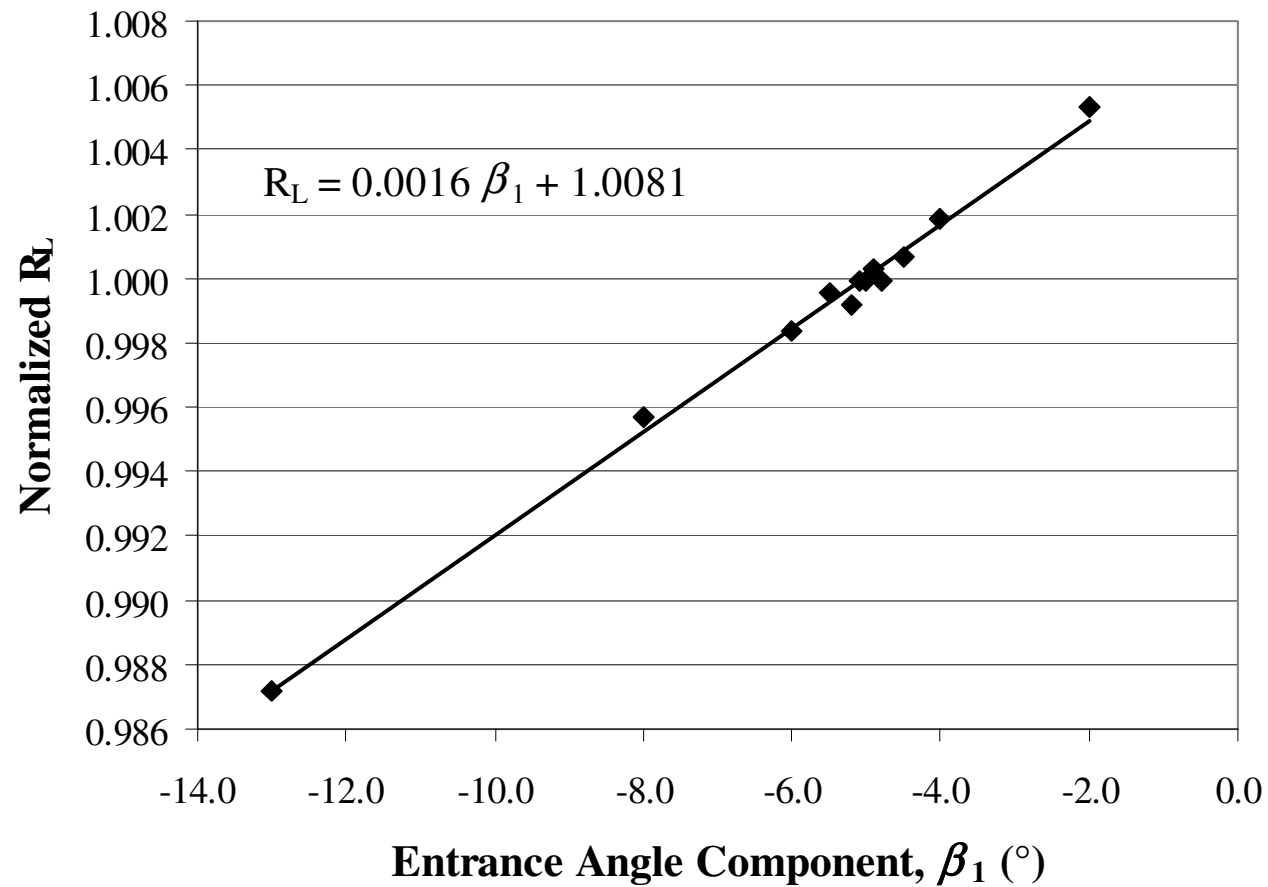
Figure 39 – Shown is the change in R_L dependent on the first entrance angle component for a white encapsulated lens signage material.

$$R_L = -4.7841 \times 10^{-5} \beta_2^{2} + 1.9139 \times 10^{-4} \beta_2 + 1.00036$$
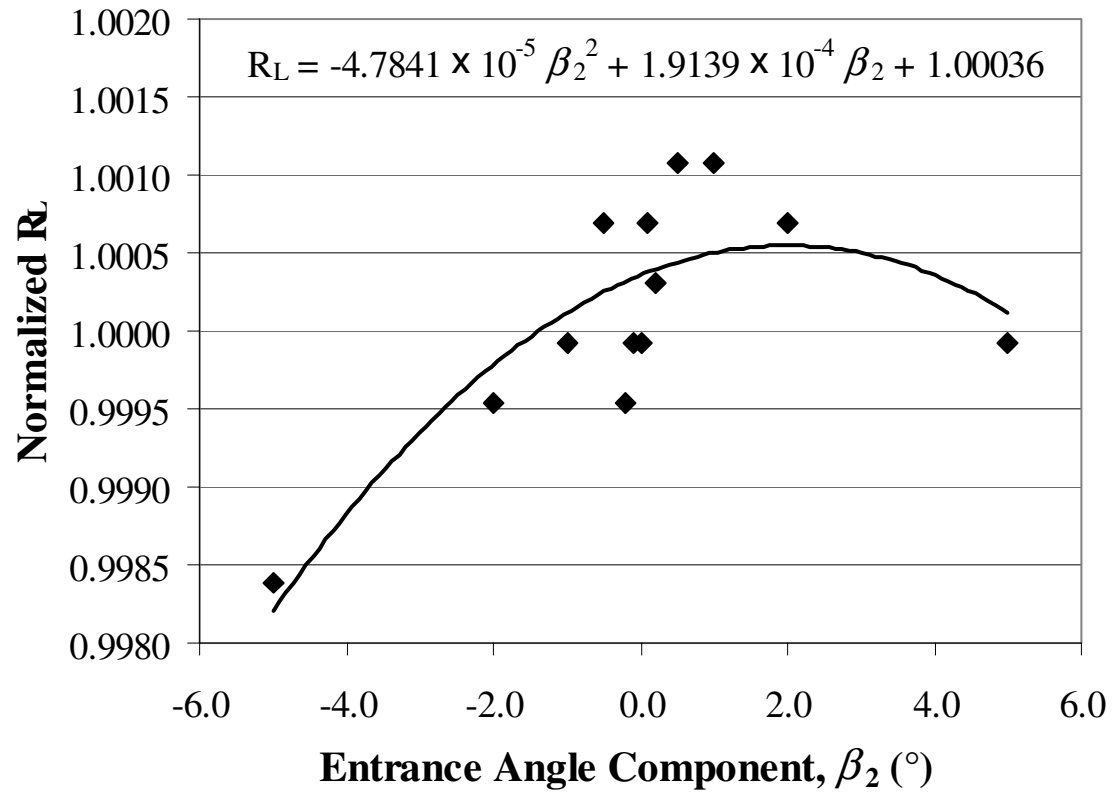
Figure 40 – Shown is the change in R_L dependent on the second entrance angle component for a white encapsulated lens signage material.
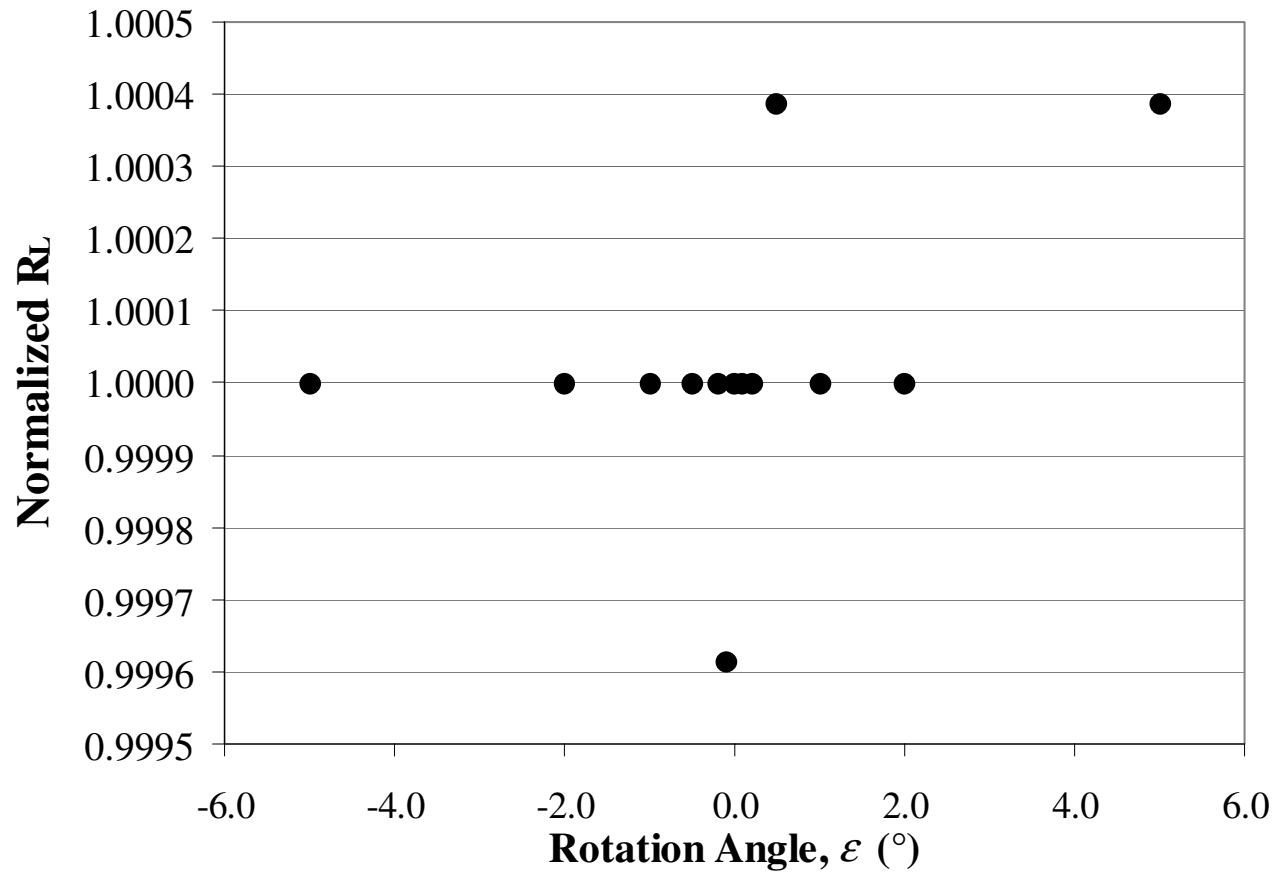
Figure 41 – Shown is the change in R_L dependent on the rotation angle for a white encapsulated lens signage material.

Figure 42 – Shown is the set of retroreflective samples used in the MAP service originally.
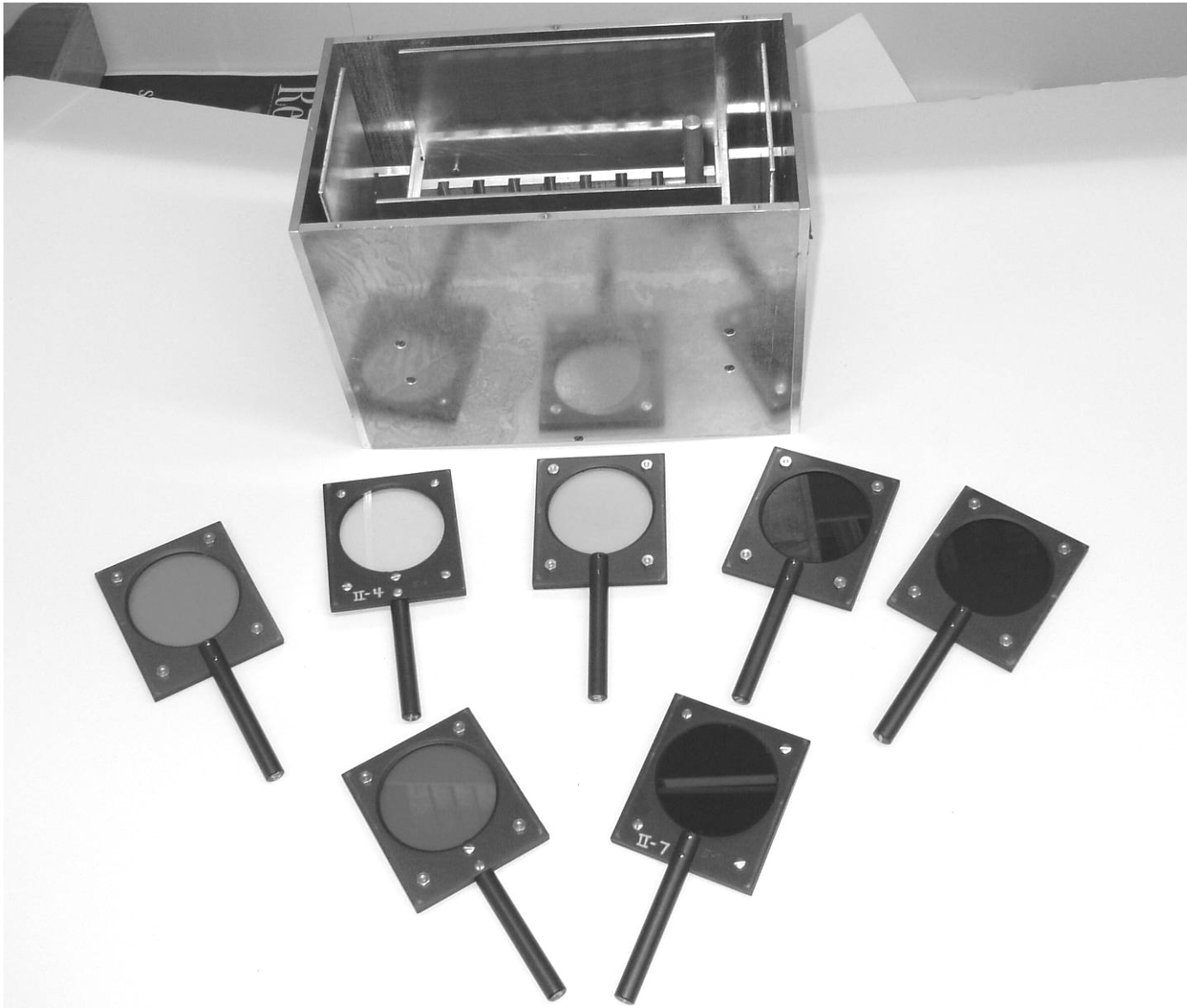
Figure 43 – Shown is the filter set used in the original MAP service.
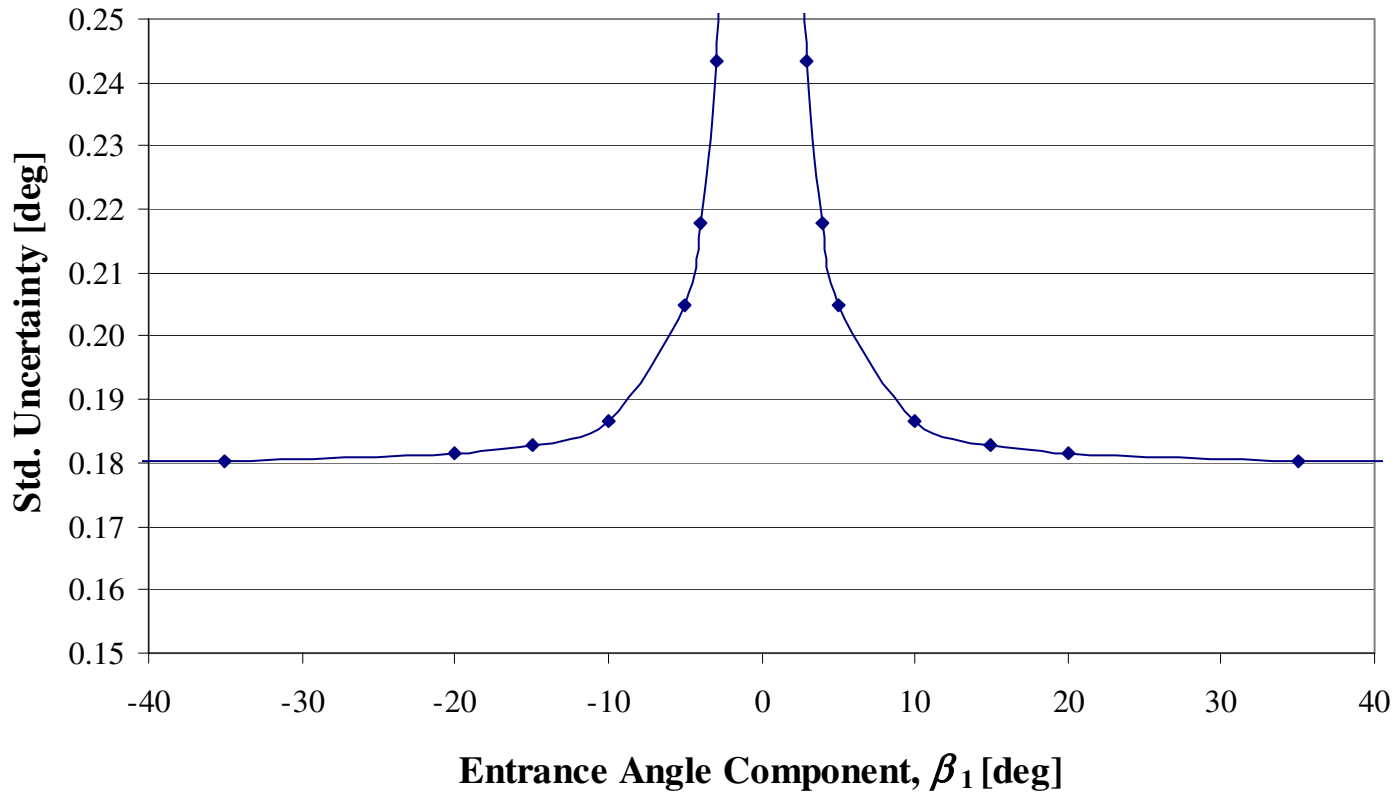
Figure B-1 – Orientation Angle Uncertainty Dependence

Table 1 - Light Spot Diameter (cm) at Sample Position with 5 mm Field Aperture

Lens Focal Length (m)	Sample Distance (m)					
	5	10	15	20	25	30
0.100	24	52.5	77	102	130	154
0.172	13	27	41	55	68	82
0.350	7	15	22	29	37	44
0.600	3.5	7	11	15	19	23
0.750	3.3	6.6	10	13	17	20

Table 2 - Summary of Source Requirements and Characterization

Characteristic	Requirement	Realization
Stability	< 1 %	short-term stability – 0.030 % ($k=2$) (monitoring) long-term stability – 0.056 % ($k=2$) (current uncertainty)
Spectral Distribution	S(λ) of Illuminant A CCT = 2856 K ± 20 K	CCT = 2856 K ± 10 K ($k=2$)
Uniformity of source aperture	not discussed	within 3 % of mean
Illuminance uniformity at specimen	within 5 % of mean	within 1.8 % of mean
Aperture size, 6' at 15 m	< 0.1'	5.96' at 15 m

C. Miller, et. al., Project 05-16

$$L_I = \frac{V}{R} C_V$$

Table 3 – Uncertainty budget for measuring the lamp current at any time within the year

No	Quantity	Symbol	Value	Standard Uncertainty	Unit	Type of evaluation	Degree of freedom	Sensivity Coefficient	Unit	Uncertainty Contribution
	X_i		x_i	$u(x_i)$			v_i	c_i		$u_i(y)$
1	Voltage Drop	V	1.67000	0.000004	V	A	30	10.00000	Ω^{-1}	0.0000400
2	Shunt Resistance	R	0.10000	0.00000125	Ω	B (cert)	∞	167.00000	A/Ω	0.0002088
3	DMM Cal Factor	C_v	1.00000	0.0000626		B (R)	∞	16.70000	A	0.0010456
	Lamp Current	L_I	**16.70000 0.0021 (k=2)**		**A**		∞			**0.00107**

$$\frac{\partial L_I}{\partial V} = \frac{L_I}{V} \qquad \frac{\partial L_I}{\partial R} = \frac{-L_I}{R} \qquad \frac{\partial L_I}{\partial C_V} = \frac{L_I}{C_V}$$

Table 4 – Uncertainty budget for measuring the lamp current over the course of a day

No	Quantity X_i	Symbol	Value x_i	Standard Uncertainty $u(x_i)$	Unit	Type of evaluation	Degree of freedom v_i	Sensivity Coefficient c_i	Unit	Uncertainty Contribution $u_i(y)$
1	Voltage Drop	V	1.67000	0.000004	V	A	30	10.00000	Ω^{-1}	0.0000400
2	Shunt Resistance	R	0.10000	0.00000125	Ω	B (cert)	∞	167.00000	A/Ω	0.0002088
3	DMM Cal Factor	C_v	1.00000	0.0000376		B (R)	∞	16.70000	A	0.0006272
	Lamp Current	L_I	**16.70000**	**0.0013 (k=2)**	**A**		∞			**0.00066**

Table 5 - Sensitivity Coefficient with respect to CCT

Material Color	CCT Expanded Uncertainty (k=2)	Sensitivity Coefficient (cd/m^2/lx/K)	Relative Expanded Uncertainty (k=2)
White	10 K	-0.0000114	0.011%
Red	10 K	-0.0001384	0.138%
Yellow	10 K	-0.0000571	0.057%
Green	10 K	0.0000551	0.055%
Blue	10 K	0.0001222	0.122%

Table 6 - Summary of goniometer motion requirements

Axis of Motion	Range of Motion	Minimum Step Size	Positioning Accuracy
Distance	10 m, 15 m, 30 m	N/A	$\pm$ 0.05 %
Entrance Angle, β_1	$\pm$ 90 °	0.02 °	<0.1 °
Entrance Angle, β_2	$\pm$ 90 °	0.02 °	<0.1 °
Rotation Angle, ε	$\pm$ 180 °	0.04 °	<0.2 °

Table 7 - Summary of realized goniometer motions and capabilities

Axis of Motion	Range of Motion	Minimum Step Size	Positioning Accuracy
X (rail – illumination axis)	3 – 33 m	< 100 μm	< $\pm$ 0.25 mm
X' (parallel to rail)	$\pm$ 46 cm	< 100 μm	< $\pm$ 0.25 mm
Y (perpendicular to rail)	$\pm$ 30.5 cm	$\pm$ 10 μm	< $\pm$ 0.050 mm
Z (vertical)	$\pm$ 30.5 cm	$\pm$ 10 μm	< $\pm$ 0.050 mm
NIST Entrance Angle, β_1'	$\pm$ 95 °	0.0002 °	<0.001 °
NIST Entrance Angle, β_2'	$\pm$ 95 °	0.0002 °	<0.001 °
Rotation Angle, ε	$\pm$ 185 °	0.0002 °	<0.001 °

$$D_I = VR - SA + D + TR$$

Table 8 – Uncertainty budget for setting the absolute position of the magnetic encoder

No	Quantity	Symbol	Value	Standard Uncertainty	Unit	Type of evaluation	Degree of freedom	Sensivity Coefficient	Unit	Uncertainty Contribution
	X_i		x_i	$u(x_i)$			v_i	c_i		$u_i(y)$
1	Source aperture	SA	0.0000	0.0254	mm	B	∞	-1.0000		-0.0254
2	Vernier distance	VR	3000.0000	0.0100	mm	B (cert)	∞	1.0000		0.0100
3	Dial indicator	D	0.0000	0.0115	mm	B (R)	∞	1.0000		0.0115
4	Tape reproducibitily	TR	0.0000	0.1732	mm	B (R)	∞	1.0000		0.1732
	Illumination dis.	D_{I0}	**3000.00**	**0.35 (*k=2*)**	**mm**		∞			**0.1757**

$$D_I = TM + CC + D + TR$$

Table 9 – Uncertainty budget for the illumination distance of a sample

No	Quantity	Symbol	Value	Standard Uncertainty	Unit	Type of evaluation	Degree of freedom	Sensivity Coefficient	Unit	Uncertainty Contribution
	X_i		x_i	$u(x_i)$			ν_i	c_i		$u_i(y)$
1	Tape measurement	TM	3000.0000	0.1757	mm	B	∞	1.0000		0.1757
2	Calibration curve	CC	0.0000	2.5000	mm	B	∞	1.0000		2.5000
3	Dial indicator	D	0.0000	0.0115	mm	B (R)	∞	1.0000		0.0115
4	Tape Reprod.	TR	0.0000	0.1732	mm	B (R)	∞	1.0000		0.1732
	Illumination dis.	D_I	**3000.00**	**5.02 (k=2)**	**mm**		∞			**2.5122**

C. Miller, et. al., Project 05-16

Table 10 – Summarizes the capabilities of the three detector stages

Stage	gear ratio motor:stage	stage distance / motor rev	encoder step size	min. step (1 motor step)	motor steps / encoder step	Uncertainty ($k=2$)
Rotation	180:1	2.00°	0.002°	0.00008°	25	0.008°
20 cm	1:1	5000 µm	1 µm	0.2 µm	5	14 µm
2 m	1:1	5000 µm	1 µm	0.2 µm	5	14 µm

Table 11 – The chromaticity differences (STARR-CHARM)

Tile Color	Δx	Δy
White	-0.0013	-0.0017
Black	-0.0021	-0.0027
Cyan	0.0030	0.0021
Yellow	0.0013	-0.0007
Red	-0.0040	0.0003

Table 12 - Uncertainty budget for setting the alignment tool

No	Quantity	Symbol	Value	Standard Uncertainty	Unit	Type of eval.	Deg. of freedom	Sensitivity Coefficient	Unit	Uncertainty Contribution
	X_i		x_i	$u(x_i)$			v_i	c_i		$u_i(y)$
1	Plate parallelism	C	0.0000	0.003252	deg	B (R)	∞	1.00000		0.003252
2	Source alignment	L	0.0000	0.001910	deg	B	∞	1.00000		0.001910
3	Goniometer unc.	G	0.0000	0.001000	deg	B	∞	1.00000		0.001000
4	Micrometer unc.	M	0.0000	0.006301	deg	B (R)	∞	1.00000		0.006301
	Alignment Tool unc.	**A**	**0.0000**	**0.0148 (k=2)**	**deg**		∞			**0.00741**

Table 13 - Uncertainty budget for setting arbitrary NIST entrance angle components

No	Quantity	Symbol	Value	Standard Uncertainty	Unit	Type of eval.	Deg. of freedom	Sensitivity Coefficient	Unit	Uncertainty Contribution
	X_i		x_i	$u(x_i)$			v_i	c_i		$u_i(y)$
1	Alignment Tool unc.	A	0.0000	0.007411	deg	B (R)	∞	1.00000		0.007411
2	Mounting sample	S	0.0000	0.006301	deg	B (R)	∞	1.00000		0.006301
3	Change in angle	$\Delta\beta$	30.0000	0.001000	deg	B	∞	1.00000		0.001000
	NIST entrance angle	$\beta_\#'$	**30.0000**	**0.0196 (k=2)**	**deg**		∞			**0.00978**

Table 14 - Uncertainty budget for calculating CIE entrance angle component, β_1

No	Quantity	Symbol	Value	Standard Uncertainty	Unit	Type of eval.	Deg. of freedom	Sensitivity Coefficient	Unit	Uncertainty Contribution
	X_i		x_i	$u(x_i)$			v_i	c_i		$u_i(y)$
1	NIST angle 1	β_1'	30.000	0.00978	deg	B	∞	1.06588		0.010424
2	NIST angle 2	β_2'	30.000	0.00978	deg	B	∞	-0.26647		-0.002606
	CIE entrance angle	β_1	**33.690**	**0.021 (k=2)**	deg		∞			**0.01074**

$$\frac{\partial \beta_1}{\partial \beta_1'} = \left[\cos^2 \beta_1' \cos \beta_2' + \frac{\sin^2 \beta_1'}{\cos \beta_2'} \right]^{-1}$$

$$\frac{\partial \beta_1}{\partial \beta_2'} = \frac{-\tan \beta_1' \sin \beta_2'}{\cos^2 \beta_2' \tan^2 \beta_1'}$$

Table 15 - Uncertainty budget for calculating CIE entrance angle component, β_2

No	Quantity	Symbol	Value	Standard Uncertainty	Unit	Type of eval.	Deg. of freedom	Sensitivity Coefficient	Unit	Uncertainty Contribution
	X_i		x_i	$u(x_i)$			v_i	c_i		$u_i(y)$
1	NIST angle 1	β_1'	30.000	0.00978	deg	B	∞	0.27735		0.002712
2	NIST angle 2	β_2'	30.000	0.00978	deg	B	∞	-0.83205		-0.008137
	CIE entrance angle	β_2	**-25.659**	**0.017 (k=2)**	deg		∞			**0.008577**

$$\frac{\partial \beta_2}{\partial \beta_1'} = \frac{\sin \beta_1' \sin \beta_2'}{\sqrt{1 - \cos^2 \beta_1' \sin^2 \beta_2'}} \qquad \frac{\partial \beta_2}{\partial \beta_2'} = \frac{-\cos \beta_1' \cos \beta_2'}{\sqrt{1 - \cos^2 \beta_1' \sin^2 \beta_2'}}$$

Table 16 - Uncertainty budget for setting the aperture separation, c

No	Quantity X_i	Symbol	Value x_i	Standard Uncertainty $u(x_i)$	Unit	Type of eval.	Deg. of freedom v_i	Sensitivity Coefficient c_i	Unit	Uncertainty Contribution $u_i(y)$
1	Little Stage Movement	y	0.018286	0.000029	m	B	∞	-0.017453		-0.000001
2	Long Stage Movement	x	1.047620	0.000029	m	B	∞	0.999848		0.000029
3	Pointing Rotation	r	0.034807	0.000140	rad	B	∞	-0.018283	m/rad	- 0.000003
	Aperture Separation	c	**1.047141 0.000058 (*k*=2)**		m		∞			**0.000029**

$$\frac{\partial c}{\partial y} = \frac{y - x\cos(\pi/2 - r)}{c} \qquad \frac{\partial c}{\partial x} = \frac{x - y\cos(\pi/2 - r)}{c} \qquad \frac{\partial c}{\partial r} = \frac{-xy\sin(\pi/2 - r)}{c}$$

C. Miller, et. al., Project 05-16

Table 17 - Uncertainty budget for observation distance, d

No	Quantity	Symbol	Value	Standard Uncertainty	Unit	Type of eval.	Deg. of freedom	Sensitivity Coefficient	Unit	Uncertainty Contribution
	X_i		x_i	$u(x_i)$			v_i	c_i		$u_i(y)$
1	Little Stage Movement	y	0.018286	0.000029	m	B	∞	-1.00000		-0.000071
2	Long Stage Movement	x	1.04762	0.000029	m	B	∞	0.00000		0.000000
3	Pointing Rotation	r	0.034807	0.000140	rad	B	∞	1.04570	m/rad	0.000146
4	Illumination Distance	s	30.00000	0.002512	m	B	∞	1.00061		0.002514
	Observation Distance	d	**30.0000**	**0.0050 (k=2)**	m		∞			**0.002519**

$$\frac{\partial d}{\partial y} = -1 \qquad \frac{\partial d}{\partial x} = \sin(r) - \frac{x\cos^2(r)}{\sqrt{s^2 - x^2\cos^2(r)}} \qquad \frac{\partial d}{\partial r} = x\cos(r) + \frac{x^2\cos(r)\sin(r)}{\sqrt{s^2 - x^2\cos^2(r)}} \qquad \frac{\partial d}{\partial s} = \frac{s}{\sqrt{s^2 - x^2\cos^2(r)}}$$

Table 18 - Uncertainty budget for arbitrary setting of the observation angle, α

No	Quantity	Symbol	Value	Standard Uncertainty	Unit	Type of eval.	Deg. of freedom	Sensitivity Coefficient	Unit	Uncertainty Contribution
	X_i		x_i	$u(x_i)$			v_i	c_i		$u_i(y)$
1	Illumination Distance	s	30.00000	0.002512	m	B	∞	-0.04714	deg/m	-0.000118
2	Observation Distance	d	30.00000	0.002519	m	B	∞	-0.04711	deg/m	-0.000119
3	Aperture Separation	c	1.04714	0.000029	m	B	∞	2.70095	deg/m	0.000078
	Observation angle	α	**2.00000**	**0.00037 (k=2)**	m		∞			**0.00019**

$$\frac{\partial \alpha}{\partial s} = \frac{d^2 - s^2 - c^2}{2s^2 d \sqrt{1 - \left(\frac{d^2 + s^2 - c^2}{2sd} \right)}}$$

$$\frac{\partial \alpha}{\partial d} = \frac{s^2 - d^2 - c^2}{2sd^2 \sqrt{1 - \left(\frac{d^2 + s^2 - c^2}{2sd} \right)}}$$

$$\frac{\partial \alpha}{\partial c} = \frac{c}{sd \sqrt{1 - \left(\frac{d^2 + s^2 - c^2}{2sd} \right)}}$$

C. Miller, et. al., Project 05-16

Table 19 - Uncertainty budget for coefficient of luminous intensity, R_I

No	Quantity	Symbol	Value	Standard Uncertainty	Unit	Type of eval.	Deg. of freedom	Sensitivity Coefficient	Unit	Uncertainty Contribution
	X_i		x_i	$u(x_i)$			v_i	c_i		$u_i(y)$
1	Specimen signal	m_T	1.0000	0.00030	lx	A	20	0.2250	m^2/lx	0.000068
2	Dark signal	m_D	0.0001	0.00030	lx	A	20	-0.2250	m^2/lx	-0.000068
3	Illuminance signal	m_S	1000.000	0.30000	lx	A	20	-0.000225	$cd/m^2/lx^2$	-0.000068
4	Observation distance	d	15.0000	0.00252	m	B	∞	0.0300	$cd/m/lx^2$	0.000076
	Coef. of Luminous Int.	R_I	**0.2250**	**0.00028 (k=2)** $cd/m^2/lx$			large			**0.00014**

$$\frac{\partial R_I}{\partial m_T} = \frac{d^2}{m_S} \qquad \frac{\partial R_I}{\partial m_D} = \frac{-d^2}{m_S} \qquad \frac{\partial R_I}{\partial m_S} = \frac{-R_I}{m_S} \qquad \frac{\partial R_I}{\partial d} = \frac{2R_I}{d}$$

Table 20 – Summary of the additional uncertainty components for white beaded material

Uncertainty Component	White Beaded Rel. Std. Unc.
Source luminance	0.028
CCT uncertainty	0.069
Source aperture uniformity	0.001
Source aperture size	0.004
Illuminance measurement	0.106
Illuminance uniformity and sample	0.100
Illumination distance	0.015
Amplifier Linearity	0.020
Illuminance unit	0.000
Luminance unit	0.000
Detector uniformity	0.003
Spectral mismatch factor	0.050
Observation distance	0.020
Entrance angle correction, β_1	0.002
Entrance angle correction, β_2	0.000
Observation angle correction	0.049
Rotation angle correction	0.002
Rotation stage correction	0.008
Long stage correction	0.023
Short stage correction	0.000
Long-term drift of NIST detector	0.025
Stray light	0.050
Sample temperature issues	0.150
Repeatability	0.125
Relative Combined Uncertainty	**0.27**
Relative Expanded Uncertainty ($k=2$)	**0.55**

Table 21 – Summary of the additional uncertainty components for red prismatic material

Uncertainty Component	Red Prismatic Rel. Std. Unc.
Source luminance	0.028
CCT uncertainty	0.069
Source aperture uniformity	0.001
Source aperture size	0.007
Illuminance measurement	0.106
Illuminance uniformity and sample	0.100
Illumination distance	0.015
Amplifier Linearity	0.020
Illuminance unit	0.000
Luminance unit	0.000
Detector uniformity	0.003
Spectral mismatch factor	0.150
Observation distance	0.020
Entrance angle correction, β_1	0.003
Entrance angle correction, β_2	0.000
Observation angle correction	0.074
Rotation angle correction	1.320
Rotation stage correction	0.012
Long stage correction	0.034
Short stage correction	0.000
Long-term drift of NIST detector	0.025
Stray light	0.050
Sample temperature issues	0.200
Repeatability	0.125
Relative Combined Uncertainty	**1.4**
Relative Expanded Uncertainty ($k=2$)	**2.7**

Table 22 – Summary of the additional uncertainty components for yellow pavement marking material

Uncertainty Component	Yellow Pavement Rel. Std. Unc.
Source luminance	0.028
CCT uncertainty	0.069
Source aperture uniformity	0.001
Source aperture size	0.007
Illuminance measurement	0.030
Illuminance uniformity and sample	0.250
Illumination distance	0.015
Amplifier Linearity	0.020
Illuminance unit	0.000
Luminance unit	0.000
Detector uniformity	0.003
Spectral mismatch factor	0.100
Observation distance	0.020
Entrance angle correction, β_1	0.002
Entrance angle correction, β_2	0.000
Observation angle correction	0.049
Rotation angle correction	0.000
Rotation stage correction	0.012
Long stage correction	0.034
Short stage correction	0.000
Long-term drift of NIST detector	0.025
Stray light	0.350
Sample temperature issues	0.150
Repeatability	0.175
Relative Combined Uncertainty	**0.51**
Relative Expanded Uncertainty ($k=2$)	**1.02**

Table 23 - Uncertainty budget for measurement of area, A

No	Quantity X_i	Symbol	Value x_i	Standard Uncertainty $u(x_i)$	Unit	Type of eval.	Deg. of freedom v_i	Sensitivity Coefficient c_i	Unit	Uncertainty Contribution $u_i(y)$
1	Sample length	l	0.20000	0.0005	m	B	∞	1.0000		0.0005
2	Sample height	h	0.20000	0.0005	m	B	∞	1.0000		0.0005
	Sample area	**A**	**0.04000**	**0.0014 (k=2)**	m^2		∞			**0.0007**

C. Miller, et. al., Project 05-16

Table B-1 - Uncertainty budget for orientation angle, ω_s

No	Quantity	Symbol	Value	Standard Uncertainty	Unit	Type of eval.	Deg. of freedom	Sensitivity Coefficient	Unit	Uncertainty Contribution
	X_i		x_i	$u(x_i)$			v_i	c_i		$u_i(y)$
1	CIE entrance angle	β_1	33.690	0.0107	deg	B	∞	1.5371		0.0165
2	CIE entrance angle	β_2	-25.660	0.0086	deg	B	∞	0.9509		0.0081
3	Rotation angle	ε	0.000	0.1800	deg	B	∞	1.0000		0.1800
	Orientation angle	ω_s	**-33.006**	**0.362 (k=2)**	deg		∞			**0.1809**

$$\frac{\partial \omega_s}{\partial \beta_1} = \frac{-\sin \beta_2}{\sin^2 \beta_1} + (\cos \beta_1 \sin \beta_2)^2$$

$$\frac{\partial \omega_s}{\partial \beta_2} = \frac{\cos \beta_2}{\left(\tan \beta_1 + \dfrac{\sin^2 \beta_2}{\tan \beta_1} \right)}$$

$$\frac{\partial \omega_s}{\partial \varepsilon} = 1$$

C. Miller, et. al., Project 05-16

Table B-2 - Uncertainty budget for presentation angle, γ

No	Quantity	Symbol	Value	Standard Uncertainty	Unit	Type of eval.	Deg. of freedom	Sensitivity Coefficient	Unit	Uncertainty Contribution
	X_i		x_i	$u(x_i)$			v_i	c_i		$u_i(y)$
1	CIE entrance angle	β_1	33.690	0.0107	deg	B	∞	0.7423		0.0079
2	CIE entrance angle	β_2	-25.660	0.0086	deg	B	∞	-3.0306		-0.0261
	Presentation angle	γ	**-40.895**	**0.054 (k=2)**	deg		∞			**0.0272**

$$\frac{\partial \gamma}{\partial \beta_1} = \frac{-\tan \beta_2 \cos \beta_1}{\sin^2 \beta_1 + \tan^2 \beta_2} \qquad \frac{\partial \gamma}{\partial \beta_2} = \frac{\sin \beta_1}{\cos^2 \beta_2 \sin^2 \beta_1 + \sin^2 \beta_2}$$

Table B-3 - Uncertainty budget for observation-elevation angle, a

No	Quantity	Symbol	Value	Standard Uncertainty	Unit	Type of eval.	Deg. of freedom	Sensitivity Coefficient	Unit	Uncertainty Contribution
	X_i		x_i	$u(x_i)$			v_i	c_i		$u_i(y)$
1	CIE entrance angle	β_1	88.760	0.00858	deg	B	∞	-1.0000		0.00858
2	CIE entrance angle	β_2	0.000	0.00858	deg	B	∞	0.0000		0.00000
3	Observation angle	α	1.050	0.00019	deg	B	∞	0.9992		0.00020
	Observation-Elevation	a	**2.290**	**0.017 (k=2)**	deg		∞			**0.0086**

$$\frac{\partial a}{\partial \beta_1} = \frac{-\sin(\beta_1 - \alpha)\cos\beta_2}{\sqrt{1-\cos^2(\beta_1 - \alpha)\cos^2\beta_2}} \qquad \frac{\partial a}{\partial \beta_2} = \frac{-\cos(\beta_1 - \alpha)\sin\beta_2}{\sqrt{1-\cos^2(\beta_1 - \alpha)\cos^2\beta_2}} \qquad \frac{\partial a}{\partial \alpha} = \frac{\sin(\beta_1 - \alpha)\cos\beta_2}{\sqrt{1-\cos^2(\beta_1 - \alpha)\cos^2\beta_2}}$$

Table B-4 - Uncertainty budget for RM First azimuthal angle, b

No	Quantity X_i	Symbol	Value x_i	Standard Uncertainty $u(x_i)$	Unit	Type of eval.	Deg. of freedom v_i	Sensitivity Coefficient c_i	Unit	Uncertainty Contribution $u_i(y)$
1	CIE entrance angle	β_1	88.760	0.00858	deg	B	∞	1.2380		0.0106
2	CIE entrance angle	β_2	0.000	0.00858	deg	B	∞	0.0000		0.0000
3	Observation angle	α	1.050	0.00019	deg	B	∞	-1.5898		-0.0003
4	Observation-Elevation	a	2.290	0.00860	deg	B	∞	-0.8348		-0.0072
	RM First Azimuthal	b	**181.179**	**0.025 (k=2)**	deg		∞			**0.0128**

$$\frac{\partial b}{\partial \beta_1} = -\operatorname{sgn}(\beta_2) \frac{\left[\dfrac{\sin(2\beta_1 - \alpha) - \sin^2 \beta_2 \sin \alpha}{\sqrt{1 - \cos^2 \beta_1 \cos^2 \beta_2}} - \dfrac{\cos \beta_1 \sin \beta_1 \cos \beta_2 \left[\sin^2 \beta_2 \cos \beta_1 \cos(\beta_1 - \alpha) + \sin \beta_1 \sin(\beta_1 - \alpha)\right]}{\sqrt[3]{1 - \cos^2 \beta_1 \cos^2 \beta_2}} \right]}{\cos a \sqrt{1 - \dfrac{\left[\sin^2 \beta_2 \cos \beta_1 \cos(\beta_1 - \alpha) + \sin \beta_1 \sin(\beta_1 - \alpha)\right]^2}{\cos^2 a \left(1 - \cos^2 \beta_1 \cos^2 \beta_2\right)}}}$$

$$\frac{\partial b}{\partial \beta_2} = -\operatorname{sgn}(\beta_2) \frac{\left[\dfrac{\sin^2 \beta_2 \cos \beta_1 \cos(\beta_1 - \alpha)}{\sqrt{1 - \cos^2 \beta_1 \cos^2 \beta_2}} - \dfrac{\cos \beta_1 \sin \beta_2 \cos \beta_2 \left[\sin^2 \beta_2 \cos \beta_1 \cos(\beta_1 - \alpha) + \sin \beta_1 \sin(\beta_1 - \alpha)\right]}{\sqrt[3]{1 - \cos^2 \beta_1 \cos^2 \beta_2}} \right]}{\cos a \sqrt{1 - \dfrac{\left[\sin^2 \beta_2 \cos \beta_1 \cos(\beta_1 - \alpha) + \sin \beta_1 \sin(\beta_1 - \alpha)\right]^2}{\cos^2 a \left(1 - \cos^2 \beta_1 \cos^2 \beta_2\right)}}}$$

$$= -\operatorname{sgn}(\beta_2) \frac{\left[\dfrac{\sin^2 \beta_2 \cos \beta_1 \sin(\beta_1 - \alpha) - \sin \beta_1 \cos(\beta_1 - \alpha)}{\cos a \sqrt{1 - \cos^2 \beta_1 \cos^2 \beta_2}} \right]}{\sqrt{1 - \dfrac{\left[\sin^2 \beta_2 \cos \beta_1 \cos(\beta_1 - \alpha) + \sin \beta_1 \sin(\beta_1 - \alpha)\right]^2}{\cos^2 a \left(1 - \cos^2 \beta_1 \cos^2 \beta_2\right)}}}$$

$$\frac{\partial b}{\partial a} = -\operatorname{sgn}(\beta_2) \frac{\left[\dfrac{\sin^2 \beta_2 \cos \beta_1 \cos(\beta_1 - \alpha) + \sin \beta_1 \sin(\beta_1 - \alpha)}{\cos^2 a \sin a \sqrt{1 - \cos^2 \beta_1 \cos^2 \beta_2}} \right]}{\sqrt{1 - \dfrac{\left[\sin^2 \beta_2 \cos \beta_1 \cos(\beta_1 - \alpha) + \sin \beta_1 \sin(\beta_1 - \alpha)\right]^2}{\cos^2 a \left(1 - \cos^2 \beta_1 \cos^2 \beta_2\right)}}}$$

Table B-5 - Uncertainty budget for Illumination Elevation angle, e

No	Quantity X_i	Symbol	Value x_i	Standard Uncertainty $u(x_i)$	Unit	Type of eval.	Deg. of freedom v_i	Sensitivity Coefficient c_i	Unit	Uncertainty Contribution $u_i(y)$
1	CIE entrance angle	β_1	88.760	0.0086	deg	B	∞	-1.0000		-0.0086
2	CIE entrance angle	β_2	0.000	0.0086	deg	B	∞	0.0000		0.0000
	Illumination Elevation	ε	**1.240**	**0.017 (k=2)**	deg		∞			**0.0086**

$$\frac{\partial e}{\partial \beta_1} = \frac{-\sin \beta_1 \cos \beta_2}{\sqrt{1-\cos^2 \beta_1 \cos^2 \beta_2}} \qquad \frac{\partial e}{\partial \beta_2} = \frac{-\sin \beta_2 \cos \beta_1}{\sqrt{1-\cos^2 \beta_1 \cos^2 \beta_2}}$$

Table B-6 - Uncertainty budget for RM Second Azimuthal angle, d

No	Quantity	Symbol	Value	Standard Uncertainty	Unit	Type of eval.	Deg. of freedom	Sensitivity Coefficient	Unit	Uncertainty Contribution
	X_i		x_i	$u(x_i)$			v_i	c_i		$u_i(y)$
1	Orientation angle	ω_s	0.000	0.1800	deg	B	∞	1.0000		0.1800
2	RM First Azimuthal	b	0.000	0.0128	deg	B	∞	1.0000		0.0128
	Illumination Elevation	d	**180.000**	**0.361 (k=2)**	deg		∞			**0.1805**

$$\frac{\partial d}{\partial \omega_s} = 1 \qquad\qquad \frac{\partial d}{\partial b} = 1$$